

**PHOTOTHERMAL INVESTIGATIONS ON
CERTAIN PLASMA POLYMERIZED THIN FILMS
AND NEAR IR OVERTONE STUDIES OF
SOME ORGANIC MOLECULES**

Thesis submitted to
Cochin University of Science and Technology
in partial fulfilment of the requirements
for the award of the degree of
DOCTOR OF PHILOSOPHY



by

Usha John

Department of Physics
Cochin University of Science and Technology
Cochin 6820 22
India

July 2006

*'It is good to give thanks to the Lord, and sing praises
to Your name, O Most High.'* Ps 92:1

*.....Dedicated to my grandparents, parents,
Albert and Jane*



Department of Physics
Cochin University of Science and Technology
Cochin 682 022

CERTIFICATE

Certified that the work presented in this thesis entitled **“PHOTOTHERMAL INVESTIGATIONS ON CERTAIN PLASMA POLYMERIZED THIN FILMS AND NEAR IR OVERTONE STUDIES OF SOME ORGANIC MOLECULES”** is based on the bonafide research work done by Ms. Usha John under my guidance in the Department of Physics, Cochin University of Science and Technology, Cochin 682 022, and has not been included in any other thesis submitted previously for the award of any degree.

Kochi-22
20 -7-2006

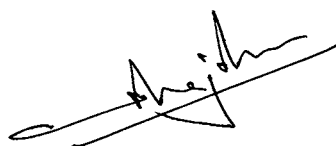
Prof. K.P Rajappan Nair
Supervising Guide
Laser and Spectroscopy Lab.
Department of Physics
CUSAT, Kochi-22

DECLARATION

I hereby declare that the present work entitled “**PHOTOTHERMAL INVESTIGATIONS ON CERTAIN PLASMA POLYMERIZED THIN FILMS AND NEAR IR OVERTONE STUDIES OF SOME ORGANIC MOLECULES**” is based on the original work done by me under the guidance of Prof. K.P. Rajappan Nair, Laser and Spectroscopy Lab., Department of Physics, Cochin University of Science and Technology, Kochi-22 and has not been included in any other thesis submitted previously for the award of any degree.

Kochi-22

20- 7-06

A handwritten signature in black ink, appearing to read 'Usha John', written over a horizontal line.

Usha John

ACKNOWLEDGEMENT

It gives me great pleasure to express my deep sense of gratitude to Dr. K. P. Rajappan Nair, Laser and Spectroscopy Laboratory, Dept. of Physics, Cochin University of Science and Technology for his excellent guidance and constant encouragement throughout the course of this research work.

I am thankful to Prof. V. C. Kurikose, Head, Dept. of Physics, Cochin University of Science and Technology and Prof. K. P. Vijayakumar, Prof. M. Sabir and Prof. Elizabeth Mathai, former Heads of the Department for providing the necessary facilities. I am thankful to Dr. T.M Abdul Rasheed and Dr. M. K. Jayaraj for their timely help. I remember with gratitude Dr. Sudha C. Kartha for all the help, support and encouragement at various stages of this work. I am thankful to all the teaching and non-teaching staff of the Dept. of Physics for their sincere co-operation.

I am extremely thankful to my co-workers in the Laser and Spectroscopy Lab., especially to Dr. Jyotsna Ravi, Dr. S. Shaji and Dr. Shibu M. Eappen from whom I have benefitted immensely. I owe a lot to Dr. Sunny Kuriakose, Dr. B. Syamalakumari, Mr. Thomas P. Zacharia, Ms. T. Nandini and Dr. K. K. Vijayan, my fellow researchers in the laboratory who contributed in different ways towards the accomplishment of this work. I thank Mr. N.V. Joshy, Ms. P.A. Subha, Ms. Chitra R. Nayak and Mr. John P. R for their timely help and assistance. During the course of my research, I have been able to communicate with Prof. B. R Henry, University of Guelph, Canada and Prof. C. Sandorfy of University of Montreal and I am thankful to them for their valuable suggestions in shaping my research work.

I am grateful to Prof. V.X. Sebastian, Principal, St-paul's College, Kalamassery and to the staff members of the Dept. of Physics for their co-operation and support. I take this opportunity to thank my colleagues, especially Dr. Sallyamma Job, Dr. M. S. Geetha, Ms. Rose Philo K, J and Ms. Beena P. J for their help and support.

I wish to thank U.G.C, India for financial assistance in the form of a minor research project sanctioned to me. I also acknowledge the analysis services rendered by Sophisticated Analytical Instrument Facility (SAIF) Cochin, a national facility sponsored by the Department of Science and Technology, Govt. of India.

I am extremely grateful to my parents, relatives and well-wishers for the support and encouragement rendered during the period of this work. Finally I express my deep sense of gratitude to my daughter, Jane for her encouragement, love, support and understanding throughout the course of this work. Above all, there is that Supreme Power without Whose blessings and kindness we cannot achieve anything in this world.

Usha John

CONTENTS

PREFACE

Chapter 1 PHOTOTHERMAL EFFECTS

1.1	Introduction	1
1.2	Detection schemes	5
1.3	Rosencwaig-Gersho 1-D theory	14
1.4	Photothermal probe beam deflection (PBD) or Mirage effect ; 3-D theory	20
	References	29

Chapter 2 PREPARATION OF R.F. PLASMA POLYMERIZED THIN FILMS AND FTIR ANALYSIS....

2.1	Introduction	32
2.2	Mechanism of plasma polymerization	34
2.3	Preparation of plasma polymerized thin films	37
2.4	FTIR analysis	39
	References	49

Chapter 3 DETERMINATION OF THERMAL DIFFUSIVITY OF R.F PLASMA POLYMERIZED THIN FILMS USING PROBE BEAM DEFLECTION METHOD

3.1	Introduction	51
3.2	Importance of thermal diffusivity	52
3.3	Experimental configurations	53
3.4	Methods of analysis	54
3.5	Transverse PBD setup	55
3.6	Thermal diffusivity of plasma polymerized thin films	62
	References	71

Chapter 4 NEAR IR VIBRATIONAL OVERTONE SPECTROSCOPY

4.1	Introduction	73
4.2	Infrared spectroscopy	74
4.3	Vibrational energy of a diatomic molecule	76
4.3.1	The Simple Harmonic Oscillator	76
4.3.2	Anharmonicity	78
4.3.3	The Anharmonic Oscillator	80
4.4	Normal modes of vibration of polyatomic molecules	83
4.5	Features of NIR spectra of polyatomic molecules	85
4.5.1	Overtone and Combination frequencies	85
4.5.2	Fermi resonance	85
4.5.3	Darling–Dennison resonance	86
4.6	Local mode model	86
4.7	Quantum mechanical description of LM model	89
4.8	Applications of overtone spectroscopy and local mode model	91
4.9	Hydrogen bonding and overtone spectroscopy	94
4.10	Present work	97
	References	98

Chapter 5	NEAR IR OVERTONE ANALYSIS OF SOME AMINES	
5.1	Analysis of the overtone spectra of 2,4-dimethylaniline and 2,6-dimethylaniline	102
5.1.1	Introduction	102
5.1.2	Experimental	103
5.1.3	Results and discussions	104
5.1.4	Conclusions	113
5.2	Analysis of the overtone spectrum of cyclohexylamine	113
5.2.1	Introduction	113
5.2.2	Experimental	114
5.2.3	Results and discussions	114
5.2.4	Conclusions	121
5.3	Analysis of the overtone spectrum of morpholine	121
5.3.1	Introduction	121
5.3.2	Experimental	122
5.3.3	Results and discussions	122
5.3.4	Conclusions	127
	References	128
Chapter 6	NEAR IR OVERTONE ANALYSIS OF SOME MODERATELY STRONG HYDROGEN BONDED SYSTEMS	
6.1	Analysis of the overtone spectra of cyclohexanol	130
6.1.1	Introduction	130
6.1.2	Experimental	131
6.1.3	Results and discussions	132
6.1.4	Conclusions	139
6.2	Analysis of the overtone spectra of cyclopentanol	140
6.2.1	Introduction	140
6.2.2	Experimental	141
6.2.3	Results and discussions	142
6.2.4	Conclusions	148
6.3	Analysis of the overtone spectra of Imidazole	149
6.3.1	Introduction	149
6.3.2	Experimental	152
6.3.3	Results and discussions	152
6.3.4	Conclusions	159
	References	160
Chapter 7	SUMMARY AND CONCLUSIONS	163
	LIST OF PAPERS PUBLISHED IN INTERNATIONAL JOURNALS	

PREFACE

Photothermal effect refers to heating of a sample due to the absorption of electromagnetic radiation. Photothermal (PT) heat generation which is an example of energy conversion has in general three kinds of applications. 1. PT material probing 2. PT material processing and 3. PT material destruction. The temperatures involved increases from 1→ 3. Of the above three, PT material probing is the most important in making significant contribution to the field of science and technology. Photothermal material characterization relies on high sensitivity detection techniques to monitor the effects caused by PT material heating of a sample. Photothermal method is a powerful high sensitivity non-contact tool used for non-destructive thermal characterization of materials. The high sensitivity of the photothermal methods has led to its application for analysis of low absorbance samples. Laser calorimetry, photothermal radiometry, pyroelectric technique, photoacoustic technique, photothermal beam deflection technique, etc. come under the broad class of photothermal techniques. However the choice of a suitable technique depends upon the nature of the sample, purpose of measurement, nature of light source used, etc. The present investigations are done on polymer thin films employing photothermal beam deflection technique, for the successful determination of their thermal diffusivity. Here the sample is excited by a He-Ne laser ($\lambda = 6328\text{\AA}$) which acts as the pump beam. Due to the refractive index gradient established in the sample surface and in the adjacent coupling medium, another optical beam called probe beam (diode laser, $\lambda = 6500\text{\AA}$) when passed through this region experiences a deflection and is detected using a position sensitive detector and its output is fed to a lock-in amplifier from which the amplitude and phase of the deflection can be directly obtained. The amplitude and phase of the signal is suitably analysed for determining the thermal diffusivity.

The production of polymer thin film samples has gained considerable attention for the past few years. Plasma polymerization is an inexpensive tool for fabricating organic thin films. It refers to formation of polymeric materials under the influence of plasma, which is generated by some kind of electric discharge. Here plasma of the monomer vapour is generated by employing radio frequency (MHz) techniques. Plasma polymerization technique results in homogeneous, highly adhesive, thermally stable, pinhole free, dielectric, highly branched and cross-linked polymer films. The possible linkage in the formation of the polymers is suggested by comparing the FTIR spectra of the monomer and the polymer.

Near IR overtone investigations on some organic molecules using local mode model are also done. Higher vibrational overtones often provide spectral simplification and greater resolution of peaks corresponding to nonequivalent X-H bonds where X is typically C, N or O. Vibrational overtone spectroscopy of molecules containing X-H oscillators is now a well established tool for molecular investigations. Conformational and steric differences between bonds and structural inequivalence of CH bonds (methyl, aryl, acetylenic, etc.) are resolvable in the higher overtone spectra. The local mode model in which the X-H oscillators are considered to be loosely coupled anharmonic oscillators has been widely used for the interpretation of overtone spectra. If we are exciting a single local oscillator from the vibrational ground state to the vibrational state v , then the transition energy of the local mode overtone is given by $\Delta E_{0 \rightarrow v} = A v + B v^2$. A plot of $\Delta E / v$ versus v will yield A, the local mode frequency as the intercept and B, the local mode diagonal anharmonicity as the slope. Here $A - B$ gives the mechanical frequency X_1 of the oscillator and $B = X_2$ is the anharmonicity of the bond. The local mode parameters X_1 and X_2 vary for non-equivalent X-H bonds and are sensitive to the inter and intra molecular environment of the X-H oscillator. The thesis contains seven chapters which are summarized as follows.

Chapter 1 gives a general introduction to photothermal effects. Common photothermal effects produced by modulated optical absorption in a sample and the

corresponding detection schemes are discussed. Various configurations for probe beam refraction (PBR) to monitor refractive index gradient (RIG) are discussed. In this thesis, major emphasis is on perpendicular probe beam refraction outside the sample (mirage effect). As the photothermal techniques are based on the heating effects, the temperature distribution in the sample as well as in the surrounding media are to be discussed, which can be related to the signal amplitude and phase. This is done in the last two sections by discussing the Rosencwaig-Gersho 1-D theory and the 3-D theory.

Chapter 2 describes the preparation of r.f plasma polymerized thin films and their FTIR analysis. Three samples namely Poly 2,6-dimethylaniline, poly diethylamine and poly dimethylamine are prepared. FTIR analysis of the monomer and polymer are done to suggest the possible linkage in the formation of the polymer.

Chapter 3 describes the determination of thermal diffusivity of all the three r.f plasma polymerized samples using the perpendicular probe beam refraction (mirage method) method. For each sample, measurements are done at two modulation frequencies. The deflection signal is analysed by phase method as well as amplitude method.

Chapter 4 starts with an introduction to vibrational spectroscopy. Vibrational energy levels of an anharmonic oscillator and appearance of overtones are discussed. The chapter outlines how the local mode model is used as a tool to analyse the overtones in the NIR region of the X-H containing molecules (X = C, N, O....).

Chapter 5 analyses the Near IR overtone spectra of four amines. The near infrared vibrational overtone absorption spectra of liquid phase 2,6-dimethylaniline and 2,4-dimethylaniline are reported in the region $\Delta v = 2, 3 \text{ \& } 4$. The aryl CH, methyl CH and NH local mode mechanical frequency values obtained from fitting the overtones are analysed and compared. Cyclohexylamine and morpholine are nonaromatic cyclic amines with six-member saturated rings. The near infrared vibrational overtone absorption spectra of these molecules in carbon tetrachloride in different concentrations are examined. The CH and NH local mode mechanical

frequency values and anharmonicity values obtained from fitting the overtones are analysed and compared. Both for cyclohexylamine and morpholine we could identify weak and broad red-shifted bands at lower overtones due to the formation of hydrogen bonds.

Chapter 6 deals with the near IR overtone analysis of some moderately strong hydrogen bonded systems. Overtone spectra of cyclohexanol in carbon tetrachloride in different concentrations are analysed using the local mode model. While the aryl CH and free OH local mode parameters are almost insensitive to the variation in concentration, the local mode parameters for the bonded OH stretching vibrations vary with concentration. The near infrared vibrational overtone absorption spectra of cyclopentanol in liquid phase are examined. The CH, bonded OH and free OH local mode mechanical frequency values and anharmonicity values obtained from fitting the overtones are analysed and compared. Due to hydrogen bonding in addition to free OH, a red shifted hydrogen bonded broad band appears in the spectrum. There is a decrease for the frequency and an increase for the anharmonicity due to intermolecular hydrogen bonding, which is in agreement with the earlier conclusions. In the case of imidazole in carbon tetrachloride, in the near IR overtone spectrum, blue-shifted hydrogen bonded NH oscillators are observed and are analysed using local mode model.

Chapter 7 is a summary of the entire work. All the conclusions are highlighted.

CHAPTER 1

PHOTOTHERMAL EFFECTS

1.1 Introduction

Photothermal effect refers to heating of a sample due to the absorption of electromagnetic radiation. After absorption, the excited sample comes to the lower state by dissipation of heat, which leads to the heating of the sample as well as the surrounding medium. These changes are referred to as photothermal effects [1,2]. It is an example of energy conversion. The photothermal effects are photo-induced changes in the thermal state of the sample. The absorption of photons by atoms or molecules will result in different types of processes in a material, as shown in Fig.1. The atoms or molecules in the excited level may lose their energy by radiative processes, such as spontaneous or stimulated emission, and by non-radiative processes which mainly result in heat generation [3-8]. If the photon energy is high enough, direct photochemical changes such as photo-decomposition, photo-ionisation, etc. of the molecule may take place. Destructive changes such as vapourisation of the material and plasma generation also may take place as a result of photon-matter interaction at very high power densities of the incident light. Only the nondestructive changes occurring in matter, subsequent to the photon absorption, will be discussed in the following sections.

Fig. 1 shows the main channels of photoinduced changes that occur in a sample. Here E_1 and E_2 represent the energies of the lower and upper levels and $E_2 - E_1 = h\nu$ is the energy of the absorbed photon. Let I and L be the incident light intensity and the sample length, respectively and β be the optical absorption coefficient. The absorbed power I_{abs} in the sample is given by

$$I_{\text{abs}} = I [1 - \exp(-\beta L)] \approx \beta I L \quad (1)$$

with $\beta L \ll 1$.

Now, the absorbed energy will be liberated through radiative, nonradiative or chemical processes and each of these processes has specific quantum yield [4,9,10]. If n_r , n_{nr} and n_{pc} are the quantum yields of radiative, nonradiative and photochemical

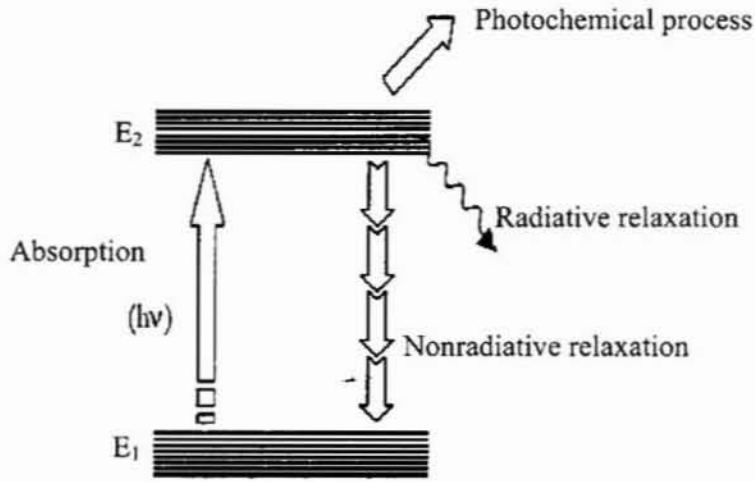


Fig. 1. Schematic representation of various photo-induced processes.

processes respectively, the total quantum yield of all the channels of de-excitation is given by

$$n_r + n_{nr} + n_{pc} = 1 \quad (2)$$

Here the intensity I_{abs} of the laser radiation absorbed will be distributed over all these channels so that

$$I_{abs} = I_r + I_{nr} + I_{pc} \quad (3)$$

where $I_r = n_r I_{abs}$, $I_{nr} = n_{nr} I_{abs}$ and $I_{pc} = n_{pc} I_{abs}$ are the amount of energy liberated through the radiative, nonradiative and photochemical processes, respectively. Measurement

of the energy absorbed or released through any of these relaxation channels facilitates the study of various properties and parameters of the sample.

Heat can be produced promptly or at various time delays (Fig. 2). The light

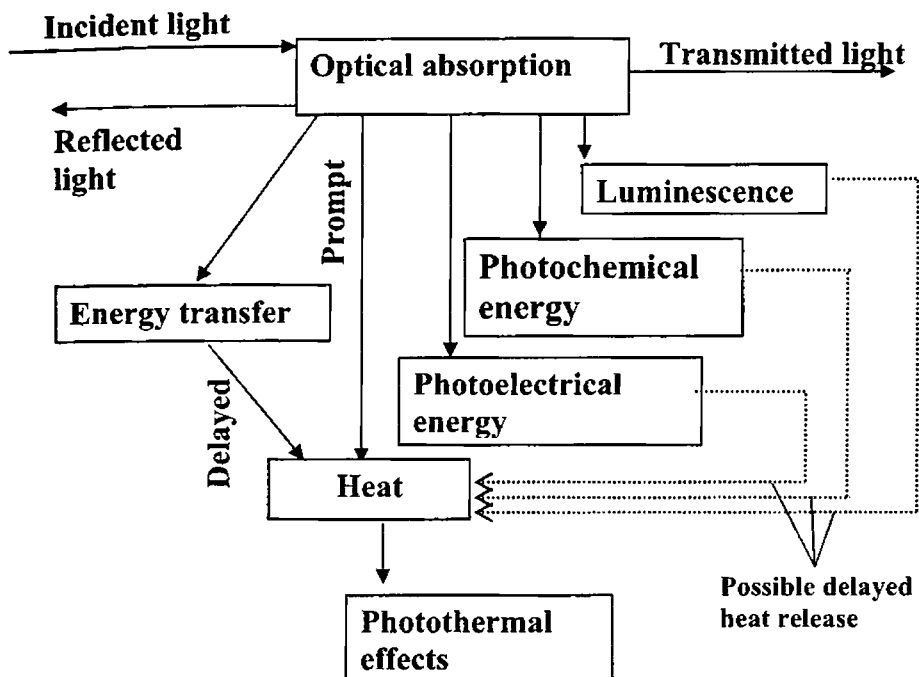


Fig. 2. Possible consequences of optical absorption leading to prompt and delayed heat production

energy absorbed and not lost by subsequent emission results in sample heating. This heating results in a temperature change as well as changes in thermodynamic parameters of the sample. Measurement of temperature, pressure, or density changes that occur due to optical absorption are ultimately the basis for the photothermal methods. The basic processes responsible for photothermal signal generation are shown in Fig. 3. Optical radiation, usually from a laser, is used to excite a sample. The sample absorbs some of this radiation resulting in an increase in the internal

energy. This followed by a non-radiative excited state relaxation results in the production of heat. The heating of the sample produces photothermal effects like temperature rise, photoacoustic waves, refractive index changes in the sample and in the adjacent fluid, IR thermal radiation changes, etc. at the same time.

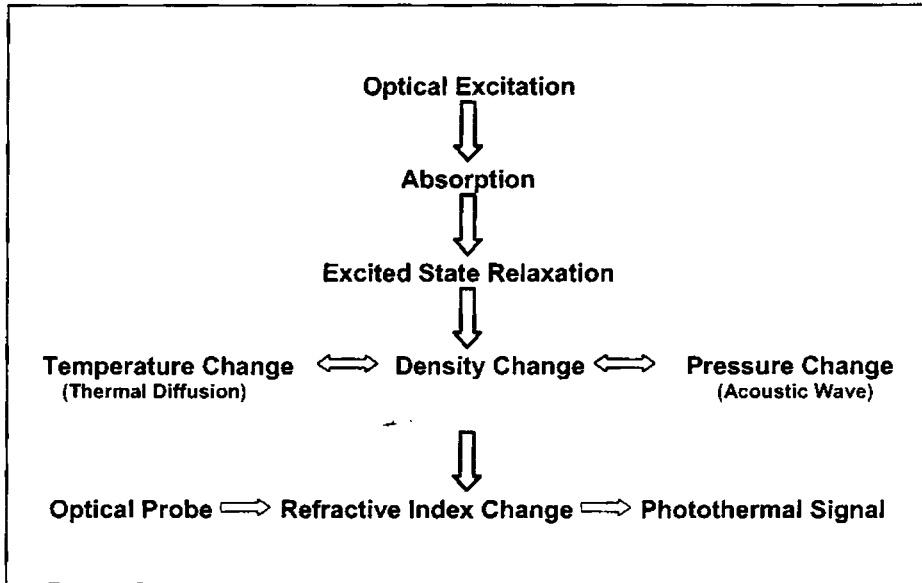


Fig. 3. Basic processes responsible for the photothermal signal generation

If we examine the history of photothermal discoveries, the oldest technical application of the photothermal effect is believed to be the communication device, the photophone, invented by Alexander Graham Bell in 1880 [11]. Bell found that audible sound could be heard coming from a tube filled with various materials when the light shining on the transparent tube was modulated. The scope of his observation was in a dormant state due to the non-availability of powerful light sources. The operational principles are now well understood. Modulation of the light impinging on an absorbing substance will produce a similar modulation in temperature due to photothermal effect. In a gas of restricted volume, temperature modulation produces a pressure modulation. The periodic pressure modulation is an acoustic signal. With the advent of lasers

many important discoveries in the field of photothermal methods were made. Historically, the birth of high sensitivity photoacoustic and photothermal methods can be traced back to that of the laser.

Photothermal spectroscopy is a of high sensitivity method used to measure optical absorption and thermal characteristics of a sample. We can consider photothermal spectroscopy as an indirect method used to measure optical absorption. In regular optical absorption spectroscopy, the intensity of the light passing out through the sample is compared to the intensity of light going into the sample. However, in photothermal spectroscopy, the transmission of light is not used in measuring, and instead, sample heating, which is a direct consequence of optical absorption is studied. Scattering and reflection losses do not produce photothermal signals. Subsequently photothermal spectroscopy more accurately measures optical absorption in scattering solutions, in solid and at interfaces. This aspect makes it particularly attractive for application to surface and solid absorption studies, and studies in scattering media. The precision of the photothermal measurements is inherently better than that of the direct transmission method [12]. The high sensitivity of the photothermal spectroscopy methods has led to application for analysis of low absorbance samples [13].

PT generation which is an example of energy conversion has in general three kinds of applications. 1. PT material probing which does not cause any sample modification. 2. PT material processing which causes the sample to change to another useful form. 3. PT material destruction which make the sample useless. The temperatures involved increases from 1→ 3. Of the above three, PT material probing is the most important in making significant contribution to the field of science and technology.

1.2 Detection Schemes

Photothermal material characterization relies on high sensitivity detection techniques to monitor the effects caused by PT material heating of a sample. Most of the photothermal effects occur simultaneously. The choice of a suitable

PT effect for detection depends on the nature of the sample and its environment, the light source used and the purpose of measurement. Common photothermal effects produced by modulated optical absorption in a sample is shown in Fig. 4. Direct effects are observed in the sample (S) and the effects observed in the transparent coupling fluid (F) adjacent to the sample are termed indirect effects. Table 1 shows the various photothermal effects and the corresponding detection schemes.

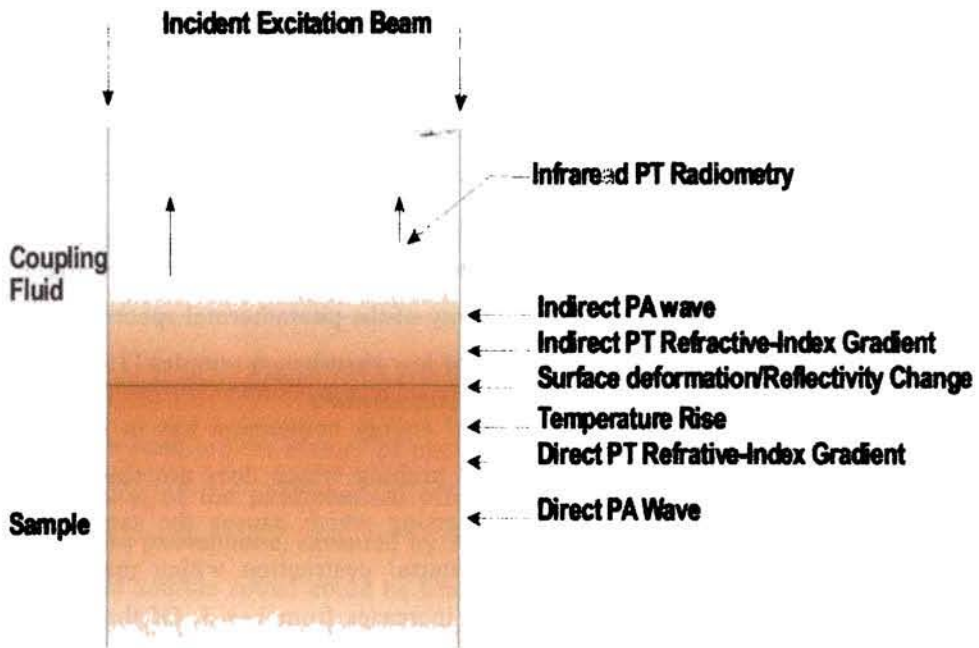


Fig. 4. Common photothermal effects produced by modulated optical absorption in a sample.

Table 1

Various photothermal effects and the corresponding detection schemes

Thermodynamic Parameter	Measured Property	Detection Technique
Temperature	Temperature	Calorimetry
	Infrared Emission	Photothermal Radiometry
Pressure	Acoustic Wave	Photoacoustic spectroscopy
Density	Refractive Index	Photothermal Lens Photothermal Interferometry Photothermal Deflection Photothermal Refraction Photothermal Diffraction
	Surface Deformation	surface Deflection

All PT detection schemes require a modulation in the excitation light. It can be a continuous modulated PT detection where the modulation is in the form of continuous train of pulses at nearly 50% duty cycle. This type of detection scheme is in the frequency domain where amplitude and phase of the PT signal are measured by lock-in detection. There is pulsed PT detection also, which is in the time domain. Here modulation is in the form of short intense pulses separated by long dark periods. Various PT effects and the detection schemes are described briefly below.

Temperature rise: Monitoring the temperature rise is called laser calorimetry or optical calorimetry or photothermal calorimetry [14,15]. For this thermocouples, thermistors or pyroelectric devices can be used. Here the advantage is that the observed temperature rise can be directly measured and can be related to absorption coefficient. But the sensitivity is low and moreover, thermal isolation is needed to avoid heat leakage from the sample. However, it was shown that fast rise time and high sensitivity for a thin film sample is possible if it is directly coated on to a thin film pyroelectric detector [16, 17].

Infrared emission change: Temperature changes can also be indirectly measured by monitoring the infrared emission, since the infrared emission is directly related to the sample temperature. This detection technique called photothermal radiometry [18], although not very sensitive, has great potential in nondestructive analysis and testing of materials. Infrared cameras can be used for the thermal imaging of large samples.

Pressure change: Pressure variation or modulation resulting from the absorption of modulated light by a sample is usually referred to as photoacoustic or optoacoustic generation [19-21]. PA generation mechanisms include electrostriction, thermoelastic expansion, volume changes due to photochemistry, gas evolution, boiling or ablation and dielectric breakdown. The pressure wave generated after light excitation contains contributions from the various sources above. For electrostriction and for thermoelastic expansion the PA generation efficiency η (acoustic energy generated/ light energy absorbed) is small compared to the breakdown mechanisms. PA generation via thermoelastic expansion is the common mechanism used in PA spectroscopy. As for the general case of PT generation, PA detection also can be direct or indirect. In direct method, the acoustic wave is detected in the sample itself while in the indirect method, the acoustic wave is detected via coupling fluid medium adjacent to the sample.

Refractive index gradients: PT heating of a sample can produce a refractive index gradient (RIG) in the sample (direct effect) or in an adjacent coupling fluid (indirect effect). Also, there are two types of RIG produced by the PT heating of the sample, namely, a thermal RIG and an acoustic RIG. The thermal RIG is produced by the decreased density of the medium (sample or coupling fluid) caused by the local temperature rise, decays in time following the diffusional decay of the temperature profile, and remains near the initial optically excited region. The acoustic RIG is associated with the density fluctuation of the medium caused by the propagation of the PA wave, decays in propagation distance following the attenuation of the PA wave, and travels at the acoustic velocity away from the initial optically excited region. Thermal RIG and acoustic RIG are related and can be used to measure similar parameters, like optical absorption coefficient, temperature, or flow velocity of the

sample. However, thermal diffusivity can only be measured by the time evolution of the thermal RIG and acoustic velocity and attenuation can only be measured by the spatial dependence of the acoustic RIG. Also, at distances farther than several thermal diffusion lengths from the excitation region, only acoustic RIG can be detected. In general, thermal RIG provides a larger signal compared to acoustic RIG.

The thermal refractive index gradient generated by the excitation beam affects the propagation of an optical beam in its vicinity, including its own propagation, resulting in the well known effect of *self-defocusing or thermal blooming* [22]. Self-defocusing generally occurs instead of self-focusing because the derivative of the refractive index with respect to temperature is usually negative, so that the temperature gradient results in a negative lens. Self-defocusing of the excitation beam provides a sensitive spectroscopic tool and Solimini [23] gave a quantitative theory for this application.

The thermal RIG can also affect the propagation of another weak 'probe' beam in the neighborhood of excitation beam. Thus, the thermal RIG can be monitored either by self defocusing or by probe beam refraction (PBR). The PBR method with an additional collinear probe beam provides higher sensitivity than the single beam self defocusing method [24-26]. This is known as *thermal lensing spectroscopy* using a probe beam. Here the thermally perturbed sample is acting as a lens (Fig. 5). This occurs when spatial dependent refractive index profiles are curved.

The PBR technique for probing the refractive index gradient need not employ collinear beams as in the thermal lens experiment. A probe beam that is parallel to but displaced from the excitation beam can also be used (Fig. 6a). It has been pointed out that the PBR method, using beams with appropriate displacements, can have higher sensitivity than thermal lens spectroscopy if the probe is positioned at the maximum refractive index gradient, which is situated at approximately one beam radius from the axis of the excitation beam [27, 28].

The probe beam need not be even parallel to the excitation beam. High spatial resolution measurements necessitate the use of 'crossed' beams (Fig. 6b). For opaque

samples, orthogonal PBR detection is generally needed because no transmission through the sample is possible (Fig. 6c). Spatial gradients in refractive index result in a direction change in the propagation of a ray of light. Thus light will exit a medium with a refractive index gradient at an angle relative to the incident ray. The study of the bending of light path is commonly called *photothermal deflection spectroscopy* [29-32]. Various configurations in Fig. 6 are all probe beam deflection schemes.

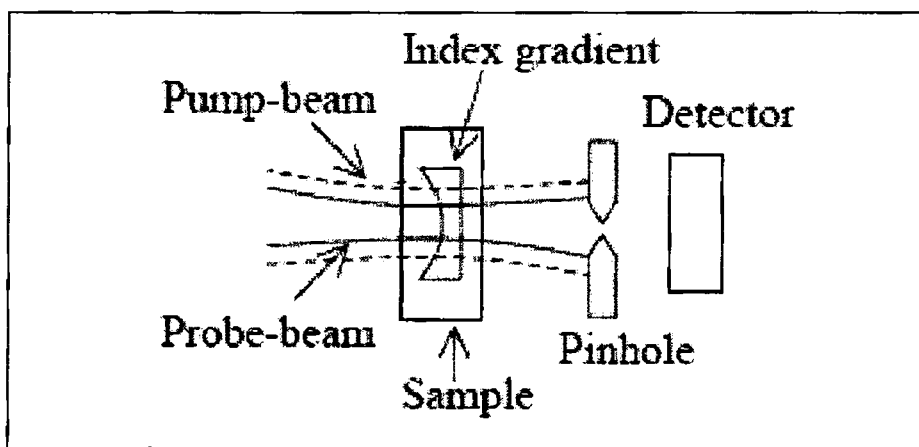


Fig. 5. Thermal lensing

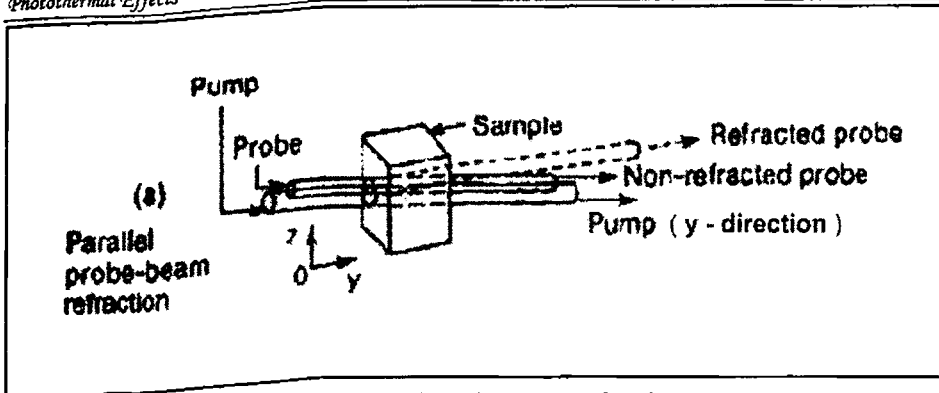


Fig. 6a. Parallel probe beam refraction

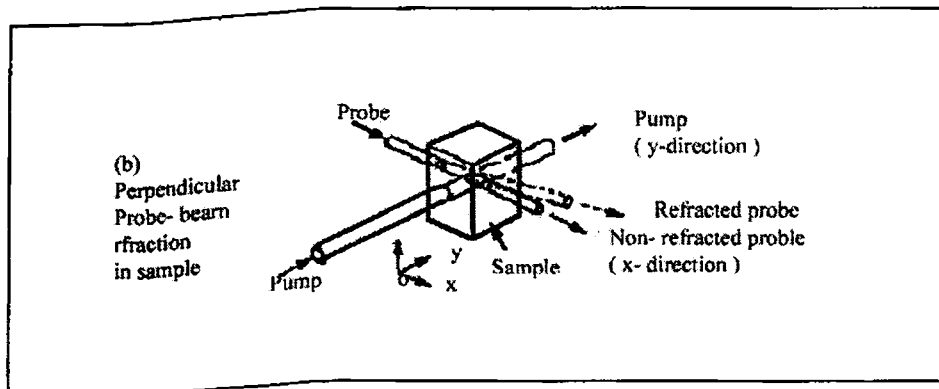


Fig. 6b. Perpendicular probe beam refraction in the sample

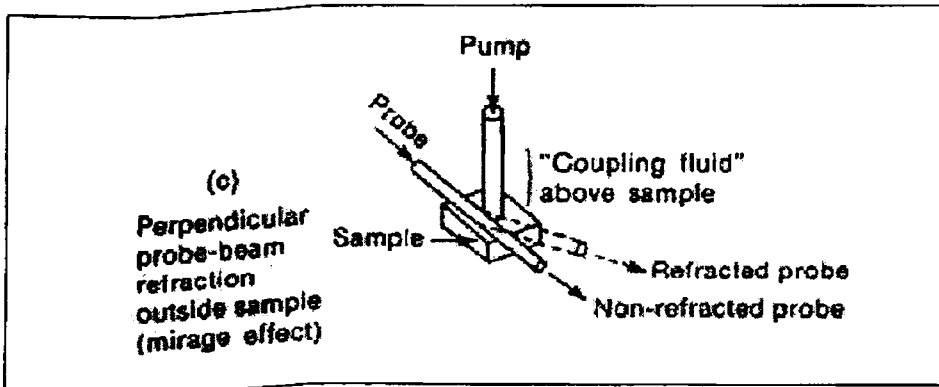


Fig. 6c. Perpendicular probe beam refraction outside the sample (Mirage effect)

Though there are several methods to detect the temperature dependent refractive index change, all these methods rely on a few basic principles of light propagation, namely, optical path length change, diffraction and refraction. The optical path length changes that occur due to the photothermal induced refractive index change can be measured with interferometry. Using interferometry, the phase of the monochromatic light passing through the heated sample, relative to the phase passing through the reference arm, results in a change in power at a photoelectric detector. There are several different interferometric schemes that can be used to detect changes in the optical path length induced by the photo thermal effect [33, 34]. These methods may all be classified as being *photothermal interferometry*.

A periodic spatial refractive index modulation results in a volume phase diffraction grating, when two pump beams cross each other inside or at the surface of the sample. This grating will refract light at an angle that meets requirements from Bragg's law. The amount of light diffracted is proportional to the refractive index change. The diffracted light is measured with a photoelectric detector. Methods used to measure spectroscopic signals based on volume phase diffraction gratings formed by the photothermal effects are called *Photothermal diffraction spectroscopy* [35, 36].

Surface deformation: The PT heating of a surface causes distortion due to thermal expansion. This distortion even though very small, can be detected. In solid samples, the density changes due to heating alter physical dimension at sample surfaces. Sample dimension changes give rise to two optical methods for monitoring the temperature change based on surface deformation. A homogeneous deformation displaces the surface of the sample. Interferometry can be used on reflective samples. Spatially heterogeneous expansion can also cause the surface angle to change. A probe beam reflected from the surface will change angle when heterogeneous expansion occurs. Measurement of the probe beam angle gives rise to the method of *photothermal surface displacement or deflection spectroscopy* [37].

Besides the more common PT effects described above that have been extensively used for PT spectroscopy and material testing application, many other PT

effects are possible, especially in special circumstances. In the case of semiconductors, besides producing a periodic thermal wave, the incident light also generates photoexcited carrier population. So besides a thermal gradient, a minority carrier population gradient also will be set up. By employing PT methods various transport properties, namely, the thermal and electronic diffusivities, the minority carrier lifetime, surface recombination rate, etc. can be studied [38]. Zapka and Tam have carried out a probe beam absorption measurement to detect the change in the Boltzmann molecular population distribution due to the PT heating of a gaseous sample [39]. Photothermal effect based techniques have a lot of applications in material and chemical analysis. Its application in biological and medical fields are well established. PT methods have been efficiently used for the measurement of acoustic velocities, thermal diffusion coefficients, sample temperature, bulk flow rates, phase transition, volume expansion coefficients, etc.

The important aspect of photothermal spectroscopy which makes it a unique approach in various applications is its flexibility to perform in different experimental configurations. On the other hand conventional optical absorption spectroscopy and luminescence studies require some specific experimental configuration and basic requirements, which limits, to some extent, their widespread use in material studies. Photothermal measurements are usually performed using laser light sources. High spectral purity and high power of the laser beam yields enhanced photothermal signals. The spatial coherence properties of the laser light also allow the light to be focused to small, diffraction limited volumes. The small volumes enhance the signal magnitude and allow the photothermal spectroscopy to be used in small volume sample analysis.

Two types of pumping mechanisms can be used for the excitation of the sample. They are the pulsed laser excitation and modulated continuous-wave (cw) laser excitation. Pulsed excitation produces transient signals of large amplitude immediately after the excitation and it decays as the sample approaches thermal equilibrium through heat diffusion. By performing the transient waveform analysis, one can obtain a variety of sample properties. Now, if the excitation is carried out

using a periodically modulated cw laser then the signal will also be periodic, the magnitude and phase of which are functions of modulation frequency. The frequency dependent phase-shift information is essentially equivalent to that contained in the time-dependent signal transients obtained from pulsed excitation.

In this thesis, major emphasis is on photothermal beam deflection (mirage) studies. As the photothermal techniques are based on the heating effects, the temperature distribution in the sample as well as in the surrounding media are to be discussed, which can be related to the signal amplitude and phase. This is discussed in the next two sections.

1.3 Rosencwaig-Gersho 1-D Theory

The Rosencwaig-Gersho (R-G) [40] theory is essentially a one-dimensional heat flow model [41], which is sufficient to describe photoacoustic (PA) signal generation. In PA technique the excitation beam is not focused so that heat diffusion takes place in one direction only. The formulation of R-G model is based on the light absorption and thermal wave propagation in an experimental configuration as shown in Fig. 7.

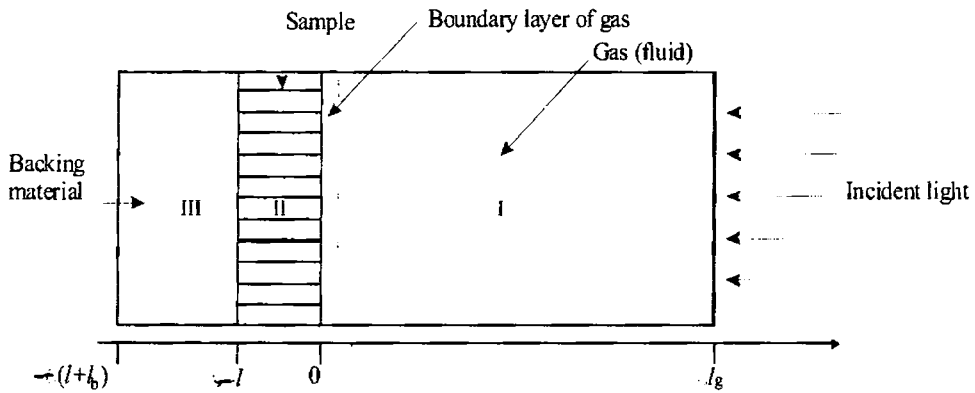


Fig. 7. Geometry of 1-D Rosencwaig-Gersho model

Consider a simple cylindrical cell of length L and diameter D as shown in Fig. 7.

Assume that the length L is small compared to the wavelength of the acoustic signal. The sample is considered to be in the form of a disk having diameter D and thickness l . The sample is mounted so that its front surface is exposed to the gas (air) within the cell and its back surface is a poor thermal conductor of thickness l_b . The length l_g of the gas column in the cell is then given by $l_g = L - l - l_b$. Further assumption is that the gas and backing materials are not light absorbing. Let k_i, ρ_i, C_i and α_i represent the thermal conductivity, density, specific heat and thermal diffusivity respectively of the material i . Then $a_i = (\omega/2\alpha_i)^{1/2}$ is the thermal diffusion coefficient and $\mu_i = 1/a_i$ is the thermal diffusion length of the material. i can take subscripts s, g and b for solid, gas and backing material respectively. ω denotes the chopping frequency of the incident light beam in radians per second. Assume that the sinusoidally chopped monochromatic light source with wavelength λ is incident on the solid with intensity $I = (1/2) I_0 (1 + \cos \omega t)$. The thermal diffusion equation in the three regions can be written as

$$\frac{\partial^2 \phi}{\partial t^2} = \frac{1}{\alpha_b} \frac{\partial \phi}{\partial t}, \quad -l - l_b \leq x \leq -l \quad \text{Region III} \quad (4)$$

$$\frac{\partial^2 \phi}{\partial t^2} = \frac{1}{\alpha_g} \frac{\partial \phi}{\partial t}, \quad 0 \leq x \leq -l_g \quad \text{Region I} \quad (5)$$

$$\frac{\partial^2 \phi}{\partial t^2} = \frac{1}{\alpha_s} \frac{\partial \phi}{\partial t} - A \exp(\beta x) [1 + \exp(j\omega t)], \quad -l \leq x \leq 0 \quad \text{Region II} \quad (6)$$

$$\text{with } A = \frac{\beta I_0 \eta}{2k_s}$$

where ϕ is the temperature, η is the light conversion efficiency and β is the absorption coefficient. The real part of the complex-valued solution $\phi(x, t)$ of the above equations is the solution of physical interest and represents the temperature in the cell relative to the ambient temperature as a function of position and time. Thus, the actual temperature field in the cell is given by

$$T(x,t) = \text{Re}[\varphi(x,t)] + \phi$$

where Re stands for 'the real part of' and ϕ is the ambient (room) temperature. The complex amplitude of the periodic temperature distribution, θ at the solid-gas boundary ($x = 0$) is given by

$$\theta = \frac{\beta I_0}{2k_s(\beta^2 - \sigma_s^2)} \left(\frac{(r-1)(b+1)\exp(\sigma_s l) - (r+1)(b-1)\exp(-\sigma_s l) + 2(b-r)\exp(-\beta l)}{(g+1)(b+1)\exp(\sigma_s l) - (g-1)(b-1)\exp(-\sigma_s l)} \right) \quad (7)$$

$$\text{where } b = \frac{k_b a_b}{k_s a_s}, g = \frac{k_g a_g}{k_s a_s}, r = (1-j)\frac{\beta}{2a_s} \text{ and } \sigma_s = (1+j)a_s$$

The main source of acoustic signal arises from the periodic heat flow from the solid to the surrounding gas. The periodic heating causes the boundary layer of gas to expand and contract periodically. This can be thought of as the action of an acoustic piston on the rest of the gas column, producing an acoustic pressure signal that travels through the entire gas column. The displacement of the gas piston due to the periodic heating can be estimated using the ideal gas law,

$$\delta x(t) = 2\pi\mu_g \frac{\bar{\phi}(t)}{T_0} = \frac{\theta\mu_g}{\sqrt{2} T_0} \exp\left[j\left(\omega t - \frac{\pi}{4}\right)\right] \quad (8)$$

where the average dc temperature of the gas boundary layer is set as dc temperature at the solid surface, $T_0 = \phi + \theta_0$, ϕ being the ambient temperature at the cell walls. Assuming that the rest of the gas responds to the action of the piston adiabatically, the acoustic pressure in the cell due to the displacement of the gas piston can be obtained from the adiabatic gas law $PV^\gamma = \text{constant}$, where P is the pressure, V is the gas volume in the cell, and γ is ratio of the specific heats. Thus the incremental pressure is

$$\delta P(t) = \frac{\gamma P_0}{V_0} \delta V = \frac{\gamma P_0}{l_g} \delta x(t) \quad (9)$$

where P_0 and V_0 are the ambient pressure and volume respectively and $-\delta V$ is the incremental volume. Then from equations (8) & (9)

$$\delta P(t) = Q \exp \left[j \left(\omega t - \frac{\pi}{4} \right) \right] \quad (10)$$

$$\text{where } Q = \frac{\gamma P_0 \theta}{\sqrt{2} I_g a_g T_0}$$

The actual physical pressure variation is given by the real part of $\delta P(t)$ and Q specifies the complex envelope of the sinusoidal pressure variation. Substituting for θ ,

$$Q = \frac{\beta I_0 \gamma P_0}{2\sqrt{2} k_s l_g (\beta^2 - \sigma_s^2)} \times \left[\frac{(r-1)(b+1)\exp(\sigma_s l) - (r+1)(b-1)\exp(-\sigma_s l) + 2(b-r)\exp(-\beta l)}{(g+1)(b+1)\exp(\sigma_s l) - (g-1)(b-1)\exp(-\sigma_s l)} \right] \quad (11)$$

Thus, equation (11) can be evaluated for obtaining the amplitude and phase of the acoustic pressure wave produced in the cell by photoacoustic effect. It can be observed that interpretation of the full expression for $\delta P(t)$ is difficult because of the complex expression of Q . Physical insight can be gained easily if certain special cases according to the optical opaqueness of solids are examined. For each category of optical opaqueness, three cases according to the relative magnitude of the thermal diffusion length μ_s , as compared to the physical length l and the optical absorption length μ_β .

$$\text{Defining } Y = \frac{\gamma P_0 I_0}{2 \sqrt{2} l_g T_0} \quad (12)$$

Case 1: Optically Transparent Solids ($\mu_\beta > 1$)

Ia : Thermally Thin Solids ($\mu_s \gg l; \mu_s \gg \mu_\beta$)

$$Q = \frac{(1-i)\beta l}{2a_g} \left(\frac{\mu_b}{k_b} \right) Y \quad (13)$$

Thus the acoustic signal is proportional to βl and varies as f^{-1} . In addition, the thermal properties of the backing material come into play in the expression for Q

Ib : Thermally Thin Solids ($\mu_s > l; \mu_s < \mu_\beta$)

Here we can set

$$\exp(-\beta l) \cong 1 - \beta l, e^{\pm \sigma l} \cong 1 \pm \sigma_s l \text{ and } |r| < 1 \text{ in equation (11)}$$

$$\text{Then } Q = \frac{(1-j)\beta l}{2a_g} \left(\frac{\mu_b}{k_b} \right) Y \quad (14)$$

This equation is identical with equation (13) and hence the acoustic signal behaves in the same fashion.

Ic : Thermally Thick Solids ($\mu_s > l; \mu_s \ll \mu_\beta$)

$$\text{In this case we set } \exp(-\beta l) \cong 1 - \beta l, e^{\pm \sigma l} \cong 0 \text{ and } |r| \ll 1 \text{ in equation(11)}$$

$$\text{Now } Q = -j \frac{\beta l}{2a_g} \left(\frac{\mu_s}{k_s} \right) Y \quad (15)$$

The acoustic signal is now proportional to $\beta\mu_s$ rather than βl . This means that light absorbed within the first thermal diffusion length contributes to the signal, although light is being absorbed throughout the length of the solid. Moreover, μ_s being less than the thickness l , thermal properties of the backing material will not influence the signal. Here the signal varies as $f^{-3/2}$.

Case II: Optically Opaque Solids

Ila: Thermally Thin Solids ($\mu_s \gg l; \mu_s \gg \mu_\beta$)

In equation (11), we set $\exp(-\beta l) \cong 0$, $-\beta l, e^{\pm\sigma l} \cong 1$ and $|r| \gg 1$

$$\text{Then we obtain } Q = \frac{(1-j)}{2a_g} \left(\frac{\mu_b}{k_b} \right) Y \quad (16)$$

Here the photoacoustic signal is independent of β . The signal depends on the thermal properties of the backing material and varies as $1/f$.

Ilb: Thermally Thick Solids ($\mu_s < l; \mu_s > \mu_\beta$)

we set $\exp(-\beta l) \cong 0, e^{-\sigma l} \cong 0$ and $|r| > 1$ in equation (11)

$$\text{We obtain } Q = \frac{(1-j)}{2a_g} \left(\frac{\mu_s}{k_s} \right) Y \quad (17)$$

Though equations (16) & (17) are similar, in the present case there is no contribution from the thermal properties of the backing material.

Ilc: Thermally Thick Solids ($\mu_s \ll l; \mu_s < \mu_\beta$)

We set

$\exp(-\beta l) \cong 0, e^{-\sigma l} \cong 0$ and $|r| < 1$ in equation (11). Then we obtain

$$Q = \frac{-j\beta\mu_s}{2a_g} \left(\frac{\mu_s}{k_s} \right) Y \quad (18)$$

The photoacoustic signal will be proportional to $\beta\mu_s$. The signal is independent of the thermal properties of the backing material and varies as $f^{-3/2}$. The theoretical analysis of the photoacoustic effect applied to different cases discussed above can be suitably applied to the study of any kind of sample.

1.4 Photothermal Probe Beam Deflection (PBD) Or Mirage Effect ; 3-D Theory

In the case of photothermal beam deflection technique [1, 30-32, 42-44], the pump beam or the excitation beam is focused. Hence, instead of the above 1-D calculation of periodic distribution of temperature, we have to resort to 3D calculations. The heat diffusion equation in cylindrical geometry [41] is given by

$$\frac{\partial T}{\partial t} = D \left(\frac{\partial^2 T}{\partial r^2} + \frac{1}{r} \frac{\partial T}{\partial r} + \frac{1}{r^2} \frac{\partial^2 T}{\partial \theta^2} + \frac{\partial^2 T}{\partial z^2} \right) \quad (19)$$

When heat flow takes place in planes through Z-axis, the heat diffusion equation becomes

$$\frac{\partial T}{\partial t} = D \left(\frac{\partial^2 T}{\partial r^2} + \frac{1}{r} \frac{\partial T}{\partial r} + \frac{\partial^2 T}{\partial z^2} \right) \quad (20)$$

The assumption that the homogeneous sample is the absorbing medium and the fluid and the backing are transparent still holds good. The heat diffusion equation in three regions can be written as

$$\frac{\partial^2 T_g}{\partial r^2} + \frac{1}{r} \frac{\partial T_g}{\partial r} + \frac{\partial^2 T_g}{\partial z^2} = \frac{1}{D_g} \frac{\partial T_g}{\partial t} \quad 0 \leq z \leq l_g \quad (21)$$

$$\frac{\partial^2 T_s}{\partial r^2} + \frac{1}{r} \frac{\partial T_s}{\partial r} + \frac{\partial^2 T_s}{\partial z^2} = \frac{1}{D_b} + \frac{\partial T_s}{\partial t} - A(r, t) \exp(\alpha z)(1 + \exp(j\omega t)) \quad (22)$$

with $-l \leq z \leq 0$.

$$\frac{\partial^2 T_b}{\partial r^2} + \frac{1}{r} \frac{\partial T_b}{\partial r} + \frac{\partial^2 T_b}{\partial z^2} = \frac{1}{D_b} \frac{\partial T_b}{\partial t} \quad -(l - l_b) \leq z \leq -l \quad (23)$$

$A(r, t) = \frac{\eta P \alpha}{k_s \pi a^2} e^{\left(\frac{-2r^2}{a^2}\right)} (1 + \cos(\omega t))$ is the heat deposited per unit volume where

P is the exciting beam power, α is the optical absorption coefficient, η is the light conversion efficiency, 'a' is the beam radius defined at $1/e^2$ intensity. The boundary conditions are

$$k_s \frac{\partial T_s}{\partial z}(z=0) = k_g \frac{\partial T_g}{\partial z}(z=0) \quad (24)$$

$$k_s \frac{\partial T_s}{\partial z}(z=-l) = k_b \frac{\partial T_b}{\partial z}(z=-l) \quad (25)$$

$$\left. \begin{aligned} T_s(z=-l, t) &= T_b(z=-l, t) \\ T_s(z=0, t) &= T_g(z=0, t) \\ T_g(z=\infty, t) &= T_b(-\infty, t) = 0 \quad \text{with } l_g \sim \infty, l_b \sim \infty \end{aligned} \right\} \quad (26)$$

Here it is assumed that l_g and l_b are very large compared to the heated area and the backward heat propagation in these two regions is neglected.

In order to obtain the periodic steady state temperature, the above differential equations are reduced to simpler partial differential equation by Hankel transformation and Laplace transformation is used to obtain ordinary differential

equation from the partial differential equation. Furthermore, the modulated source is replaced by the unit source $A(r)\delta(t)$.

$$-\lambda^2 T_0(\lambda, z, p) + \frac{\partial^2 T_0(\lambda, z, p)}{\partial z^2} = \frac{p}{D_g} T_0(\lambda, z, p) \quad (27)$$

$$-\lambda^2 T_0(\lambda, z, p) + \frac{\partial^2 T_0(\lambda, z, p)}{\partial z^2} = \frac{p}{D_s} T_0(\lambda, z, p) - A_0(\lambda) \exp(\alpha z) \quad (28)$$

$$-\lambda^2 T_0(\lambda, z, p) + \frac{\partial^2 T_0(\lambda, z, p)}{\partial z^2} = \frac{p}{D_b} T_0(\lambda, z, p) \quad (29)$$

where

$$\begin{aligned} A_0(\lambda) &= \int_0^\infty A(r) J_0(\lambda r) r dr = \frac{\alpha P \eta}{k_s \pi a^2} \int_0^\infty e^{-\frac{2r^2}{a^2}} J_0(\lambda r) r dr \\ &= \frac{\alpha P \eta}{4 k_s \pi} e^{-\frac{\lambda^2 a^2}{8}} \end{aligned}$$

Assuming solution of the form to eq. (27)

$$T_0(\lambda, z, p) = e^{\sqrt{\lambda^2 + \frac{p}{D}} z}$$

The general solution is

$$T_0(\lambda, z, p) = T_s(\lambda, p) e^{-\sqrt{\lambda^2 + \frac{p}{D}} z} + B(\lambda, p) e^{\sqrt{\lambda^2 + \frac{p}{D}} z}$$

$B(\lambda, p) = 0$ since the fluid is supposed to be very thick. Equations (28) and (29)

can be solved similarly. Thus solution to equations (27), (28) and (29) are

$$T_0(\lambda, z, p) = T_s(\lambda, p) e^{-\sqrt{\lambda^2 + \frac{p}{D}}z} \quad (30)$$

$$T_0(\lambda, z, p) = U(\lambda, p) e^{\sqrt{\lambda^2 + \frac{p}{D}}z} + V(\lambda, p) e^{-\sqrt{\lambda^2 + \frac{p}{D}}z} - \frac{A_0(\lambda) e^{\alpha z}}{\alpha^2 - \left(\lambda^2 + \frac{p}{D}\right)} \quad (31)$$

$$T_0(\lambda, z, p) = W(\lambda, p) e^{\sqrt{\lambda^2 + \frac{p}{D}}z} \quad (32)$$

After applying the Hankel inversion to the above three equations the steady periodic state solution obtained is of the form

$$T(r, z, t) = T_0(r, z, p)|_{p=j\omega} \exp(j\omega t) \quad (33)$$

Thus the expressions for the modulated temperature field in the three regions are

$$T_g(r, z, t) = \int_0^\infty T_s(\lambda) \exp(-\beta_g z) \exp(j\omega t) J_0(\lambda r) \lambda d\lambda \quad (34)$$

$$T_b(r, z, t) = \int_0^\infty W(\lambda) \exp(-\beta_b(z+l)) \exp(j\omega t) J_0(\lambda r) \lambda d\lambda \quad (35)$$

$$T_s(r, z, t) = \int_0^\infty \left[U(\lambda) \exp(\beta_s z) + V(\lambda) \exp(-\beta_s z) - E(\lambda) \exp(\alpha z) \right] \times \exp(j\omega t) J_0(\lambda r) \lambda d\lambda \quad (36)$$

where

$$E(\lambda) = \frac{p\eta}{\pi k_s} \frac{\exp\left(\frac{-\lambda^2 a^2}{8}\right)}{\left(-\lambda^2 - j\frac{\omega}{D_s} + \alpha^2\right)} \quad (37)$$

The final temperature distribution is obtained by substituting the following expressions in the above equations.

$$T_s(\lambda) = -E(\lambda) + U(\lambda) + V(\lambda) \quad (38)$$

$$W(\lambda) = -E(\lambda)\exp(-\alpha l) + U(\lambda)\exp(-\beta_s l) + V(\lambda)\exp(\beta_s l) \quad (39)$$

$$U(\lambda) = \left[(1-g)(b-r)\exp(-\alpha l) + (g+r)(1+b)\exp(\beta_s l) \right] \frac{E(\lambda)}{H(\lambda)} \quad (40)$$

$$V(\lambda) = \left[(1+g)(b-r)\exp(-\alpha l) + (g+r)(1-b)\exp(-\beta_s l) \right] \frac{E(\lambda)}{H(\lambda)} \quad (41)$$

and

$$H(\lambda) = (1+g)(1+b)\exp(\beta_s l) - (1-g)(1-b)\exp(-\beta_s l) \quad (42)$$

$$\text{with } g = \frac{k_g \beta_g}{k_s \beta_s}, \quad b = \frac{k_b \beta_b}{k_s \beta_s} \quad \text{and} \quad r = \frac{\alpha}{\beta_s}$$

$$\overline{T_s(\lambda)} = \frac{p\eta}{4k_s\pi\beta_s} \frac{r}{r^2-1} \frac{e^{-\lambda^2 a^2/8} \left[\frac{2(b-r)e^{-a l} + (1+b)(r-1)e^{\beta_s l} + (1-b)(r+1)e^{-\beta_s l}}{(1+g)(1+b)e^{\beta_s l} - (1-g)(1-b)e^{-\beta_s l}} \right]}{\quad} \quad (43)$$

The surface temperature can be written as

$$T_s(0, t) = \int_0^\infty \overline{T_s(\lambda)} J_0(\lambda r) \lambda d\lambda \exp(j\omega t) \quad (44)$$

The geometry for the mirage deflection is as shown in Fig. 8. The propagation of the beam through the spatially varying index of refraction is given by

$$\frac{d}{ds} \left(n \frac{dr_0}{ds} \right) = \nabla_{\perp} n(r, t) \quad (45)$$

where r_0 is the perpendicular displacement of the beam from its original direction, n is the uniform index of refraction and $\nabla_{\perp} n(r, t)$ is the gradient of the index of refraction perpendicular to S (the ray path). This relation can be integrated over the ray path S

$$\frac{dr_0}{ds} = \frac{1}{n} \int_{\text{path}} \nabla_{\perp} n(r, t) ds \quad (46)$$

Since the deviation is small, one can get the expression of the deflection $\theta(t)$

$$\theta = \frac{dr_0}{ds} = \frac{1}{n} \frac{\partial n}{\partial T} \int \nabla_{\perp} T(r, t) ds \quad (47)$$

$$= \frac{1}{n} \frac{\partial n}{\partial T} \int_{-\infty}^{+\infty} \nabla T_g \times ds$$

In our case, the probe beam is propagating through the fluid along the x-direction. Hence, the probe deflects with components in x-y plane and z-x plane so that after calculating the vector product in the integrand of the above expression, we get the transverse θ_t and the normal θ_n components of the deflection, respectively.

$$\theta_n = \frac{1}{n} \frac{dn}{dT} \int_{-\infty}^{+\infty} \frac{\partial T_g}{\partial z} dx \hat{j} \quad (48)$$

$$\theta_t = \frac{1}{n} \frac{dn}{dT} \int_{-\infty}^{+\infty} \sin \alpha \frac{\partial T_g}{\partial r} dx \hat{k} \quad (49)$$

θ_n and θ_t are the deflections normal and parallel to the sample surface.

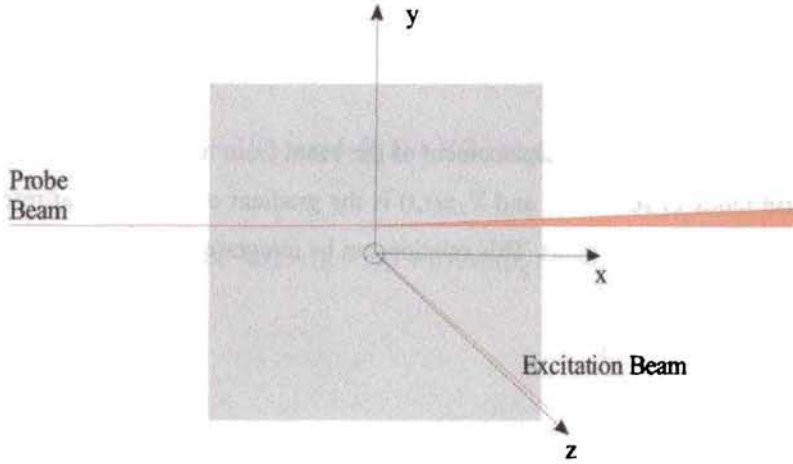


Fig. 8. Geometry for 'mirage' deflection. The probe is along x direction and the pump beam is along z direction

Using the standard result

$$\int_{-\infty}^{+\infty} T_s(x) dx = 2 \int_0^{\infty} \overline{T_s}(\lambda) \cos(\lambda y) d\lambda \quad (50)$$

and substituting for the integral in equation (37) we get

$$\theta_n = \frac{2}{n} \frac{dn}{dT} \exp(j\omega t) \int_0^{\infty} \overline{T_s}(\lambda) \beta_g \exp(-\beta_g z) \cos(\lambda y) d\lambda \hat{k} \quad (51)$$

Similar treatment of the integral in equation (38) results in

$$\theta_t = \frac{2}{n} \frac{dn}{dT} e^{j\omega t} \int_0^{\infty} \overline{T_s}(\lambda) \lambda \exp(-\beta_g z) \sin(\lambda y) d\lambda \hat{k} \quad (52)$$

Substituting the value of $T_s(\lambda)$ from equation (33) in the above equation the general expression for θ_t and θ_n can be obtained. θ_n is related to the heat diffusion process perpendicular to the surface whereas θ_t represents the heat diffusion process parallel to the sample surface. Depending upon the optical absorption coefficient, sample can be divided into optically opaque and optically transparent. According to the thermal properties, each are subdivided into thermally thick and thermally thin. Equation (33) will be modified accordingly for each of these special cases [45]. The basic assumption is that the thermal diffusivity of the sample is greater than that of fluid as well as backing i.e. $b = g \sim 0$

Case I: Optically Opaque ($\alpha l \gg 1$)

In these materials, the optical absorption length is much smaller than the sample thickness.

$$\frac{r}{1+r} = \frac{\alpha}{\beta_s + \alpha} \approx 1$$

$$\frac{r}{1-r} = \frac{\alpha}{\beta_s - \alpha} \approx -1$$

Then the expression for the tangential component of deflection

$$\theta_t = -\frac{1}{n} \frac{dn}{dt} \frac{p}{2k_s \pi} e^{j\omega t} \int_0^\infty \lambda \sin(\lambda y) e^{-\beta_g z} e^{\lambda^2 a^2 / 4} \frac{1}{\beta_s} \left[\frac{1 + e^{-2\beta_s l}}{1 - e^{-2\beta_s l}} \right] d\lambda \hat{k} \quad (53)$$

and that of normal component is given by

$$\theta_n = \frac{1}{n} \frac{dn}{dT} \frac{p}{2k_s \pi} e^{j\omega t} \int_0^\infty \beta_s \cos(\lambda y) \exp\left(\frac{-\lambda^2 a^2}{4}\right) \frac{1}{\beta} \left(\frac{1 + \exp(-2\beta_s l)}{1 - \exp(-2\beta_s l)} \right) \exp(-\beta_g z) d\lambda \hat{j} \quad (54)$$

For thermally thick solids, $l > \mu$, Hence $\exp(-\beta_s l) \sim 0$ and the integrands are further reduced. For thermally thin solids, $l < \mu$ and the equations are suitably modified.

Case II: Optically Transparent solids ($\alpha l \ll 1$)

$$\frac{r}{1+r} \approx \frac{r}{1-r} \approx \frac{\alpha}{\beta_s}$$

Now the tangential component and normal components are given by

$$\theta_t = \frac{1}{n} \frac{dn}{dT} \frac{p}{2k_s \pi} \exp(j\omega t) \int_0^{\infty} \lambda \sin(\lambda y) e^{-\frac{\lambda^2 a^2}{4}} \frac{\alpha}{\beta_s^2} e^{-\beta_g z} d\lambda \hat{k} \quad (55)$$

$$\theta_n = \frac{1}{n} \frac{dn}{dT} \frac{p}{2k_s \pi} \exp(j\omega t) \int_0^{\infty} \beta_g \cos(\lambda y) \exp\left(-\frac{\lambda^2 a^2}{4}\right) \frac{\alpha}{\beta_s^2} \exp(-\beta_g z) d\lambda \hat{j} \quad (56)$$

Both the above mentioned cases are again classified into two according to the thermal properties. For thermally thick solids, $l > \mu$. Hence $\exp(-\beta_g l) \sim 0$ and the integrands are further reduced. For thermally thin solids, $l < \mu$ and the equations are suitably modified.

The two techniques detailed in this chapter can be suitably applied to various materials for the optical as well as thermal characterization non-destructively. PTD signal analysis for thermal characterization of certain plasma polymerized thin films is done in chapter 3 using the 'Mirage' technique.

REFERENCES

- [1] J.A. Sell, *Photothermal Investigations of Solids and Liquids*, Academic Press, Inc., New York, 1988.
- [2] S.E. Bialkowski, *Photothermal Spectroscopy Methods for Chemical Analysis*, John Wiley & Sons, Inc., New York, 1996.
- [3] D.S. Kliger, *Ultrasensitive Laser Spectroscopy*, Academic Press, New York, 1983.
- [4] K.K.R. Mukherjee, *Fundamentals of Photochemistry*, New Age International publishers, New Delhi, 1978.
- [5] J.D. Winefordner, *Chemical Analysis: A Series of Monographs on Analytical Chemistry and its Applications*, John Wiley & Sons, Inc., 1996.
- [6] G.M. Hieftje, J.C. Travis, F.E Lytle, *Lasers in Chemical Analysis*, Humana:Clifton, New Jersey, 1981.
- [7] C.V. Bindhu., *Studies on Laser Induced Photothermal Phenomena in Selected Organic Compounds and Fullerenes*, Ph.D Thesis, Cochin University of Science and Technology, 1998.
- [8] N.A. George, *Photoacoustic and Phtothermal Deflection Studies on Certain Selected Photonic Materials*, Ph.D. thesis, Cochin University of Science and Technology, 2001.
- [9] V.P. Zharov, V.S. Letokhov, *Laser Optoacoustic Spectroscopy*, Springer-Verlag, Berlin, 1986.
- [10] R.P. Bauman, *Absorption Spectroscopy*, John Wiley & Sons, New York, 1962.
- [11] A.G. Bell, *Am. J. Sci.* 20 (1880) 305.
- [12] S.E. Bialkowski, X. Gu, P.E. Poston, L.S Powers, *Appl. Spectrosc.* 46 (1992) 1335.
- [13] N.J. Douchi, *Critical Reviews in Analytical Chemistry* 17 (1987) 357.
- [14] G.H. Brilmyer, A. Fujishima, K.S.V. Santhanam, A.J Bard, *Anal. Chem.* 49 (1977) 2057.
- [15] M. Bass, L. Lion, *J. Appl. Phys.* 56 (1984) 184.
- [16] H. Coufal, P. Hefferle, *Appl. Phys. A* 38 (1985) 213.

-
- [17] H. Coufal, P. Hefferle, *Can. J. Phys.* 64 (1986) 1200.
- [18] P.E. Nordal, S.O. Kanstad, *Phy. Scr.* 20 (1979) 659.
- [19] A. Rosenzwaig, *Photoacoustics and Photoacoustic Spectroscopy*, John Wiley & Sons, New York, 1980.
- [20] A. Rosenzwaig, J.B. Willis, *J. Appl. Phys.* 51 (1980) 4361.
- [21] D.A. Hutchins, A.C. Tam, *IEEE Transactions on Ultrasonics, Ferroelectrics and Frequency Control*, Vol. UFFC – 33 (5) (1986) 429.
- [22] R.C. Leite, R.S. Moore, J.R. Whinnery, *Appl. Phys. Lett.* 5 (1964) 141.
- [23] D. Solimini, *Appl. Opt.* 5 (1966) 1931.
- [24] R.L. Swofford, M.E. Long, A.C. Albrecht, *J. Chem. Phys.* 65 (1976) 179.
- [25] D.S. Kliger, *Acc. Chem. Res.* 13 (1980) 129.
- [26] S.E. Bialkowski, *Appl. Opt.* 24 (1985) 2792.
- [27] A.C. Boccara, D. Fournier, W. Jackson, N.M. Amer, *Opt. Lett.* 5 (1980) 377.
- [28] W.B. Jackson, N.M. Amer, A.C. Boccara, D. Fournier, *Appl. Opt.* 20 (1981) 1333.
- [29] A.C. Boccara, D. Fournier, J. Badoz, *Appl. Phys. Lett.* 36 (1979) 130.
- [30] J.C. Murphy, L.C. Aamodt, *J. Appl. Phys.* 51 (1980) 4580.
- [31] L.C. Aamodt, J.C. Murphy, *J. Appl. Phys.* 52 (1981) 4903.
- [32] J.C. Murphy; L.C. Aamodt, *Appl. Phys. Lett.* 39 (1981) 519.
- [33] J. Stone, *J. Opt. Soc. Amer.* 62 (1972) 327.
- [34] F. Lepoutre, J.P. Roger, D. Fournier, A.C. Boccara, *J. Appl. Phys.* 54 (1983) 4586.
- [35] J.F. Power, M.S. Schweitzer, *Opt. Eng.* 36 (1997) 521.
- [36] S.E. Bialkowski, A. Chartier, *Appl. Opt.* 36 (1997) 6711.
- [37] M.A. Olmstead, N.M. Amer, *Phy. Rev. Lett.* 52 (1984) 1148.
- [38] R.A. Smith, *Semiconductors*, Cambridge University Press, 1978.
- [39] W. Zapka, A.C. Tam, *Opt. Lett.* 7 (1982) 86.
- [40] A. Rosenzwaig, A. Gersho, *J. Appl. Phys.* 47 (1976) 64.

-
- [41] H.S. Carslaw, J.C. Jaeger, *Conduction of Heat in Solids*, Oxford, Clarendon, 1959.
- [42] A. Figari, *J. Appl. Phys.* 71 (1992) 3138.
- [43] F. Lepoutre, B.K. Bein, L.J. Inglehart, *Can. J. Phys.* 64 (1986) 1037.
- [44] A. Hadj-Sahraoui, G. Louis, B. Mangeout, P. Peretti, J. Billard, *Phy. Rev. A* 44 (1991) 5080.
- [45] A. Salazar, A. Sanchez-Lavega, J. Fernandes, *J. Appl. Phys.* 65 (1989) 4150.

CHAPTER 2

PREPARATION OF R.F. PLASMA POLYMERIZED THIN FILMS AND FTIR ANALYSIS

2.1 Introduction

The concept of plasma dates back to Irving Langmuir, who in 1928 introduced the term plasma in his studies of electrified gases in vacuum tubes. Plasmas are quasi-neutral particle systems in the form of gaseous or fluid-like mixtures of free electrons and ions, frequently also containing neutral particles (atoms, molecules), with a large mean kinetic energy of the components. In addition, there are a large amount of excited molecular conditions, which by emitting electromagnetic radiation turns back to the ground state and this gives the characteristic luminance of the plasma. Plasma occurs in the sun, in lightnings and flames. Plasmas are frequently subdivided into low and high-temperature plasmas. Arc Plasma at normal pressure and low-pressure glow discharge are low-temperature plasmas, while fusion plasmas are high-temperature plasmas [1-6]. Plasmas are used in fluorescent tubes and in recent times, in the surface technique.

Plasma polymerization is a new material preparation process. It refers to formation of polymeric materials under the influence of plasma, which is generated by some kind of electric discharge. Here gaseous monomers, stimulated through a plasma, condense on freely selectable substrates, as high cross-linked layers. Plasma polymerization covers a wide interdisciplinary area of physics, chemistry, interfaces, materials and so on [1]. Because the most practical means of carrying out plasma polymerization involves the use of an electric glow discharge in a vacuum, the term *glow discharge polymerization* has been used synonymously with plasma polymerization. The well-recognized concept of polymerization today is based on the molecular processes by which the size of the molecules increases. In contrast to such

molecular processes, polymer formation in plasma has been recognized as an atomic (non molecular) process [7]. If one wants to coat a certain substrate with a conventional polymer, several steps are required. In coating by plasma polymerization, in contrast, all these functional steps are replaced by an essentially one-step process to produce a good polymer coating. Initially polymers formed under the plasma condition were recognized as an insoluble deposit that provided only difficulty in cleaning and nothing else. The two most important characteristics of this undesirable deposit, which are the most sought later, in modern technology of coatings are excellent adhesion to substrate materials and strong resistance to most chemicals. Plasma polymerization is an inexpensive tool for fabricating organic thin films. This technique results in homogeneous, highly cross-linked and thermally stable polymer thin films. Fig. 1 gives a comparison of the structures of plasma polymers and conventional polymers.

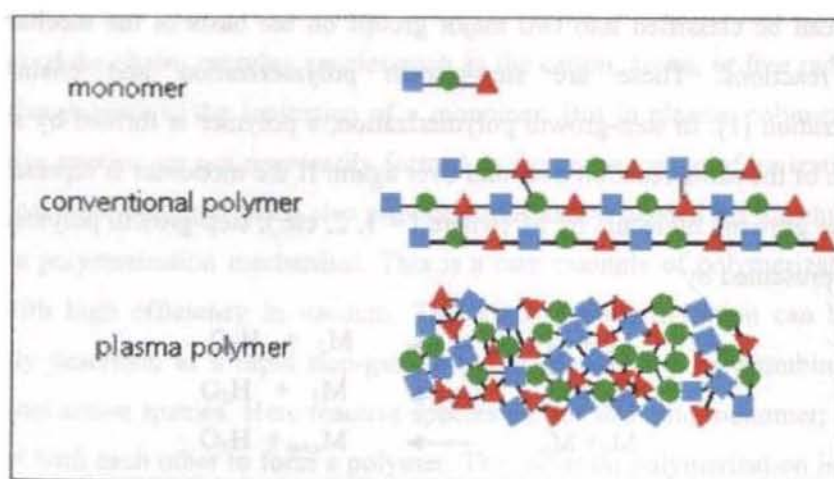
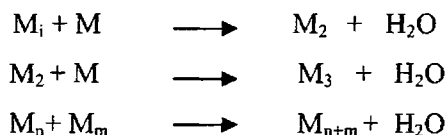


Fig. 1. Comparison between the plasma polymer and the conventional polymer of the same monomer

The dielectric properties of the plasma polymerized thin films have potential applications in microelectronics. These films are used in the production of microcapacitors and in the deposition of passivation layers onto semiconductor devices [1]. A good passivation layer must fulfil two requirements; it has to shield the device from outside influence but at the same time should not interrupt its operations [8]. Plasma polymerized thin films are finding use in fabricating storage batteries, LEDs, sensors, super capacitors, etc. Films with low dielectric permittivity are potential candidates as intermetallic dielectrics in microelectronics [9]. Now a days multilayer optical interference films have been developed [10, 11] out of plasma polymerization techniques.

2.2 Mechanism of Plasma Polymerization

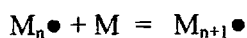
The mechanism by which plasma polymerization occurs is complex. Before discussing in detail the mechanisms of formation of polymeric materials in plasma, it is necessary to review some fundamental aspects of polymerization. Polymerization reaction can be classified into two major groups on the basis of the mechanism of growth reactions. These are step-growth polymerization and chain-growth polymerization [1]. In step-growth polymerization, a polymer is formed by stepwise repetition of the same reaction over and over again. If the monomer is represented by M and the growing molecule by M_i (where $i = 1, 2, \text{etc.}$), step-growth polymerization can be represented by



Here all the reactions at each step is identical to the first reaction.

In chain growth polymerization, a long-chain molecule is formed by a series of consecutive steps that is completed in a very short time. In this case, the products are only final polymers. Unlike the case of step-growth polymerization, intermediate-size molecules cannot be isolated. Consequently, the entire polymer formation can be

considered an essentially one-step process, as long as the concept of chemical reactions that relies on the identification of the reactants and the products is concerned. When the chain-carrying species is indicated by $M\bullet$ and the monomer by M , the chain-growth mechanism can be shown by



and

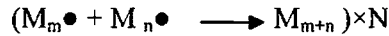


The first three reactions represent the propagation reaction and the last reaction in which the chain-carrying species is lost is the termination reaction.

In the elucidation of mechanisms of plasma polymerization a brief review of *radiation polymerization* and *parylene polymerization* is extremely helpful since they are closest to plasma polymerization. Polymerization initiated by ionizing radiation such as γ rays from ^{60}Co or high energy beams is radiation polymerization. Here the formation of the chain-carrying species such as the cation, anion, or free radical is a consecutive process to the ionization of a monomer. But in plasma polymerization, the reactive species are not necessarily formed as the consequence of ionization. The study of parylene polymerization also provides information needed for the elucidation of plasma polymerization mechanism. This is a rare example of polymerization that occurs with high efficiency in vacuum. This kind of polymerization can be more adequately described as a rapid step-growth polymerization by polycombination of difunctional active species. Here reactive species do not add onto monomer; instead, they react with each other to form a polymer. The radiation polymerization is similar to plasma polymerization since the primary step in both is ionization of monomers. However, radiation polymerization does not yield polymers in vacuum. The similarity between plasma polymerization and parylene polymerization is in the formation of polymer deposits in vacuum and differ in that parylene polymerization does not involve the ionization process. In short, plasma polymerization can be viewed as a

hybrid of these two polymerization mechanisms.

The overall plasma polymerization mechanism proposed by Yasuda is based on the rapid Step-growth mechanism [1]. The deposition of a plasma polymer can be envisaged as occurring by rapid step-growth polymerization (RSGP)



where N represents the number of repetitions of similar reactions. In 1973 Yasuda and Lamaze pointed out that an elementary reaction product was not immune to reactivation in plasma polymerization [12]. Therefore the combination of two monofunctional reactive species, such as a radical or cation ($M_m\bullet + M_n\bullet \longrightarrow M_{m+n}$) is not necessarily a termination step as it is in conventional polymerization. Instead, plasma polymerization, proceeds via the stepwise fragmentation and recombination of molecules and/or oligomers to form macromolecules [1,13]. In Fig. 2, M_x refers to a neutral species that can be the original monomer molecule or any of the dissociation products, where $x = i, j, k$, etc. indicates a size difference between species.

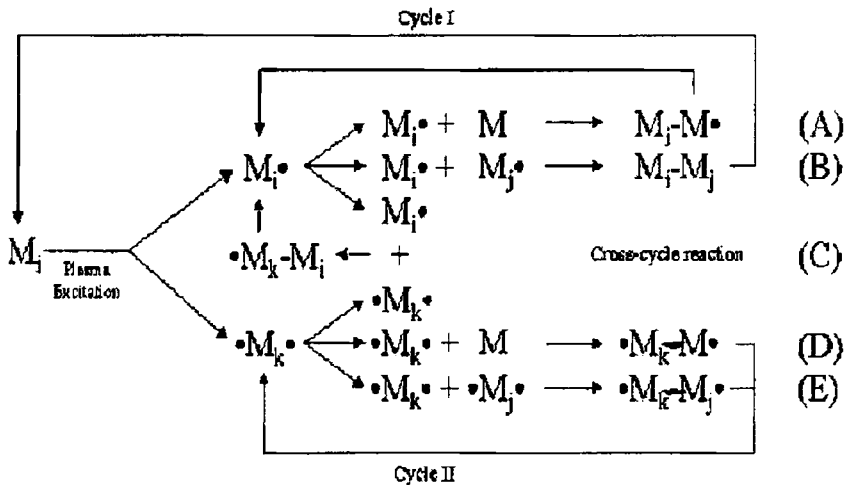


Fig. 2. Schematic representation of the bicyclic rapid step-growth polymerization mechanism proposed by Yasuda

The overall reaction cycle of plasma polymerization occurs via two major routes of rapid step growth. The first route or cycle I is the repeated activation of reaction products derived from monofunctional activated species. The second route or cycle II occurs through the formation of bifunctional or multifunctional activated species, similar to what is found in parylene polymerization. Reactions A and D in Fig.2 are the same as the first step of propagation by the addition mechanism. Therefore these reactions require a chemical structure that allows for the addition of $M\bullet$. Reaction D is essentially the same as reaction A, with the monofunctional reactant replaced by a bifunctional reactant. Reaction B is essentially a termination by the recombination mechanism and reaction C is similar to reaction B, with one of the reactants being bifunctional. Reaction E is a combination reaction between bifunctional intermediates. Plasma polymers are formed through any combination of the different routes, as a result of the RSGP mechanism. Anyway, the chain growth mechanism is absent here. The reaction between a cation and an anion ($M_i^+ + M_k^- \longrightarrow M_{i+k}$) is the only combination of ionic species that can contribute to the reaction scheme in Fig. 2 as $M\bullet$. Plasma polymerization is mainly dominated by free radical chemistry. It seems quite probable that plasma polymerization proceeds mainly via reactions of neutral species, although ions do indeed exist in plasma.

2.3 Preparation of Plasma Polymerized Thin Films

In plasma polymerization, plasma of the monomer vapour is generated by employing d.c., a.c. (50Hz.), radio frequency (MHz) or microwave (GHz) techniques. At frequencies above 1MHz, no direct contact between electrodes and plasma is necessary. Hence in r.f. plasma polymerization, the energy can be fed to plasma by inductive or capacitive coupling. Hence r.f. plasma can be initiated and sustained by external electrodes at a much lower voltage than it is required for maintaining d.c. glow discharge.

The schematic of the plasma polymerization unit is shown in Fig. 3. The system comprises of an r.f. generator source that uses four 807 RCA tetrode valves.

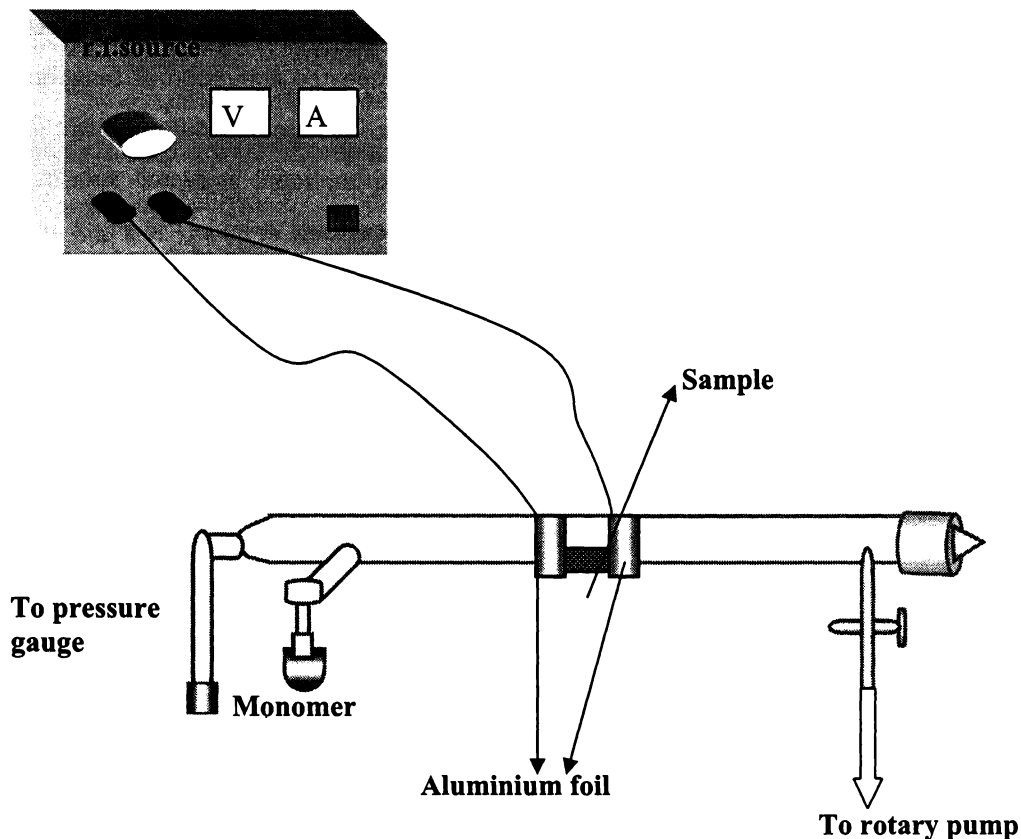


Fig. 3. Schematic of the plasma polymerization unit.

The r.f. source oscillates in the frequency range 5 – 13MHz and has an output power of \approx 35 watts. The deposition chamber is a long glass tube of length 35 cm and diameter of 3.5 cm. For maintaining plasma the energy is fed to the deposition chamber by capacitive coupling using aluminium foils. The tube is connected to a rotary pump and is evacuated to a pressure of 10^{-2} Torr. The monomer flow in the tube is regulated using a manually operated needle valve.

In order to prepare the polymer films flat glass slides (5 x 2 cm) are used. These glass substrates are first cleaned in running water and are immersed in chromic acid for 1-2 hours

in order to remove alkaline impurities. The slides are then washed in distilled water and are cleaned ultrasonically. The microscopic impurities are striped off by ultrasonic agitation in water. The glass slides are then dried and placed inside the deposition chamber in between the aluminum foil electrodes, which are wrapped around the glass tube and are capacitatively coupled. First, the chamber is evacuated to a pressure of 10^{-2} Torr, keeping the monomer needle valve closed. The r.f. power is switched on and bluish glow appears in between the electrodes. The monomer needle valve is opened gradually and a glow discharge is obtained in between the electrodes by applying a current in the range 60-80 mA. After a time interval of 30 minutes to 1 hour, a thin film of the corresponding polymer is coated on the glass substrate. Three different polymers namely poly 2,6-dimethylaniline, poly diethylamine and poly dimethylamine are prepared in the above described set up.

2.4 FTIR Analysis

Functional groups present in the plasma polymerized films can be identified through Fourier Transform Infrared Analysis (FTIR). New bond formations to any significant degree can be determined by this method. Even though the complex nature of plasma polymers makes the precise interpretation of their IR spectra difficult, much useful information concerning the general nature of polymers can be obtained [1,14]. Before analysing the FTIR spectra of plasma polymers let us have a brief discussion of the method.

FTIR method: In almost all spectrometers the recorded spectrum has a background fluctuation called noise. In order for the real spectral peak to be well distinguished, the signal to noise ratio (s/n) of atleast 3 or 4 is necessary. In the regions of the electromagnetic spectrum where sources are weak and detectors are less sensitive it is always advantageous to use Fourier Transform Spectroscopy. Another major disadvantage of the conventional dispersive method of recording a spectrum is its slowness. Here the frequency is swept smoothly across the whole span of the spectrum by rotating the monochromator. This method is very inefficient in some cases. For example, suppose a spectrum with one or two lines in it is needed. Here we have to sweep from one end to the other in order to find the lines, but most of the time is spent recording nothing but the background noise. An FTIR instrument gives the same information as a simple infrared spectrophotometer, however, the

performance of the former overweighs with respect to speed, sensitivity and much smaller requirements of the sample [15].

Fourier Transform Spectroscopy provides almost instantaneous recording of the whole spectrum with the help of computers [16, 17]. In the IR region FT method is the transfer of the information from time (t) domain to frequency (ν) domain by a mathematical analysis known as Fourier transformation, which is performed with the help of computers. A function $f(y)$ in the time domain is related to a function $f(x)$ in the frequency domain by the relation.

$$f(x) = \int_{-\infty}^{+\infty} f(y) \exp(-ixy) dy$$

Here $f(x)$ is said to be the Fourier transform of $f(y)$. Or the intensity in the frequency domain is given as

$$I(\nu) = \int_{-\infty}^{+\infty} I(t) \exp(-i\nu t) dt$$

In the frequency domain spectrum intensity variation with frequency is shown while in time domain spectrum intensity variation with time is shown. All FT spectrometers consist of an interferometer unit [18, 19]. Michelson's interferometer invented by Albert Abraham Michelson in 1880 forms the basis for the development of FTIR. The interferometer unit is for obtaining the time domain spectrum. Performing the Founier transform on this signal will give the original frequencies and intensities emitted by the source. But this process is time consuming. The invention of computers and the advances of computers to perform mathematical operations made FTIR a reality. A great advantage of the FTIR method is that the radiation of all wavenumbers from the source falls on the detector all the time. This is called multiplex advantage, which gives a gain of \sqrt{n} in signal-to-noise ratio for an FTIR spectrum over the same total time on a dispersive spectrum [20, 21]. Here n is the number of resolution elements. Besides multiplex advantage, rapid scanning and constant resolving power over the entire spectrum are added advantages of the FTIR method over the ordinary IR method where dispersive measurements are made.

Sampling techniques for FTIR spectroscopy depend on the nature of the sample

[22, 15]. In the case of liquid samples, the easiest way is to place one drop of sample between two IR transparent plates of rock salt (NaCl) or potassium bromide. Solid samples can be milled with KBr to form a very fine powder. This powder is then compressed into a thin pellet, which can be analyzed.

Analysis of monomer and polymer spectra : In the present work, the FTIR spectra of the monomer samples namely, 2,6-dimethylaniline, diethylamine and dimethylamine (structures in Fig. 4) and the corresponding polymers are recorded in the range 400cm^{-1} – 4000cm^{-1} .

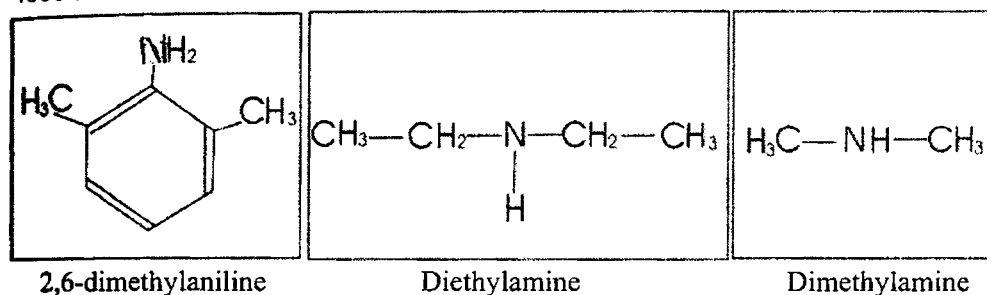


Fig.4.structure of the monomers

The FTIR spectra of the 2,6 dimethylaniline monomer and polymer are shown in Figs. 5 and 6 respectively. The introduction of two *ortho* methyl groups into aniline brings 2,6-dimethylaniline. In the monomer spectrum 3078 , 3025 and 2965cm^{-1} correspond to the three ring CH or aromatic CH stretch frequencies corresponding to the three ring CH bonds of the benzene ring. The frequency at 2965cm^{-1} is present in the polymer spectrum also, which implies that the benzene ring is retained in the polymer. The presence of group frequencies 2925 and 2866cm^{-1} in the polymer spectrum indicates the presence of the methylene group in the polymer [23, 24]. These are frequencies corresponding to asymmetric and symmetric stretch of CH_2 . This implies that the methyl group of the monomer is changed to methylene group. The most important observation made by comparing the two spectra is that pertaining to NH stretching frequencies. 2,6-dimethylaniline being a primary amine, there are two bands in the monomer spectrum in the NH stretch region corresponding to asymmetric (3462cm^{-1}) and symmetric (3383cm^{-1}) stretch. But in the polymer spectrum only a single frequency (3343cm^{-1}) is there. The

presence of this single frequency is characteristic of a secondary amine, which has only one NH bond. Hence it can be inferred that NH_2 group in the monomer is changed to NH group in the polymer. Thus the possible linkage is through the hydrogen abstraction of the NH_2 group in the monomer. This is the linkage reported for poly aniline [25]. Hence by comparing the FTIR spectra of monomer and polymer samples of 2,6 dimethylaniline, we can come to the conclusion that there are two linkages, one of which is from the amino group and the other from the methyl group. This substantiates the highly branched and cross-linked nature of the r.f plasma polymers.

Figs. 7 and 8 show the FTIR spectra of diethylamine monomer and polymer samples. Diethylamine is an aliphatic secondary amine and shows only one NH stretch (3409 cm^{-1}) in the monomer spectrum. In the polymer spectrum the broad NH stretch at 3337 cm^{-1} rather than at $\approx 3400\text{ cm}^{-1}$ implies intermolecular hydrogen bonding, as might be expected in a highly branched polymer [1]. The four peaks within $2800 - 3000\text{ cm}^{-1}$ in the monomer spectrum correspond to CH stretching frequencies of methyl and methylene groups. Of these 2965 and 2839 cm^{-1} are associated with the asymmetric and symmetric stretch of methyl group while 2919 and 2806 cm^{-1} are those of methylene group. In the polymer spectrum only two frequencies are there in this region. Or those two frequencies corresponding to the symmetrical stretching of methyl and methylene groups are absent. This suggests that the possible linkage has taken place through both methyl and methylene groups of diethylamine.

The FTIR Spectra of the dimethylamine monomer and polymer are shown in Figs. 9 and 10. Being a secondary amine, dimethylamine also shows only one NH Stretch (3443 cm^{-1}) in the monomer spectrum. Just as in diethylamine here also in the polymer spectrum we have the broad NH Stretch at a lower value of 3290 cm^{-1} due to the intermolecular hydrogen bonding expected in a highly branched polymer [1].

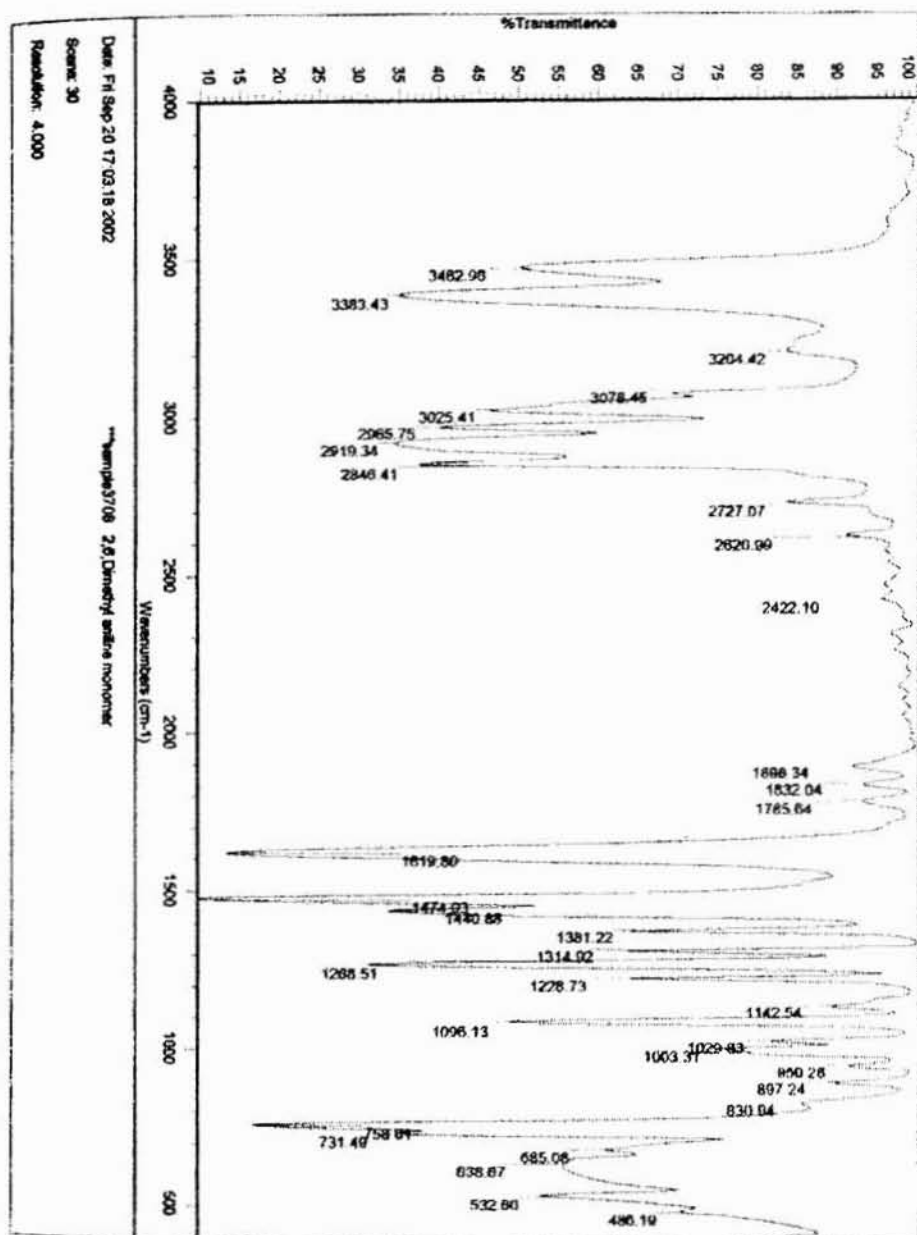


Fig. 5. FTIR spectrum of 2,6-dimethylaniline monomer

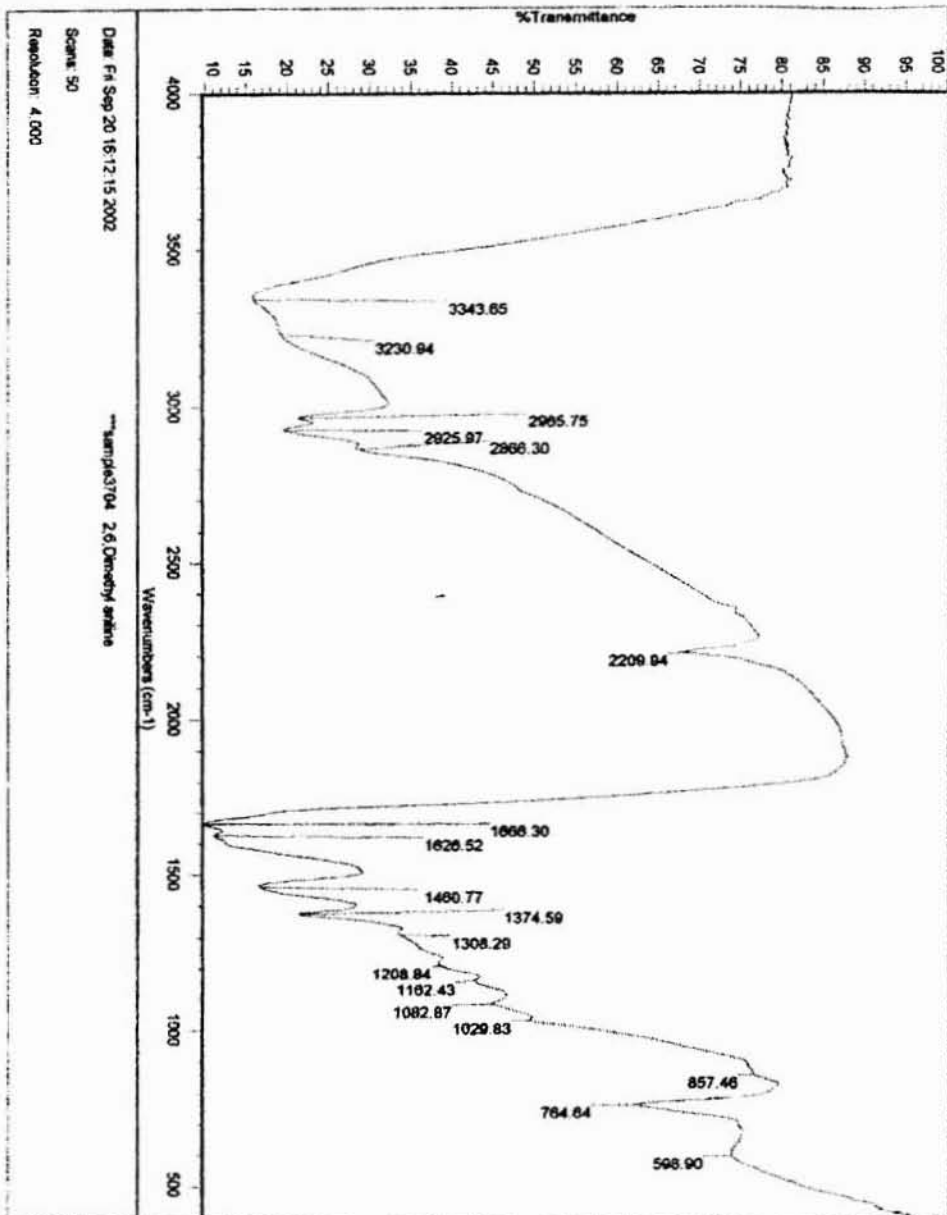


Fig. 6. FTIR spectrum of 2,6- dimethylaniline polymer

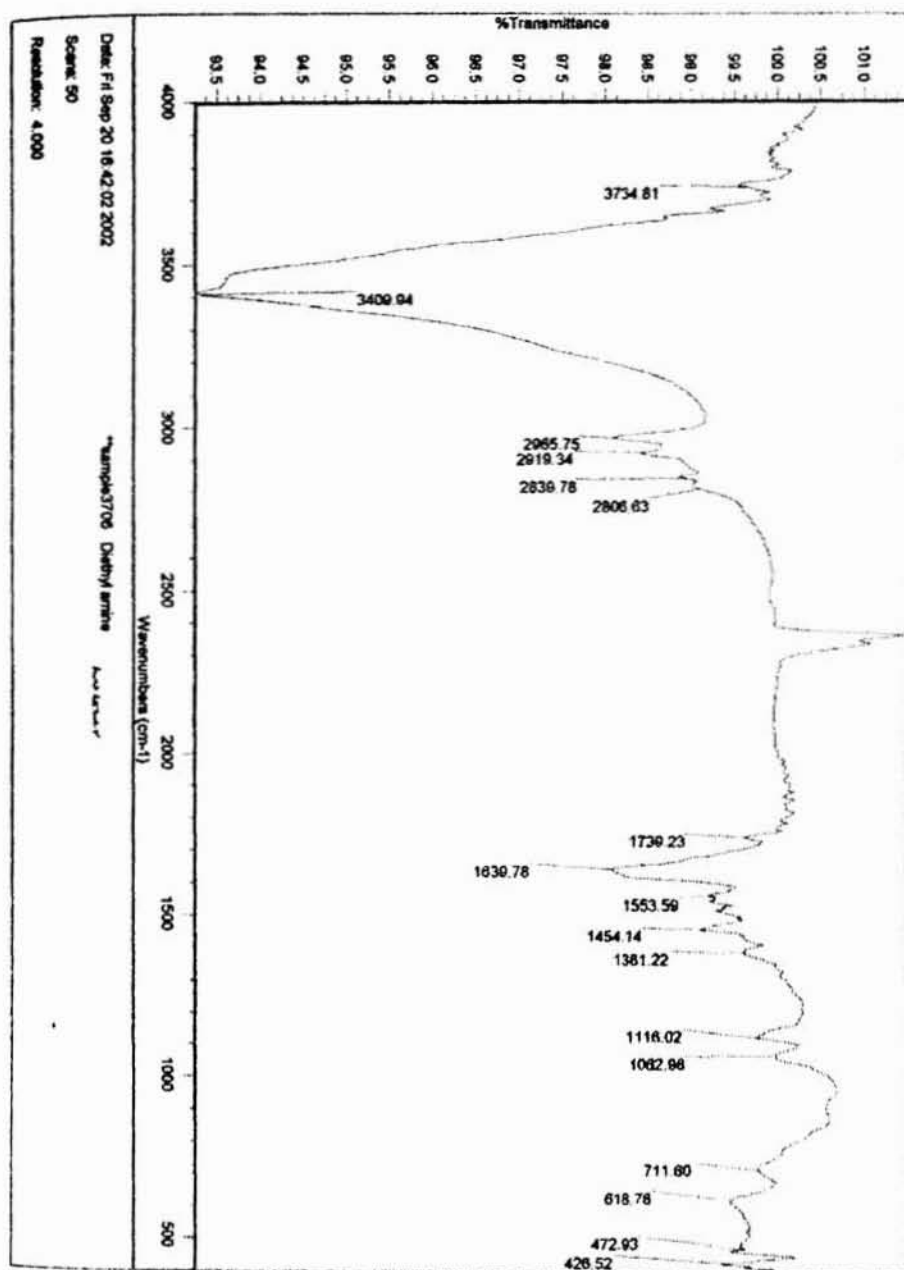


Fig. 7. FTIR spectrum of diethylamine monomer

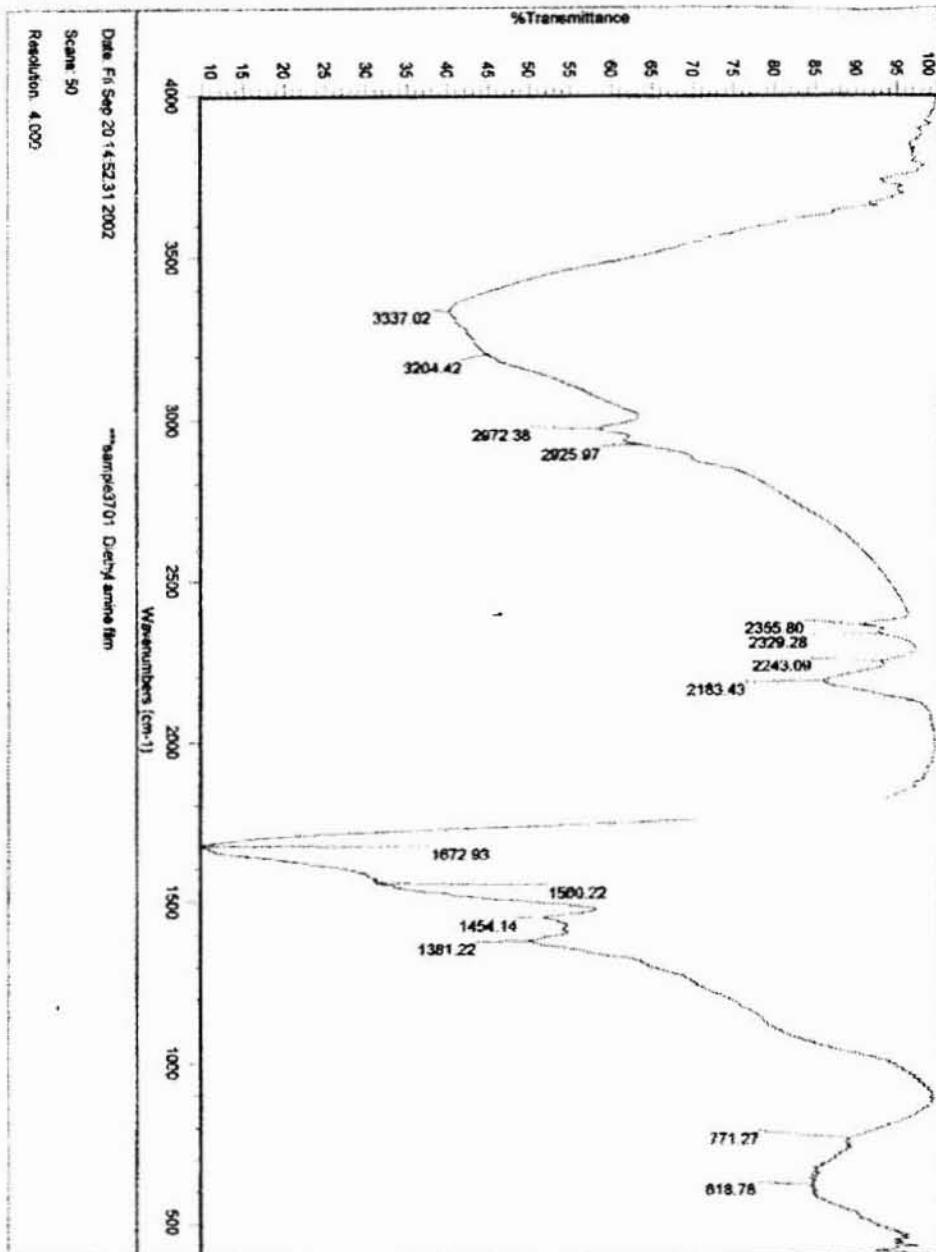


Fig. 8. FTIR spectrum of diethylamine polymer

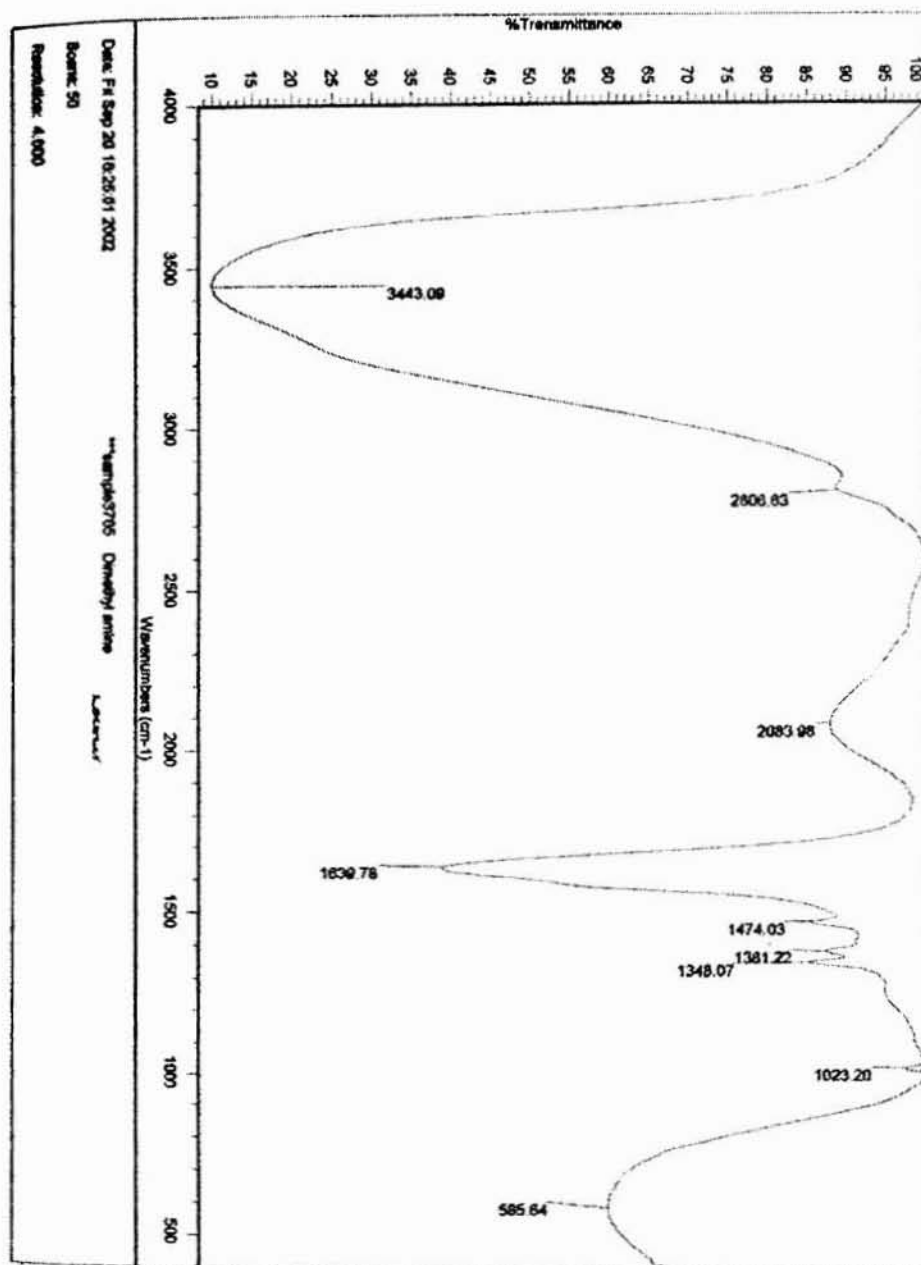


Fig. 9. FTIR spectrum of dimethylamine monomer

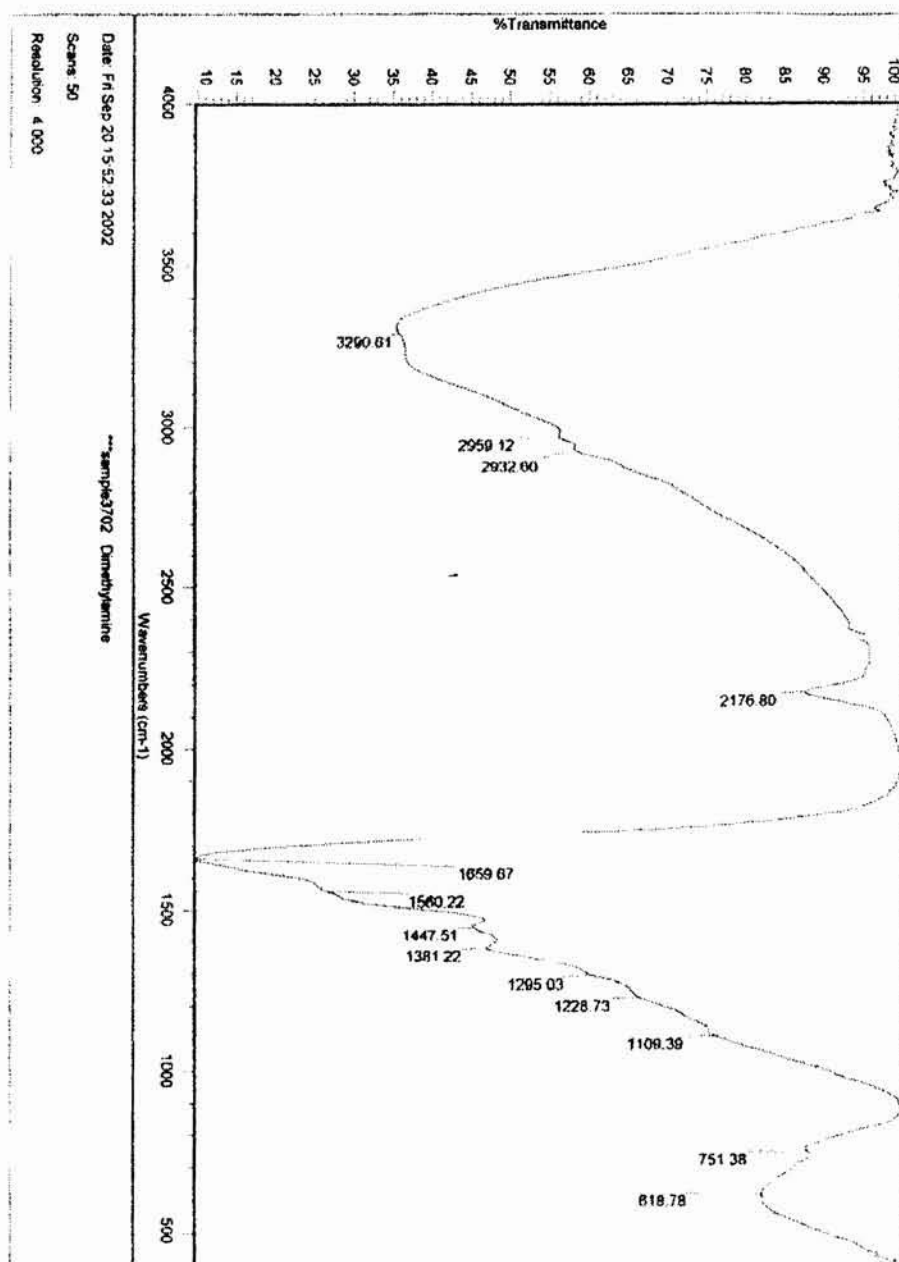


Fig. 10. FTIR spectrum of dimethylamine polymer

REFERENCES

- [1] H. Yasuda, Plasma Polymerization, Academic Press, Inc., Orlando, 1985.
- [2] R. Hippler, S. Pfau, M. Schmidt, K.H. Schoenbach, (Eds.), Low Temperature Plasma Physics, Wiley-Vch, Berlin, 2000.
- [3] A. Gill, Cold Plasma in Materials Fabrications, IEEE Press, New York, 1994.
- [4] J.R. Roth, Industrial Plasma Engineering, Volume 1 & 2, IOP, Philadelphia, USA, 2001.
- [5] H. Biederman, Y. Osada, Plasma Polymerization Processes, Elsevier, New York, 1970.
- [6] M. Shen, Plasma Chemistry of Polymers, Marcel Dekker, Inc., New York, 1976.
- [7] H. Yasuda, Contemp. Top. Polym. Sci. 3 (1979) 103.
- [8] Y. Segui, Bui Ali, Thin Solid Films 50 (1978) 321.
- [9] S.Saravanan, C. J. Mathai, S. Venkatachalam, M.R. Anantharaman, New J. Phys. 6 (2004) 64.
- [10] H. Jiang, W.E. Johnson, J.T. Grant, K. Eyink, E.M. Johnson, D.W.Tomlin, T.J.Bunning, Chem. Mater. 15 (2003) 340.
- [11] E. M. Johnson, Plasma Polymerization for the Fabrication of Optical Stacks, Ph.D Thesis, University of Cincinnati, 2001.
- [12] H. Yasuda et al., J.Appl. Polym. Sci.17 (1973) 1533.
- [13] N. Inagaki et al., J.Appl. Polym. Sci. 30 (1985) 3385.
- [14] H.Yasuda, H.C. Marsh, M.O. Burgarner, N. Morosoff, J. Appl. Polym. Sci. 19 (1975) 2845.
- [15] P.S. Kalsi, Spectroscopy of Organic Compounds, 4th edn., New Age International (p) Ltd., Publishers, New Delhi, 1999.
- [16] B.C. Smith, Fundamentals of Fourier Transform Infrared Spectroscopy, CRC Press, New York, 1996.
- [17] K. Nakanishi, P.H. Solomon, Infrared Absorption Spectroscopy, II edition, Holden-Day, Inc., Sanfrancisco, 1977.
- [18] G. Aruldas, Molecular Structure and Spectrosopy, Prentice Hall of India Pvt. Ltd., New Delhi, 2002.
- [19] B.K. Sharma, Spectroscopy, 15th edn., Goes Pub.House, Meerut, India, 2002.

-
- [20] J.M. Hollas, High Resolution Spectroscopy, John Wiley & Sons Ltd., Chichester, 1998.
- [21] C.N. Banwell, E.M. McCash, Fundamentals of Molecular Spectroscopy, Tata Mc Graw-Hill Publishing Company Limited, New Delhi, 1995.
- [22] B.P. Straughan, S. Walker, Spectroscopy (Vol.2), Chapman and Hall Ltd., London, 1976.
- [23] R.M. Silverstein, F.X. Webster, Spectrometric Identification of Organic Compounds, John Wiley & Sons, New York, 1998.
- [24] B.S. Furniss, A.J. Hannaford, V. Rogers, P.W.G. Smith, A.R. Tatchell, A Text Book of Organic Chemistry, Longman Group Ltd., England, 1978.
- [25] C.J. Mathai, S. Saravanan, M.R. Anantharaman, S. Venkatachalam, S. Jayalekshmi, J. Phys. D: Appl.Phys. 35 (2002) 240.

CHAPTER 3

DETERMINATION OF THERMAL DIFFUSIVITY OF R.F. PLASMA POLYMERIZED THIN FILMS USING PROBE BEAM DEFLECTION METHOD

3.1 Introduction

Development of new and improved materials and their characterization is one of the most active areas of research in the progress of science and technology. The conventional thermal characterization techniques include differential scanning calorimetry, contact transient methods, etc. These techniques are time consuming and need large sample quantity. In these methods the sample must be in contact with the detector, producing fluctuations in the thermal field to be measured. This can explain the thermal data dispersion which appears in the literature. Non-contact tools like *laser flash methods* where temperature is measured as a varying function of time are also used [1-3]. Here IR radiation emitted from the hot sample is detected. Radiation losses, destructive tendencies of the sample, etc. are some major disadvantages of the technique.

Meanwhile, a set of highly sensitive non-contact techniques, which are non-destructive also are developed and are commonly known as photothermal techniques [4, 5], as mentioned in chapter 1. These PT techniques are best suited for thermal characterization of solids, liquids and gases. Thermal diffusivity is an important parameter which is measured by applying the suitable technique depending upon the thermo-optical properties and structure of samples. Photoacoustic methods [6-9] and photothermal beam deflection methods [10-15] are widely used for thermal diffusivity measurements. Thermal diffusivity of the plasma polymerized thin films described in chapter 2 are measured here using a transverse probe beam deflection experimental setup.

3.2 Importance of Thermal Diffusivity

Thermal conduction is a process by which heat is transferred from one part of the sample to another as a result of the temperature gradient. Both electrons and phonons are instrumental in transferring energy from one place to another in a solid. Electrons are primary carriers in metals and these materials have fairly large thermal conductivities. Heat conduction in insulators can be considered as the diffusion of phonons from the hot to the cold end. Jean Fourier derived a basic law defining the one-dimensional propagation of heat in solids as

$$\frac{\partial Q}{\partial t} = -kA \frac{\partial T}{\partial x}$$

This equation is known as the Fourier equation. Here Q is the quantity of heat conducted, A is the conducting area normal to the flow path, $\frac{\partial T}{\partial x}$ is the temperature gradient along the path and k is thermal conductivity of the conducting material. The formal definition of thermal diffusivity arises from the expression for a transient temperature field in a conducting solid, which is given by

$$\nabla^2 T = \frac{1}{\alpha} \frac{\partial T}{\partial t}$$

where the thermal diffusivity α is given by $\alpha = \frac{k}{\rho C}$

Here 'k' is the thermal conductivity, 'ρ' is the density and 'C' is the specific heat of the material. The thermal diffusivity (α) is expressed in $m^2 s^{-1}$. It is evident from the units that, α represents the rate of heat flow.

Thermal diffusivity is an important physical parameter in thin film characterization. In the case of polymers, knowledge of thermal diffusivity is required for studying the relation between molecular structures and crucial thermal properties [16]. Moreover thermal diffusivity or thermal conductivity are often vital parameters in the applications of polymers [17]. In superconductivity studies,

Thermal diffusivity and conductivity give useful information of electron-phonon coupling [18, 19], phonon scattering [20], lattice anisotropy [21–23] and thermal boundary resistance at the film-substrate interface of superconducting samples [21, 22]. Thermal diffusivity can also be used to check the quality of thin films [24].

3.3 Experimental Configurations

As discussed in chapter 1 the photothermal beam deflection (PBD) technique uses two laser beams, one for heating the sample (pump) and the other to probe the refractive index gradient produced (probe). According to the alignment of pump and probe with respect to each other we have collinear PBD and transverse PBD [4]. The pump and probe are parallel to each other in collinear PBD while they are perpendicular to each other in transverse PBD. The probe beam can be directed to the sample surface in two ways. They are the skimming configuration and bouncing configuration [25-27].

Skimming configuration: In this configuration, the probe beam just grazes the sample surface. This implies that the probe beam travels at a certain height above the sample surface, which is determined by the size of the probe beam. The main problem connected with the skimming configuration is related to the size of the probe beam. Though the probe beam is focused to a small spot size, it increases at the edge and in order to avoid probe beam scattering the beam has to travel a distance 'z' far from the surface which is at least $z = \sqrt{\lambda L/\pi}$. Here λ = wavelength of the probe beam and L = sample size along the probe beam path.

Bouncing configuration: This is also called *surface reflection scheme*. Here the probe beam impinges on the sample surface at a certain angle and the deflection of the reflected beam is noted. The height of the probe beam above the sample surface is zero. In the bouncing configuration, the probe beam deflection is obtained as a result of two different mechanisms, the thermal gradient in the areas near to the heated sample (mirage) and the sample deformation due to thermal expansion. The

bouncing scheme however cannot be applied to absorbing, rough or non-reflecting samples where there is no relevant probe reflection.

The effects introduced in both the configurations by the finite size of the heating beam, finite height of the probe beam above the sample surface, the secondary effects like finite size of the probe beam, sample temperature, optical misalignment, diffusivity of the deflecting medium, etc. are discussed in detail by Salazar et al. [25].

In the present work in order to measure the deflection, the *transverse scan method* is preferred. In this method, the pump beam is fixed to a particular position on to the sample surface. The probe beam is then scanned across sample surface perpendicular to the pump beam. Hence the separation between the pump and the probe beams (transverse offset 'y') is a variable. Thus, the normal and tangential beam deflection profiles are measured about the center position of the exciting laser beam.

3.4 Methods of Analysis

As already explained, photothermal beam deflection experiment consists of a pump source for excitation of the sample, which is modulated using a chopper and a probe source to probe the refractive index gradient. The deflection of the probe beam is detected using a position sensitive detector. The vectorial nature of the deflection implies that the magnitude has two spatial components. The components are referred to as the normal component φ_n and tangential component φ_t [4, 12]. Different methods are developed by many workers to analyse the amplitude and phase data for the determination of thermal diffusivity. They are zero crossing [14], multiparameter fitting, thermal wave coupling, phase method [28, 29], amplitude method [30, 31], etc. In the present work the phase and amplitude methods are used.

Phase method: This method utilizes the phase of the tangential component of deflection signal φ_t . Theoretically,

$$\varphi_t = \varphi_0 \exp [-j (y/l_t + \phi) - j\omega t]$$

This implies that the phase varies linearly with the pump-probe offset 'y'. l_1 is the characteristic length, which is the distance corresponding to one radian phase shift. From the slope s of the plot of phase vs. 'y', the thermal diffusivity of the sample can be determined using the relation

$$D = \pi f / s^2$$

Direct determination is possible only if the thermal diffusivity of the sample is greater than that of the coupling medium. On the contrary, if the thermal diffusivity of the sample is lower than that of the coupling medium, modified phase method must be applied. In such a case, slope 's' is determined for various modulation frequencies 'f' and a graph is plotted between $1/s$ and $1/\sqrt{f}$. The slope of this straight line graph, s' , gives the thermal diffusivity using the relation

$$D = \pi s'^2$$

Amplitude method: The method developed by Quelin et al. took into account the linear variation of logarithm of amplitude of the tangential component of the deflection signal with the pump-probe offset. The three-dimensional thermal conductivity tensor of a polymer crystal is determined in the front configuration where the pump and probe runs on the same side of the sample [30]. This is similar to the Phase method and the thermal diffusivity is obtained from the relation $D = \pi f / s'^2$ where s' is the slope of graph between $\ln [A_t]$ and 'y'. Further they observed that only a numerical simulation led to the thermal conductivity coefficient perpendicular to the sample surface. Hence in order to determine the thermal conductivity coefficient in the normal direction, they used amplitude of normal component of deflection in the rear configuration, which means that the pump and probe are running on either side of the sample [31].

3.5 Transverse PBD Setup

The essential components for the mirage (PBD) setup are: 1) pump source 2) probe source 3) chopper 4) sample cell 5) detection & data acquisition assembly consisting

of the position sensitive detector (bicell, quadrant cell, etc.), preamplifier and lock-in amplifier.

1) Pump source: Lasers are used as light sources in photothermal experiments. Besides the monochromaticity, high spectral brightness, etc., the laser output is highly collimated with cylindrical beam symmetry. The basic theory of the probe beam refraction treats the excitation beam as gaussian. The strength or amplitude of the photothermal signal is directly proportional to the amount of laser light absorbed and to the laser power. However the high excitation power is found to cause deformation of the probe beam [30]. In the present work, a He-Ne laser ($\lambda=6328 \text{ \AA}$, power 20mW) with geometrical dimensions of length 50 cm and diameter 5 cm is used as the excitation source. The ($1/e^2$) beam diameter is .7mm and the divergence is 1.2 milliradians. The beam is focused using a lens of focal length 10 cm and hence the beam is focused to a spot size of $\approx 110 \mu\text{m}$.

2) Probe source: Usually all the traditional setups use He-Ne laser as the probe source. Since the power required for the probe source in mirage experiment is small, only a low power semiconductor laser is required. Here a diode laser ($\lambda= 6328 \text{ \AA}$, 5mW) is used as the probe beam. The size of the laser is about 7 cm long and 1.5 cm in diameter and is focused using a lens of focal length 5cm to a spot size of $\approx 52 \mu\text{m}$. The other advantages of using the semiconductor lasers include easy power stabilization and absence of high frequency pointing noise.

3) Chopper: Light from the excitation source should be modulated for observing the photothermal signal. The two main types of modulation are amplitude modulation and frequency modulation of which the former one is the most common technique. The amplitude modulation can be achieved by mechanical, electrical, electro-optic or acousto-optic choppers. In the present set up, a mechanical chopper (Stanford Model SR 540) is used, which is the most inexpensive, efficient and easy way to modulate with the depth of modulation being 100%. The unit can chop light beam at rates of 4Hz-4 kHz. The whole frequency range operation requires two blades: a 6-slot blade

for operation in the frequency range 4Hz-400 Hz and 30-slot blade for 400 Hz - 4 kHz.

The modulation frequency has a major role in determining whether the sample is thermally thick or thermally thin. This is due to the fact that the thermal diffusion length follows an inverse relation with the square root of modulation frequency. As mentioned earlier in chapter 1, the sample is classified into thermally thick or thermally thin according to whether the thermal diffusion length is less than or greater than the thickness of the sample. Hence by controlling the modulation frequency, the sample can be changed from thermally thick to thermally thin or vice versa. However, in the mirage measurements for thermal diffusivity, the technique can be applied irrespective of whether the sample is thermally thin or thermally thick. Only the analysis of the deflection signal must be made appropriately.

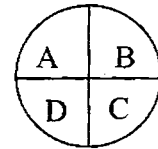
4) Sample cell: The sample cell used is a quartz cuvette of dimensions 1cm x 1cm x 5 cm. High purity carbon tetrachloride is used as the coupling fluid surrounding the sample, mainly due to the high value of dn/dT compared to air. This implies that for each degree temperature rise there will be considerable change in the refractive index, which will lead to an appreciable beam deflection. The comparatively low values of thermal conductivity ($k=0.099 \text{ Wm}^{-1}\text{K}^{-1}$) specific heat capacity ($C_p= 0.85 \text{ Jg}^{-1}\text{K}^{-1}$) and thermal diffusivity ($0.731 \times 10^{-3} \text{ cm}^2\text{s}^{-1}$) also make carbon tetrachloride an ideal coupling fluid for thermal diffusivity measurements.

5) Detector & data acquisition assembly: This assembly consists of a position sensitive detector, a pre-amplifier and a lock-in amplifier. Silicon photodetectors are commonly used for light power measurements in wide range of applications such as spectroscopy, photography, optical remote control, optical switches, analytical instrumentation, medical imaging, laser printers, bar code readers and many more. However there is another application that utilizes the photodetectors as optical position sensors and hence are referred to as *position sensitive detectors* (PSD). Under this head they are widely used in ultra fast accurate auto focusing schemes for a variety of optical systems, human eye movement monitoring, etc. The position of

beam with fractions of microns can be obtained using PSDs and hence are conveniently used in beam deflection or mirage experiments. The PSDs are broadly classified into segmented PSDs and lateral effect PSDs .

Segmented PSDs are common substrate photodiodes divided into either two or four segments or photodiode elements separated by a gap or dead region and are referred to as bicell and quadrant cell respectively. The photodiode elements are generally masked onto a common substrate so that their cathode is shared. A symmetrical optical beam generates equal photocurrents on all segments, if positioned at the centre. The relative position is obtained by measuring the output current of each segment. The bicell is used for one dimensional measurement where as the quadrant cell is used for two dimensional measurements. A quadrant cell with segments A, B, C and D are shown in the figure below. The light spot diameter should be larger than the gap between the photodiode elements.

Lateral effect PSDs are continuous single element planar diffused photodiodes with no gaps or dead areas.



In the present work a bicell (SPOT 2D from M/S UDT

Sensors Inc.) is used as the position sensitive detector for the probe beam deflection measurements. The important features of this bicell include high accuracy, excellent resolution, high-speed response, ultra low dark current and excellent response match. They have fast response times necessary for high speed or pulsed operation and position resolutions of better than $0.1 \mu\text{m}$.

A *pre-amplifier* is used to obtain the amplified output since the deflection signal is usually small. The block diagram of the pre-amplifier circuit used in the present set up is as shown in Fig. 1. Giving common signal from a function generator to the two different inputs initially tests the pre-amplifier and it is ensured that the output is zero. Furthermore, two different inputs are fed to obtain the same result as expected theoretically.

The output of the pre-amplifier is fed to a lock-in amplifier for detection. The lock-in amplifier is used to detect and measure very small a.c signals using a technique known as phase-sensitive detection in order to single out the component of the signal at a specific reference frequency and phase. The signals at other frequencies regarded as noise are rejected and do not affect the measurement. Lock-in amplifiers use a phase locked loop (PLL) to generate the reference signal. The PLL locks the internal reference oscillator to the external reference signal provided to the lock-in amplifier resulting in a reference sine wave of a particular frequency and a fixed phase shift. In the present work, SR830 (Stanford Research Model) is used. The SR 830 operates from 100 V, 120 V, 220 V or 240 V nominal a.c. power source having line frequency 50 Hz or 60Hz and can measure voltage from 2 nV to 1 V.

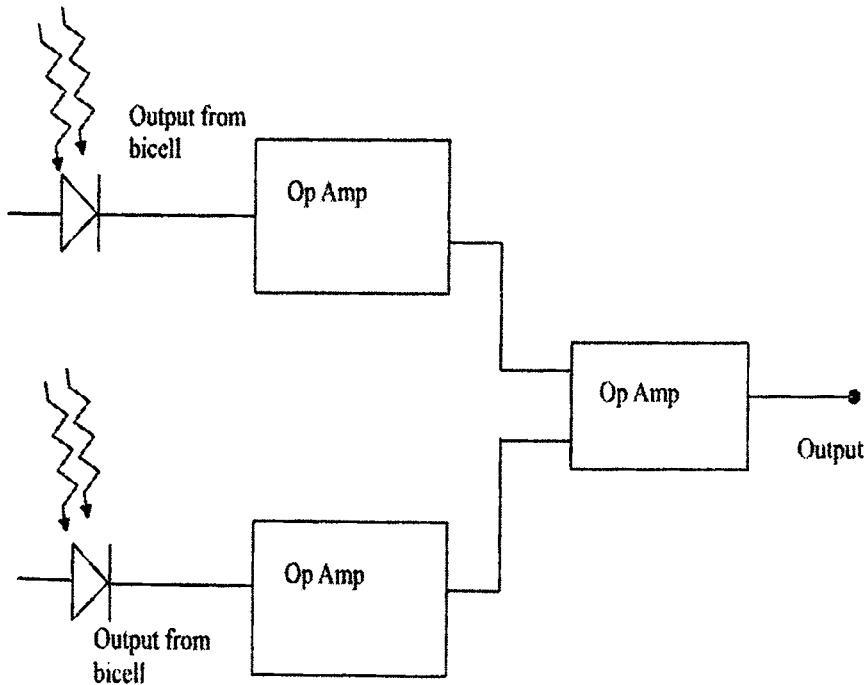


Fig. 1. Block diagram of the pre-amplifier

Schematic of the experimental setup: The schematic of the experimental setup used for the measurement of thermal diffusivity is as shown in Fig. 2. A photograph of the same is shown in Fig. 3. In the present work, the transverse scan method is employed. The measurements are performed by varying the distance between the pump and probe beams. This is achieved by fixing the pump beam and scanning the probe beam across the sample surface, since our pump source is bulky compared to the probe source. In traditional mirage experimental set ups, usually the probe beam is fixed and the pump beam scans across the sample surface with the help of a mirror arrangement. This is because probe beam scanning requires a synchronous movement

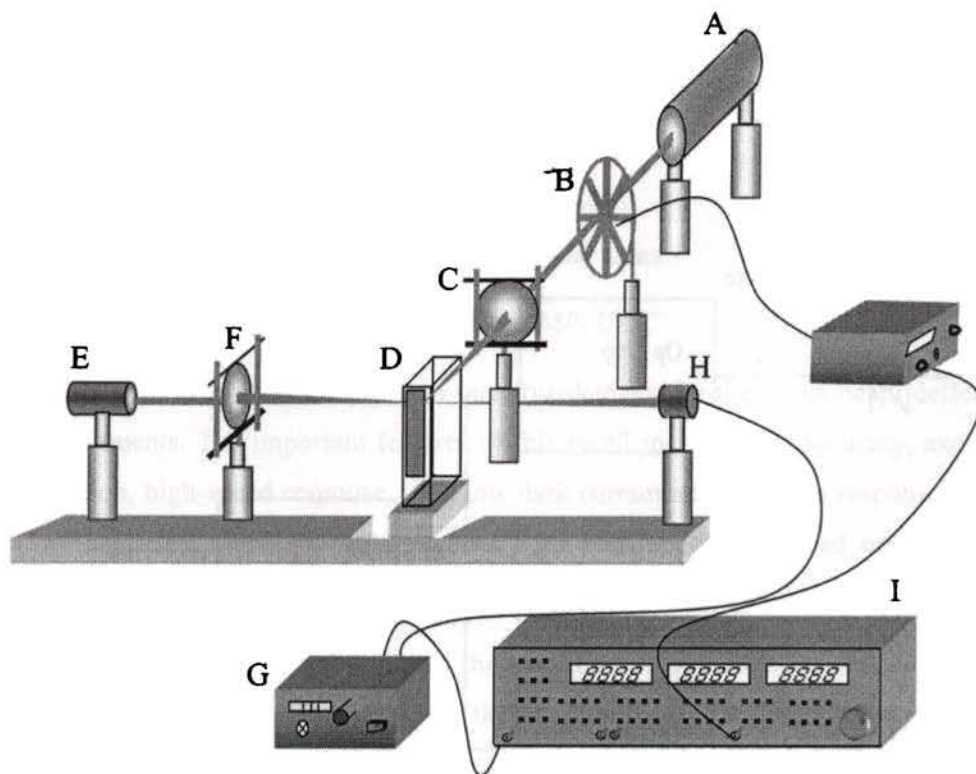


Fig. 2 .Schematic diagram of the experimental setup
A:He-Ne laser, B:Mechanical chopper, C: Lens, D:Sample cell,
E:Diode laser, F:Lens, G: Amplifier, H: Bicell detector, and
I: Lock-in amplifier.

of the lens focusing the probe beam and the detector, which makes the system complex, especially when the probe source is bulky. Here since the probe laser is of small size that, it together with the focusing lens and detector could be fixed on an aluminium flat of length 30 cm and width 1cm, which in turn is fixed onto an XYZ translation stage, so that all the three move in synchrony. The sample placed in the cuvette is also fixed on a translation stage. The pump laser and these two translation stages are fixed on an optical breadboard with honeycomb structure, placed on a granite table so as to minimize the errors due to mechanical vibrations. The experimental setup is standardized for thermal diffusivity using InP wafer [32].

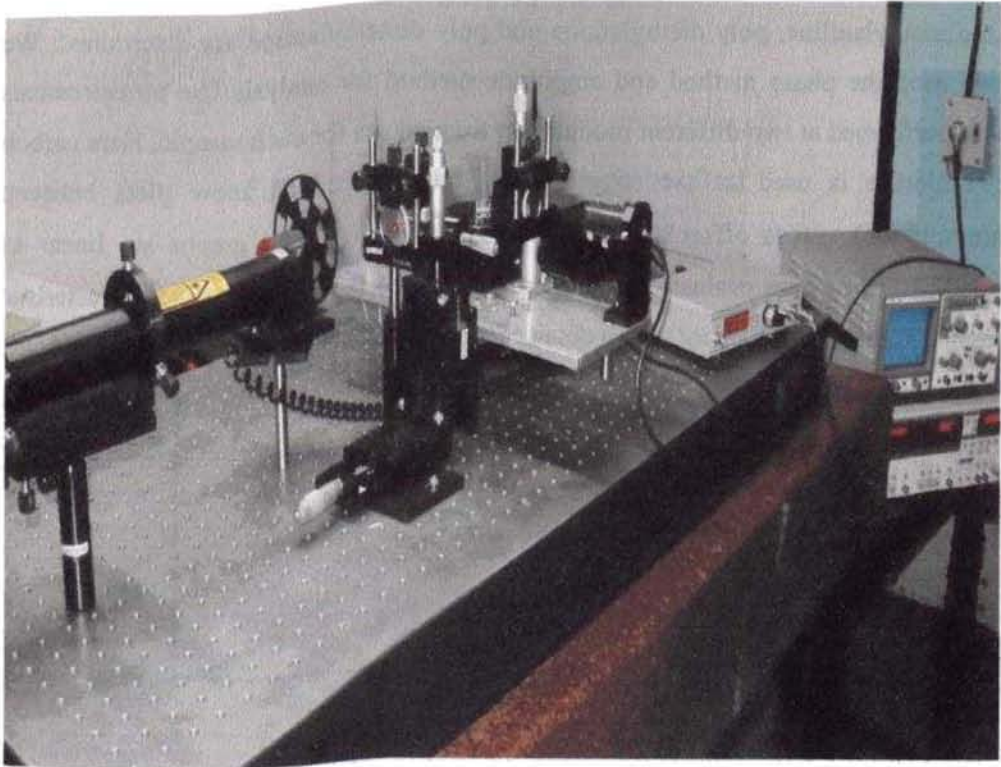


Fig. 3. Photograph of PBD experimental setup

3.6 Thermal Diffusivity of Plasma Polymerized Thin Films

As mentioned in Chapter 2 plasma polymerized thin films find innumerable applications ranging from corrosion free adhesive coating materials to sensor technology and microelectronics [33-38]. The thermal diffusivity (and hence conductivity) is an equally important parameter like electrical conductivity, which is to be known for effectively applying these materials for different purposes. The thermal conduction parameters of polymers are very low that the determination is really challenging and the sample being in thin film form adds to the difficulty. By employing the photothermal beam deflection setup described in section 3.5 the thermal diffusivity values of the three r.f plasma polymerized thin films namely, poly 2,6-dimethylaniline, poly diethylamine and poly dimethylamine are determined. We have used the phase method and amplitude method for analysis. The measurements were performed at two different modulation frequencies for each sample. Here carbon tetrachloride is used as the coupling medium. Figs. 4-15 show plots between $\ln(\text{amplitude})$ versus offset and phase versus offset. All the graphs are linear as expected. The slopes evaluated from these graphs are the inverse of the characteristic length and thermal diffusivity values obtained from the slopes are tabulated in Table I.

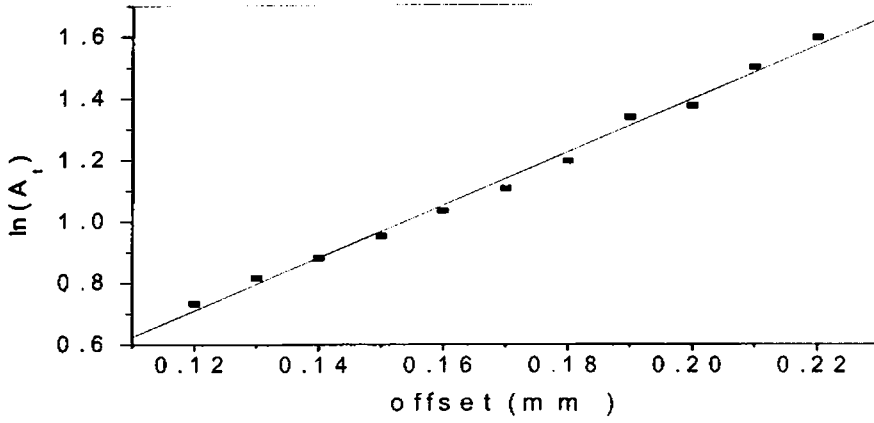


Fig. 4. $\ln(\text{amplitude})$ vs. pump-probe offset for 2,6-dimethylaniline at 8 Hz

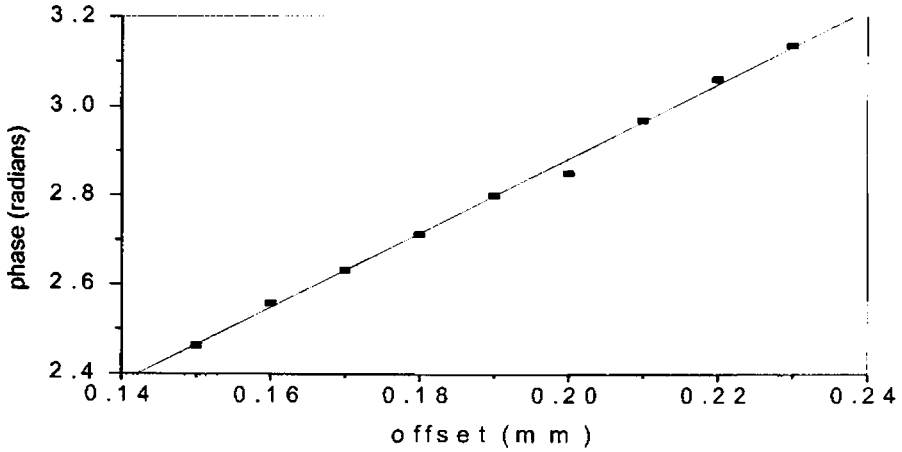


Fig. 5. Phase vs. pump-probe offset for 2,6-dimethylaniline at 8 Hz

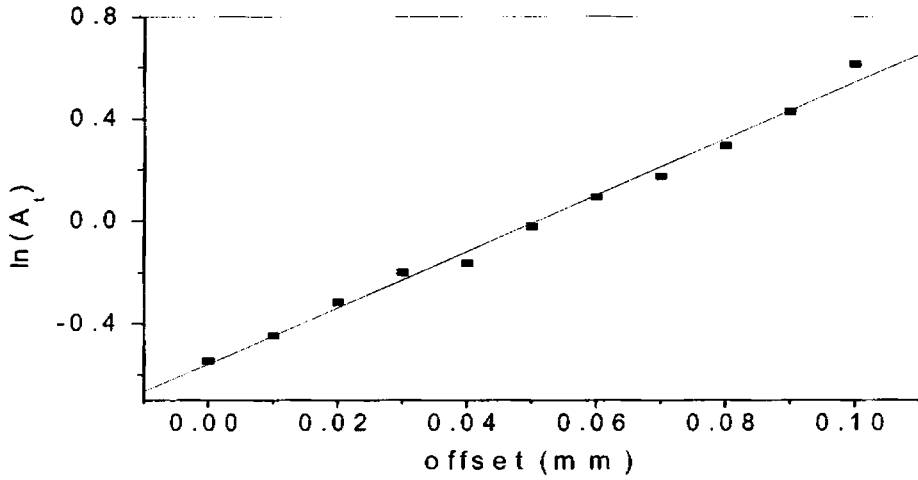


Fig. 6. $\ln(\text{amplitude})$ vs. pump-probe offset
for 2,6-dimethylaniline at 12 Hz

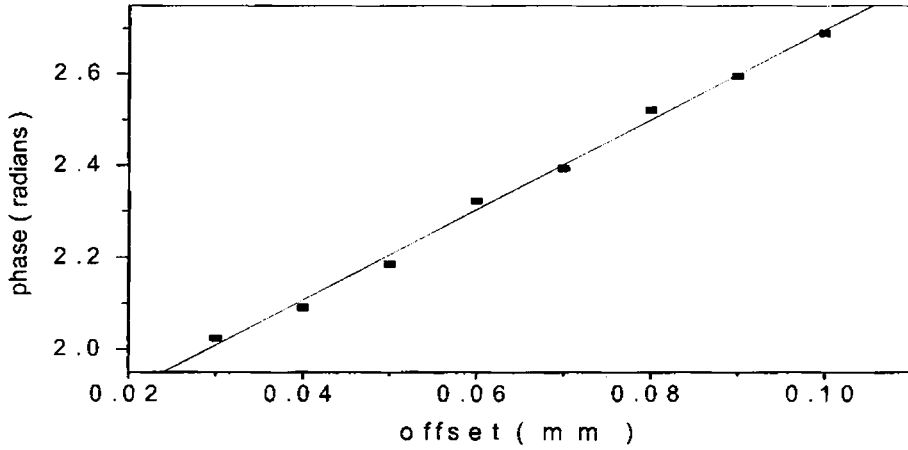


Fig. 7. Phase vs. pump-probe offset
for 2,6-dimethylaniline at 12 Hz

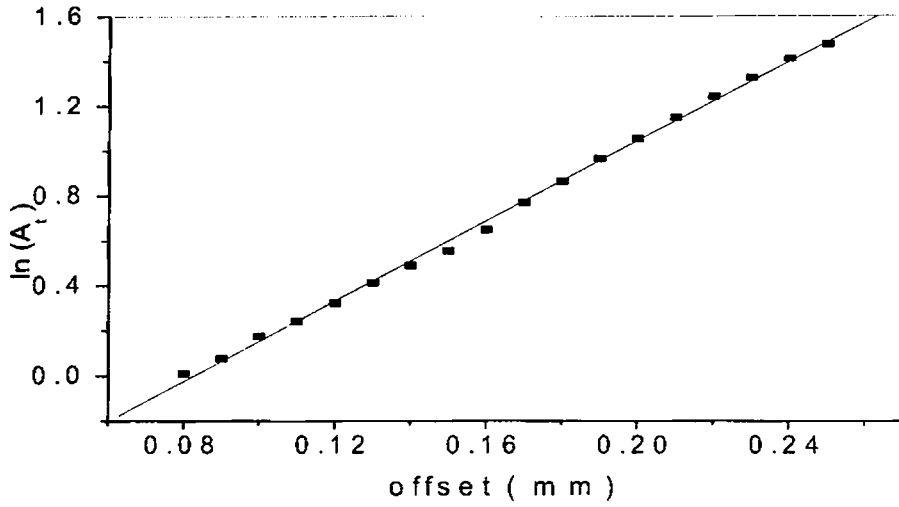


Fig. 8. $\ln(\text{amplitude})$ vs. pump-probe offset for diethylamine at 8 Hz

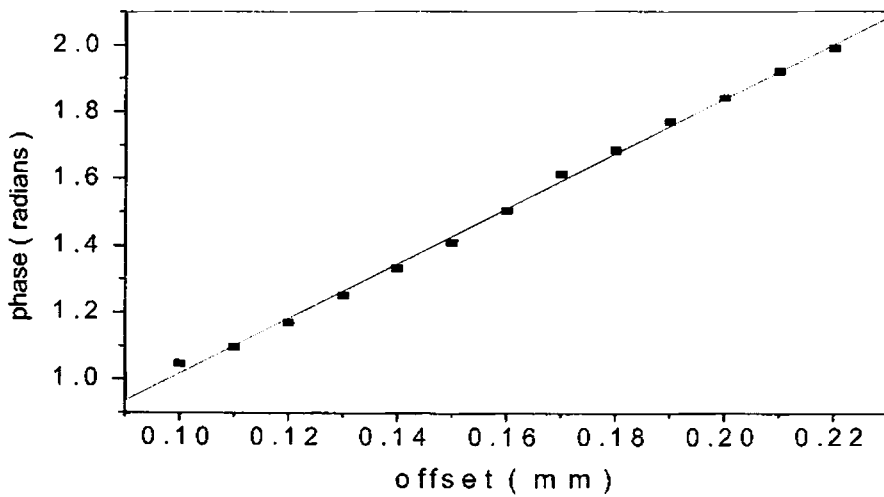


Fig. 9. Phase vs. pump-probe offset for diethylamine at 8 Hz

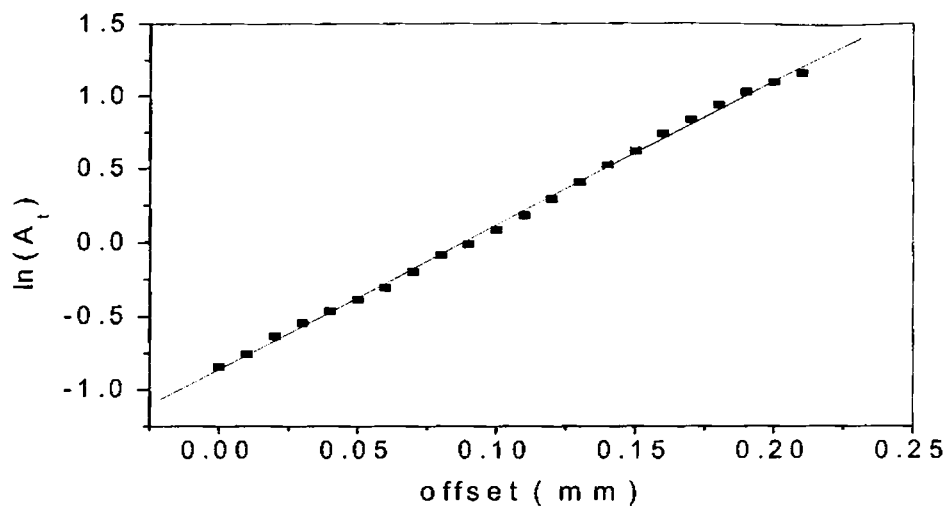


Fig. 10. $\ln(\text{amplitude})$ vs. pump-probe offset
for diethylamine at 10 Hz

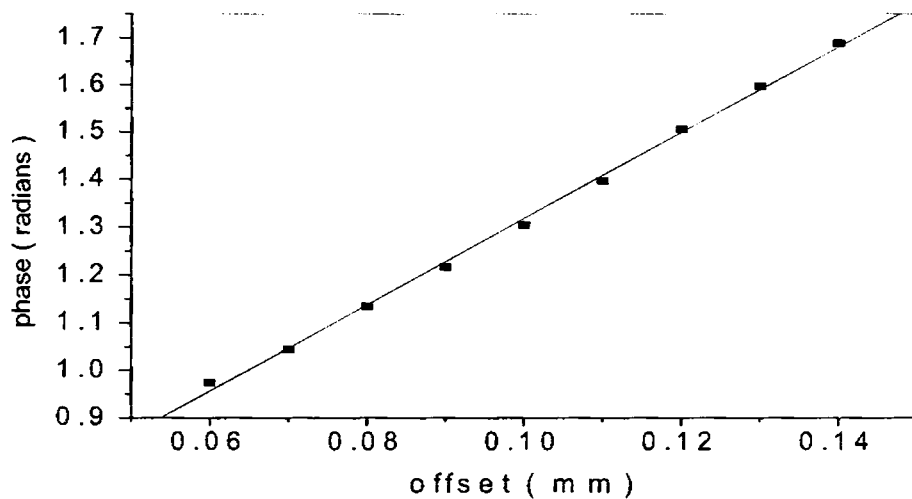


Fig. 11. Phase vs. pump-probe offset
for diethylamine at 10 Hz

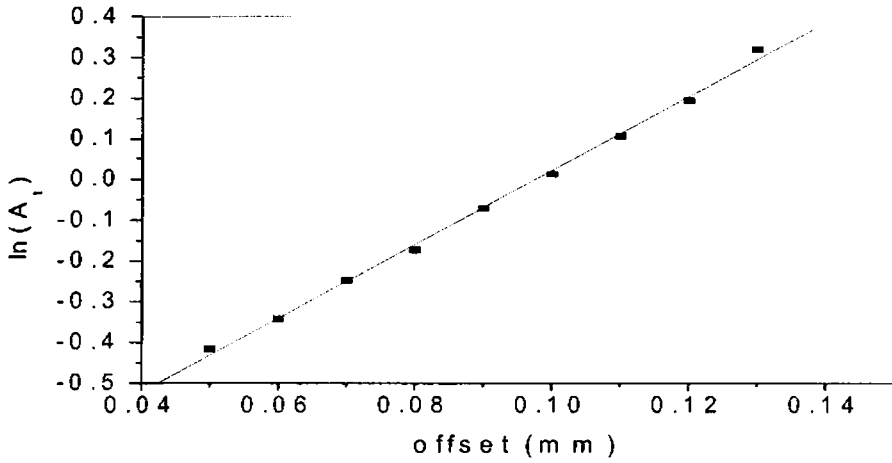


Fig. 12. $\ln(\text{amplitude})$ vs. pump-probe offset for dimethylamine at 4 Hz

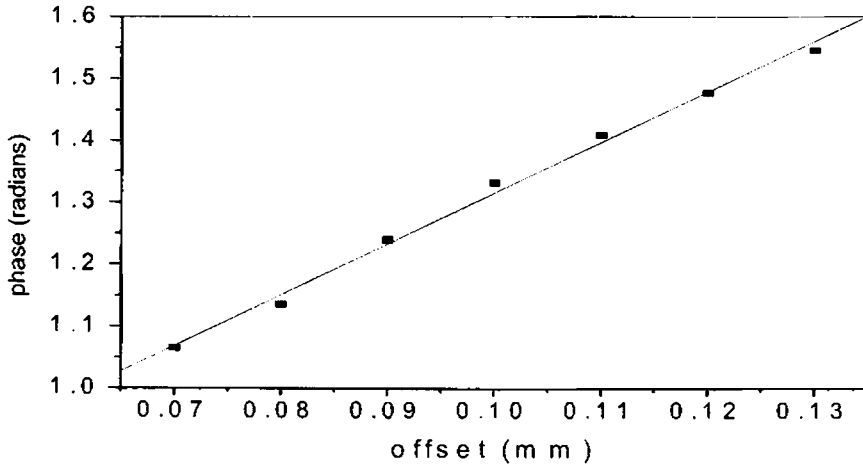


Fig. 13. Phase vs. pump-probe offset for dimethylamine at 4 Hz

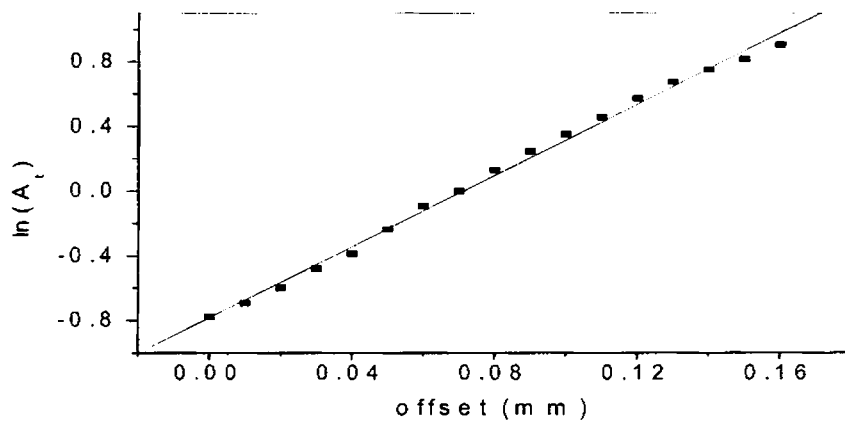


Fig. 14. $\ln(\text{amplitude})$ vs. pump-probe offset
for dimethylamine at 6 Hz

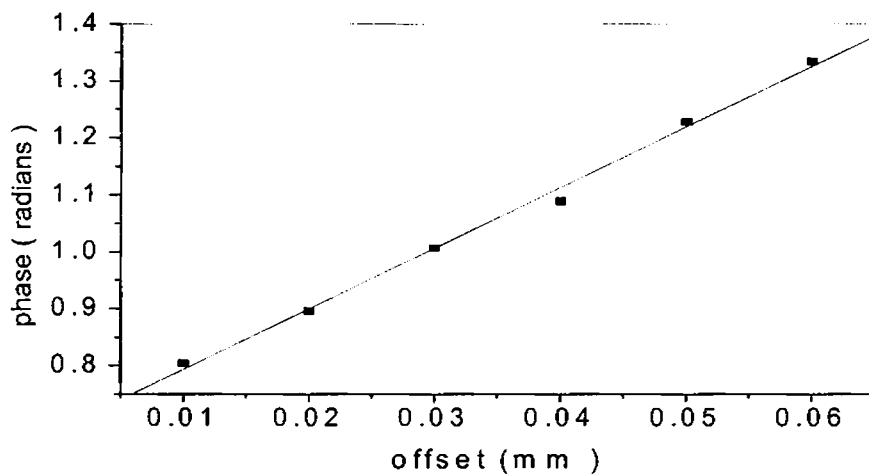


Fig. 15. Phase vs. pump-probe offset
for dimethylamine at 6 Hz

Table 1

Thermal diffusivity values obtained for the three samples

Sample	Method of Analysis	Frequency (Hz)	Thermal Diffusivity ($10^{-2} \text{ cm}^2 \text{ s}^{-1}$)
Poly 2,6-dimethylaniline	Phase Method	8	.365 ± .016
		12	.391 ± .020
	Amplitude Method	8	.343 ± .018
		12	.312 ± .019
Poly diethylamine	Phase Method	8	.374 ± .010
		10	.384 ± .010
	Amplitude method	8	.319 ± .007
		10	.327 ± .006
Poly dimethylamine	Phase Method	4	.187 ± .012
		6	.166±.011
	Amplitude Method	4	.155±.006
		6	.156±.005

Two basic factors that need to be considered in the photothermal beam deflection technique are the effects of coupling media and substrate on which the samples are coated. If there were any contribution from the coupling media, then the thermal diffusivity value calculated would have been different for different modulation frequencies [28]. The contribution from the coupling fluid to the photothermal signal becomes dominant in the skimming configuration only when the thermal diffusivity of the coupling fluid is greater than that of the sample. In the present work, although the thermal diffusivity of the samples under study are low, the carbon tetrachloride ($D_{CCl_4} \sim 0.731 \times 10^{-3} \text{ cm}^2\text{s}^{-1}$) which is used as the coupling medium in our measurements has still a lower thermal diffusivity value. In conclusion, in our measurements, the thermal properties of the coupling medium do not influence the photothermal measurements. However, in the present work, the samples are coated onto a glass substrate, which is perfectly non-absorbing at the pump beam wavelength. Hence the effect of substrate on the photothermal measurements can also be neglected [39].

While dealing with the polymer samples, another important factor to be dealt with is the effect of the temperature rise on the expansion of the samples. However, the temperature rise in the heated area is estimated to be approximately 1 degree, which can cause a surface deformation of only $< 1\text{nm}$. This expansion can affect the photothermal measurements only when the bouncing configuration is employed. In the present work skimming configuration is used where the probe beam skims the sample surface and the height of the probe beam above the sample surface is limited by the spot size of the probe beam. Due to the large spot size of the probe beam compared to the surface deformation, any error in the photothermal measurements caused by the thermal expansion of polymers also is completely eliminated.

In conclusion, the thermal diffusivity values of r.f. plasma polymerized thin films of poly 2, 6-dimethylaniline, poly diethylamine and poly dimethylamine are determined. The values obtained for all the samples lie in the same order as those of polymer thin film samples [40, 41].

REFERENCES

- [1] W.J. Parker, R.J. Jenkins, C.P. Butler, G.L. Abbott, *J. Appl. Phys.* 32 (1961) 1679.
- [2] L.M. Clark III, R.E. Taylor, *J. Appl. Phys.* 46 (1975) 714.
- [3] M.A. Sheikh, S.C. Taylor, D.R. Hayburst, R. Taylor, *J. Phys. D: Appl. Phys.* 33 (2000) 1536.
- [4] J.A. Sell, *Photothermal Investigations of Solids and Liquids*, Academic Press, Inc., New York, 1988.
- [5] S.E. Bialkowski, *Photothermal Spectroscopy Methods for Chemical Analysis*, John Wiley & Sons, Inc., New York, 1996.
- [6] A. Rosencwaig, A. Gersho, *J. Appl. Phys.* 47 (1976) 64.
- [7] A. Rosencwaig, *Photoacoustics and Photoacoustic Spectroscopy*, John Wiley & Sons, New York, 1980.
- [8] C. Garcia-Segundo, M. Villagran-Muniz, S. Muhi, *J. Phys. D: Appl. Phys.* 31 (1988) 165.
- [9] A. Rosencwaig, T.W. Hindley, *Appl. Opt.* 20(1981) 606.
- [10] A.C. Boccara, D. Fournier, J. Badoz, *Appl. Phys. Lett.* 36 (1980) 130.
- [11] J.C. Murphy, L.C. Aamodt, *J. Appl. Phys.* 51 (1980) 4580.
- [12] L.C. Aamodt, J.C. Murphy, *J. Appl. Phys.* 52 (1981) 4903.
- [13] M.A. Schweitzer, J.F. Power, *Appl. Spectro.* 48 (1994) 1076.
- [14] P.K. kuo, E.D. Sandler, L.D. Favro, R.L. Thomas, *Can. J. Phys.* 64 (1986) 1168.
- [15] W.B. Jackson, N.M. Amer, A.C. Boccara, D. Fournier, *Appl. Opt.* 20 (1981) 1333.
- [16] J. Rantala, L. Wei, P.K. Kuo, J. Jaarinen, M. Luukkala, R.L. Thomas, *J. Appl. Phys.* 73 (1993) 2714.
- [17] B. Skagerberg, J. Jaarinen, J. Rantala, *Photoacoustic and Photothermal Phenomena III*, Springer, Berlin, 1992.
- [18] L. Gomes et al., *J. Appl. Phys.* 63 (1988) 5044.
- [19] V. Bayot et al., *Solid State Commun.* 63 (1987) 983.
- [20] J.T. Fanton, D.B. Mitzi, A. Kapitulnik, B.T. Khuri-Yakub, G.S. Kino, D. Gazit, R. S. Feigelson, *Appl. Phys. Lett.* 55 (1989) 598.
- [21] C.D. Marshall, I.M. Fishman, R.C. Dorfman, C. B. Eom, M. D.Fayer, *Phys. Rev. B* 45 (1992) 10009.

- [22] C.D. Marshall, A. Tokmakoff, I.M. Fishman, C.B. Eom, J.M. Phillips, M.D. Fayer, *J. Appl. Phys.* 13 (1993) 850.
- [23] P.K. Wong, P.C.W. Fung, H.L. Tam, J. Gao, *Phys. Rev. B* 51 (1995) 523.
- [24] X. Zhang, C. Gam, Z. Xu, S. Zhang, H. Zhang, *Photoacoustic and Photothermal Phenomena II*, Springer, Berlin, 1990.
- [25] A. Salazar, A. Sanchez-Lavega, J. Fernandez, *J. Appl. Phys.* 69 (1991) 1216.
- [26] M. Bertolotti, G.L. Liakhov, R. Li Voti, S. Paoloni, C. Sibilìa, *J. Appl. Phys.* 83 (1998) 966.
- [27] M. Bertolotti, G.L. Liakhov, R. Li Voti, S. Paoloni, C. Sibilìa, *Appl. Phys. B* 67 (1998) 641.
- [28] M. Bertolotti, R. Li Voti, G. Liakhov, C. Sibilìa, *Rev. Sci. Instrum.* 64 (1993) 1576.
- [29] M. Bertolotti, R. Li Voti, G. Liakhov, C. Sibilìa, *Rev. Sci. Instrum.* 66 (1995) 277.
- [30] X. Quelin, B. Perrin, G. Louis, P. Peretti, *Phys. Rev. B* 48 (1993) 3677.
- [31] X. Quelin, B. Perrin, G. Louis, *J. Appl. Phys.* 77 (1995) 2292.
- [32] J. Ravi, *Photothermal and Photoacoustic Investigations on Certain Polymers and Semiconducting Materials*, Ph.D Thesis, Cochin University of Science and Technology, 2003.
- [33] R.H. Turner, I. Segall, F.J. Boerio, G.D. Davis, *Adhesion* 62 (1997) 1.
- [34] M.R. Alexander, T.M. Duc, *Polymer* 40 (1999) 5479.
- [35] M.R. Alexander, T.M. Duc, *J. Mater. Chem.* 8 (1998) 937.
- [36] S. Kurosawa, N. Kamo, D. Matsui, Y. Kobatake, *Anal. Chem.* 62 (1990) 353.
- [37] S. Kurosawa, E. Tawara-Konda, N. Kamo, *Anal. Chim. Acta.* 43 (1997) 175.
- [38] Y. Segui, Bui Ai, *Thin solid Films* 50 (1978) 321.
- [39] G. Amato, G. Benedetto, M. Maringelli, R. Spagnolo, *Appl. Phys. A* 52 (1991) 280.
- [40] E.T. Ogawa, Chuan Hu, P.S. Ho, *J. Appl. Phys.* 86 (1999) 6018.
- [41] K.N. Madhusoodanan, M.R. Thomas, J. Philip, *J. Appl. Phys.* 62 (1987) 1162.

CHAPTER 4

NEAR IR VIBRATIONAL OVERTONE SPECTROSCOPY

4.1 Introduction

Spectroscopy deals with the measurement and interpretation of the interaction of electromagnetic radiation with matter [1-8]. The interaction can be absorption or emission of radiant energy, when atoms or molecules of matter move from one energy level to another. Spectroscopic methods are used routinely by chemists and physicists to provide information about the nature of chemical substances [9]. The scope and power of spectroscopic techniques have been increased substantially in recent years by major advances in instrumentation.

The part of the spectrum located between the mid-infrared and visible region is the near infrared (NIR) spectrum. Over the last few years, near infrared spectroscopy has rapidly developed into an important and extremely useful method of analysis and much exciting progress has brought it to the attention of spectroscopists in various fields. The growing interest in near infrared spectroscopy has arisen from improvements in instrumentation and in data analysis as well as from the introduction of optical fibres allowing delivery and transfer of NIR energy and information. The NIR region which covers the range between approximately 12,800 and 4,000 cm^{-1} (0.780–2.5 μm), contains absorption bands corresponding to overtones and combinations of fundamental C–H, O–H and N–H vibrations. An NIR spectrum is expected to be much simpler than a conventional mid-IR (4000–400 cm^{-1}) spectrum. As the overtones and combination bands are much weaker than the fundamental absorption bands (usually by a factor of 10 to 100), NIR spectroscopy allows the analysis of samples up to several millimeters thick [10, 11].

Among the advantages offered by NIR spectroscopy, the speed, the simplicity of sample preparation and the non-destructive nature of the technique should be mentioned. One of the strengths of the NIR technology is that it allows several constituents to be measured concurrently. In addition, for each fundamental vibration

there exists a corresponding series of overtone and combination bands with each successive overtone band approximately an order of magnitude less intense than the preceding one. This provides a built-in dilution series which allows several choices of absorptions of different intensities containing the same chemical information. The greatest disadvantage of NIR is probably its weak sensitivity to minor constituents. NIR spectroscopy has proved to be a powerful tool for research in agriculture, food, pharmaceutical, chemical, polymer and petroleum industries. An NIR spectrum cannot be interpreted in such a straightforward manner as a mid-IR spectrum. Effectively, mid-IR spectra exhibit sharp and narrow peaks essentially related to fundamental modes, while NIR spectra often contain broad bands which are the result of many individual overlapped peaks. Additionally, the presence of Fermi resonances can also increase the complexity of the NIR spectra. Therefore, many band assignments can only be tentative or unresolved which limits the usefulness of the NIR region. Fortunately, the emergence of statistical methods has allowed qualitative and quantitative information to be obtained from complex NIR spectra [12, 13]. Since the introduction of these statistical analyses, the development of various mathematical techniques and the wide availability of software have contributed to the tremendous expansion and to the current state of popularity of NIR spectroscopy.

4.2 Infrared Spectroscopy

Of the different types of energies a molecule possesses, the vibration of its atoms with respect to each other has the next larger energy level spacing after the rotation of molecules. The atoms in molecule do not remain in fixed relative positions, but vibrate about their mean position, i.e. they execute different types of vibrational motion. The energy of most of these molecular vibrations is quantized and corresponds to that of the infrared region of the electromagnetic spectrum. When infrared radiation of the same frequency is allowed to fall on the molecule the system absorbs energy, causing the excitation of the molecule to higher vibrational levels. When a molecule absorbs radiation, its energy increases in proportion to the energy of the photon, and can be expressed as

$$\Delta E = h \nu = \frac{hc}{\lambda} \quad (1)$$

where, h is Planck's constant, ν the frequency of radiation, λ the wavelength of radiation and c the velocity of light. Considering molecule as an assembly of nearly independent structural units, one could consider IR spectrum of a molecule as a combination of sets of bands associated with the different groups. The absorption of IR radiation (quantised) causes the various bonds in a molecule to stretch and bend with respect to one another.

Once the vibrational frequencies are obtained, valuable information regarding molecular structure, symmetry, bond strength, inter and intramolecular interactions, etc. can be derived. There are two types of spectroscopy that involve vibrational transitions – Infrared Spectroscopy and Raman Spectroscopy. A mode of vibration of molecules will be infrared active if dipole moment changes during the vibration. On the other hand a mode of vibration will be Raman active if polarizability changes during the corresponding vibration [3, 8]. Infrared spectroscopy gives considerable information on the structural features and provides fingerprints of molecules. The IR region of the electromagnetic spectrum is considered to cover the range from 50 to 12,800 cm^{-1} approximately. It is subdivided into near infrared (12,800 – 4000 cm^{-1}), middle infrared (4000 – 400 cm^{-1}) and far infrared (400 – 50 cm^{-1}) regions. The middle IR is the region most commonly employed for standard laboratory investigations as it covers most of the vibrational transitions. The far IR is also important when we deal with solid samples.

The infrared spectrum of a molecule consists of two major regions, the group frequency region and finger print region. Group frequencies are vibrations that are associated with certain structural units such as $-\text{CH}_3$, $-\text{NH}_2$, $-\text{OH}$, etc. and appear fairly at constant regions in the spectrum. The region 900 – 1450 cm^{-1} is very rich in absorption bands and contains mainly bending and certain stretching vibrations. A molecular or structural moiety may often be identified by the assignments of the bands in this region. Though molecules having similar groups show very similar

spectra outside this region, they show bands typical of the molecule in this region. Hence the name finger print region. The factors affecting group vibrations are

(1) Internal factors involving changes in atomic mass, vibrational coupling resonance field effects, hydrogen bonding, etc.

(2) External factors involving physical state (gas, liquid, solid, solution, solvent and concentration) and temperature. Often one factor is isolated from the rest, so that its influence upon one particular group frequency can be studied along with intensities.

4.3 Vibrational Energy of a Diatomic Molecule

At ordinary temperatures, organic molecules are in a constant state of vibration, each bond having its characteristic stretching and bending frequency, and being capable of absorbing light of that frequency. The vibrations of atoms joined together by a chemical bond can be likened to the vibrations of two balls joined by a spring. Using this analogy, we can rationalise several features of infrared spectra.

4.3.1 The Simple harmonic oscillator

Consider the vibrations of a system of two masses m_1 and m_2 connected by a spring. If the spring is compressed and released, the system executes simple harmonic motion with fundamental frequency ω_{osc} of the harmonic oscillator with masses replaced by the reduced mass μ of the system .

$$\omega_{osc} = \frac{1}{2\pi} \sqrt{\frac{k}{\mu}} \text{ Hz} \quad (2)$$

where k is the force constant and

$$\mu = m_1 m_2 / m_1 + m_2 \quad (3)$$

Quantum mechanically, the vibrational energy of such a harmonic system is given by

$$E_v = \left(v + \frac{1}{2}\right) h\omega_{osc} \text{ joules} \quad (4)$$

where $v = 0, 1, 2, \dots$ is the vibrational quantum number. Expressing energy in cm^{-1} , we get

$$\epsilon_v = \frac{E_v}{hc} = \left(v + \frac{1}{2}\right) \frac{\omega_{\text{osc}}}{c} = \left(v + \frac{1}{2}\right) \bar{\omega}_{\text{osc}} \quad (5)$$

where $\bar{\omega}_{\text{osc}}$ is the frequency in cm^{-1} . These energy levels are equally spaced and the energy of the lowest state ($v = 0$) is given by

$$\epsilon_0 = \frac{1}{2} \bar{\omega}_{\text{osc}} \quad \text{cm}^{-1} \quad (6)$$

is called the zero point energy. That is, the vibrational energy is not zero even at the lowest vibrational level. The selection rules which state which transitions are active or allowed can be deduced from the examination of the transition moment given by the expression

$$P_{v' \rightarrow v''} = \int \psi_{v'}^* \epsilon \psi_{v''} d\tau \quad (7)$$

where $\psi_{v'}$ and $\psi_{v''}$ are the wave functions of the v' and v'' states (the * indicates the complex conjugate of $\psi_{v'}$) and ϵ is the dipole moment which may be expressed as a linear function of x for small displacements about the equilibrium configuration.

$$\epsilon = \epsilon_0 + \left(\frac{d\epsilon}{dx}\right)x \quad (8)$$

where ϵ_0 is the dipole moment at the equilibrium internuclear distance. The transition moment for the transition $v'' \rightarrow v'$ may be calculated by substitution of the appropriate wave functions and dipole moment [equation (8)] into equation (7). Transitions are allowed for a non-zero value of the transition moment. This occurs if the vibration is accompanied by a dipole moment change which implies that only heteronuclear diatomic molecules will exhibit vibrational spectral transition. In the quantum mechanical harmonic oscillator, a further restriction concerns the vibrational quantum number which can change only by one unit, i.e. $\Delta v = \pm 1$. Therefore, transitions are allowed only if $\left(\frac{d\epsilon}{dx}\right) \neq 0$.

From the Boltzmann distribution, most molecules at room temperature exist in the ground vibrational level $v = 0$ and consequently the allowed transition

$v = 0 \rightarrow v = 1$, called fundamental transition, dominates the infrared absorption spectrum. This transition is responsible for most of the infrared absorptions of interest to a chemical spectroscopist.

The other allowed transitions such as $v = 1 \rightarrow v = 2$, $v = 2 \rightarrow v = 3$, etc. originate from vibrationally excited levels ($v \neq 0$). The corresponding bands are much weaker than the fundamental absorption band. Their designation as “hot bands” comes from the fact that the excited levels have a relatively low population and increasing temperature will increase this population and thus, the intensity of the bands. For the harmonic oscillator, the transitions giving rise to the hot bands have the same frequency as that of the fundamental transition. Applying the selection rule $\Delta v = \pm 1$ we get,

$$\epsilon_{v \rightarrow v+1} = (v+1 + \frac{1}{2})\bar{\omega}_{\text{osc}} - (v + \frac{1}{2})\bar{\omega}_{\text{osc}} = \bar{\omega}_{\text{osc}} \text{ cm}^{-1} \quad (9)$$

Thus the transition between any two neighboring states will give rise to the same energy change and the wave number of the spectral line is given by

$$\bar{\nu}_{\text{spectroscopic}} = \epsilon_{v \rightarrow v+1} = \bar{\omega}_{\text{osc}} \text{ cm}^{-1} \quad (10)$$

Thus the vibrating molecule will absorb energy only from the radiation with which it can coherently interact and this must be radiation of its own oscillation frequency. But real molecules do not obey exactly the laws of simple harmonic motion since the molecular vibrations are anharmonic.

4.3.2 Anharmonicity

Two experimental observations give evidence that molecules are not ideal oscillators. First, the hot bands do not have exactly the same frequency as the fundamental band, which comes from the fact that the vibrational energy levels are no longer equally spaced. Second, overtones transitions such as $v = 0$ to $v = 2, 3, 4$, etc. are allowed. This deviation from harmonic behaviour may be expressed by two effects [11, 14].

The first effect called mechanical anharmonicity, arises from the effect of cubic and higher terms in the potential-energy expression

$$V = \frac{1}{2}kx^2 + k'x^3 \dots\dots\dots k' \ll k \quad (11)$$

The above expression is used in the Schrodinger equation to deduce the energy levels of the allowed states of the anharmonic oscillator. The solution is obtained by an approximation or perturbation method and leads to energy levels (in cm^{-1}) as described in section 4.3.3.

The second effect called electrical anharmonicity is responsible for the appearance in the infrared spectra of overtones corresponding to transitions between energy levels differing by two or three vibrational quantum number units ($\Delta v = +2, +3, \dots$). The electrical anharmonicity arises from the effect of square and higher terms in the dipole-moment expression

$$\epsilon = \epsilon_0 + \left(\frac{d\epsilon}{dx} \right) x + \frac{1}{2} \left(\frac{d^2\epsilon}{dx^2} \right) x^2 + \dots\dots\dots (12)$$

As it can be seen in the following section 4.3.3 for the anharmonic oscillator, the frequencies of the overtone absorptions are not exactly 2, 3, ... times that of the fundamental absorption. On the other hand, on account of the mechanical anharmonicity, the frequency of the hot bands is less than that of the fundamental transition.

Deviation from the harmonic approximation is generally referred to as anharmonicity. Anharmonicity then must account for the fact that at large internuclear distances the vibrational potential varies more slowly than quadratically with distance and eventually becomes constant at the dissociation energy of the oscillator. The effects of anharmonicity will be to reflect this change in potential and, as a result, to destroy the purely Hermite polynomial character of the vibrational wave functions. The physical manifestations of anharmonicity are that transitions, forbidden in a

purely harmonic approximation, become allowed to some extent. Also, dissociation and chemical reactions involving bond breaking become possible.

4.3.3 The Anharmonic oscillator

Real bonds, although elastic, are not so homogenous as to obey Hooke's law. If the bond between atoms is stretched, for instance, there comes a point at which it will break and the molecule dissociates into atoms [3]. In diatomic molecules, the actual potential energy curve is not of simple harmonic type but is generally modelled by the Morse function [15]. Morse potential is given by

$$U = D_e [1 - \exp\{a (r_{eq} - r)\}]^2 \quad (13)$$

where D_e is the dissociation energy, 'a' is a constant for the given molecule and r_{eq} is the internuclear distance at the minimum energy. This potential energy function is called the Morse function. Fig. 4.1 shows the shape of the energy curve for a typical diatomic molecule, together with the ideal, simple harmonic parabola (dashed). With the potential in the above equation, the Schrodinger equation of an anharmonic oscillator gives the allowed vibrational energy eigen values as

$$\epsilon_v = (v + \frac{1}{2})\bar{\omega}_e - (v + \frac{1}{2})^2 x_e \bar{\omega}_e + (v + \frac{1}{2})^3 y_e \bar{\omega}_e \quad (14)$$

Here $\bar{\omega}_e$ is the oscillation frequency of the anharmonic system in cm^{-1} , x_e and y_e are anharmonicity constants which are very small and positive for band stretching vibrations. Retaining the first anharmonic term, we get

$$\epsilon_v = (v + \frac{1}{2})\bar{\omega}_e - (v + \frac{1}{2})^2 x_e \bar{\omega}_e \quad \text{cm}^{-1} \quad (15)$$

As x_e is positive, the effect of anharmonicity is to crowd more closely the vibrational levels. These energy levels are shown in Fig. 4.2. With increasing value of v the separations of adjacent levels decreases and become zero at the limit of dissociation. The exact zero point energy is obtained by substituting $v = 0$ in equation (11). Thus we get

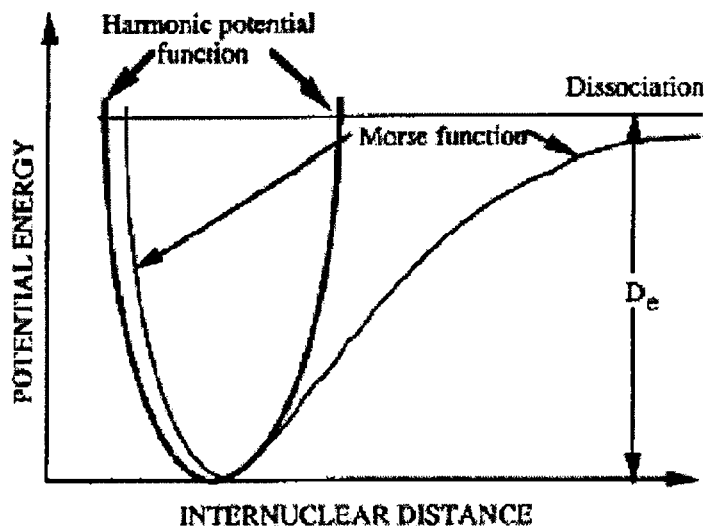


Fig. 4.1. Harmonic and Anharmonic potential functions for a diatomic oscillator.

$$\epsilon_0 = \frac{1}{2} \left(1 - \frac{1}{2} x_e\right) \bar{\omega}_e \quad (16)$$

The spectroscopic dissociation energy D_e is the sum of the chemical dissociation energy D_0 and the zero point energy ϵ_0 .

Rewriting equation (11)

$$\epsilon_v = \bar{\omega}_e \left\{1 - x_e \left(v + \frac{1}{2}\right)\right\} \left(v + \frac{1}{2}\right) \quad (17)$$

and equating this to equation (5) of simple harmonic oscillator we get

$$\bar{\omega}_{\text{osc}} = \bar{\omega}_e \left\{1 - x_e \left(v + \frac{1}{2}\right)\right\} \quad (18)$$

Thus the anharmonic oscillator behaves like the harmonic oscillator but with an oscillation frequency that decreases with increasing v . If we set $v = -\frac{1}{2}$, then $\epsilon_v = 0$

and $\bar{\omega}_e = \bar{\omega}_{osc}$. Therefore $\bar{\omega}_e$ is considered as the (hypothetical) equilibrium oscillation frequency of the anharmonic system. The selection rules for the anharmonic oscillator are found to be $\Delta v = \pm 1, \pm 2, \pm 3$, etc. But due to intensity considerations we will restrict ourselves to the following three transitions.

1. $v = 0 \rightarrow v = 1$, $\Delta v = +1$, with considerable intensity.

$$\begin{aligned} \Delta \epsilon &= \epsilon_{v=1} - \epsilon_{v=0} \\ &= \left(1 + \frac{1}{2}\right) \bar{\omega}_e - x_e \left(1 + \frac{1}{2}\right)^2 \bar{\omega}_e - \left\{ \frac{1}{2} \bar{\omega}_e - \left(\frac{1}{2}\right)^2 x_e \bar{\omega}_e \right\} \\ &= \bar{\omega}_e (1 - 2x_e) \text{ cm}^{-1} \end{aligned} \quad (19)$$

2. $v = 0 \rightarrow v = 2$, $\Delta v = +2$, with small intensity.

$$\begin{aligned} \Delta \epsilon &= \left(2 + \frac{1}{2}\right) \bar{\omega}_e - x_e \left(2 + \frac{1}{2}\right)^2 \bar{\omega}_e - \left\{ \frac{1}{2} \bar{\omega}_e - \left(\frac{1}{2}\right)^2 x_e \bar{\omega}_e \right\} \\ &= 2\bar{\omega}_e (1 - 3x_e) \text{ cm}^{-1} \end{aligned} \quad (20)$$

3. $v = 0 \rightarrow v = 3$, $\Delta v = +3$, with normally negligible intensity.

$$\begin{aligned} \Delta \epsilon &= \left(3 + \frac{1}{2}\right) \bar{\omega}_e - x_e \left(3 + \frac{1}{2}\right)^2 \bar{\omega}_e - \left\{ \frac{1}{2} \bar{\omega}_e - \left(\frac{1}{2}\right)^2 x_e \bar{\omega}_e \right\} \\ &= 3\bar{\omega}_e (1 - 4x_e) \text{ cm}^{-1} \end{aligned} \quad (21)$$

These three transitions are shown in Fig. 4.2. To a good approximation, since $x_e \approx 0.01$, the three spectral lines lie very close to $\bar{\omega}_e$, $2\bar{\omega}_e$, and $3\bar{\omega}_e$. The line near $\bar{\omega}_e$ is called the fundamental absorption, while those near $2\bar{\omega}_e$ and $3\bar{\omega}_e$ are called the first and second overtones, respectively.

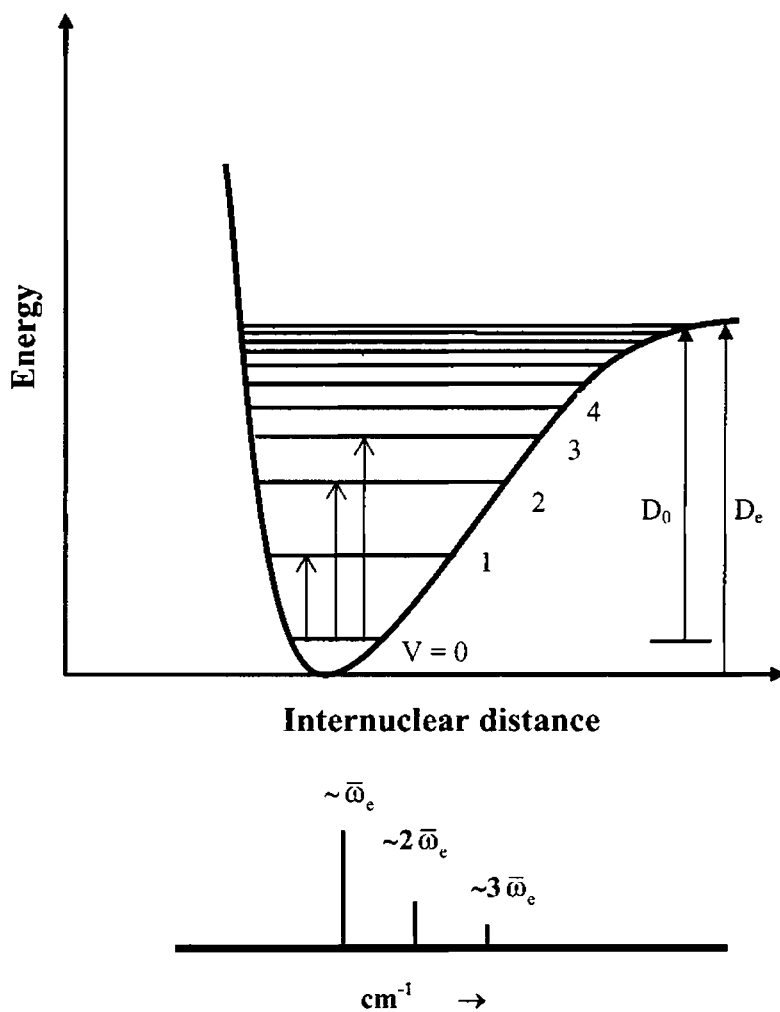


Fig. 4.2. Vibrational energy levels, associated transitions and spectrum for a diatomic molecule undergoing anharmonic oscillations

4.4 Normal Modes of Vibration of Polyatomic Molecules

The standard treatment for the problem of the vibrational motion of a polyatomic molecule begins with the assumption that the vibrational amplitudes are infinitesimal, which implies that the potential energy is a purely quadratic function of the vibrational coordinates [2, 16]. Then the problem can be reduced to that of a set of uncoupled oscillators, which is elementary. The total vibrational energy equals the

sum of the energies of the simple harmonic oscillations or normal modes. The concept of a normal mode plays an important part in vibrational theory whether for molecules, musical instruments or engineering structures. A molecule containing N atoms will have $(3N-6)$ vibrational degrees of freedom ($3N-5$ for linear molecules). The number of vibrational degrees of freedom gives the number of fundamental vibrational frequencies of the molecule or the number of different "normal" modes of vibration. A normal mode of vibration of a given molecule corresponds to internal atomic motions in which all atoms move in phase with the same frequency but with different amplitudes. Each normal mode of vibration is equivalent to a quantum mechanical harmonic oscillator with characteristic frequency. During a normal vibration, the center of gravity of the molecule remains unchanged. Any general vibrational motion of a molecule can be considered as a superposition of $(3N-6)/(3N-5)$ normal modes of vibrations.

The vibrating polyatomic molecule may be considered, in a good approximation, as a superposition of $(3N - 6)$ simple harmonic motions. The vibrational energy of the molecule would be given by

$$G(v_1, v_2, v_3, \dots) = \sum_i \bar{\omega}_i \left(v_i + \frac{1}{2} \right) \quad (22)$$

Here $\bar{\omega}_i$ are the vibrational frequencies measured in cm^{-1} units and v_1, v_2, v_3 , etc. are the vibrational quantum numbers corresponding to the normal vibrations. Taking into account the anharmonicity terms (higher than quadratic terms, cubic, quartic...) leads to a vibrational energy which is no longer a sum of independent terms corresponding to the different normal vibrations but contains cross terms containing the vibrational quantum numbers of two or more normal vibrations. In the general case of polyatomic molecules (without degenerate vibrations) the solution of the Schrodinger equation gives the vibrational term values

$$\sum_i G(v_i) = \sum_{i < j} \bar{\omega}_i \left(v_i + \frac{1}{2} \right) + \sum_{i < j} X_{ij} \left(v_i + \frac{1}{2} \right) \left(v_j + \frac{1}{2} \right) \quad (23)$$

where $\bar{\omega}_i$ are the fundamental vibration wave numbers for infinitely small displacements from the equilibrium configuration. The X_{ij} are anharmonic constants.

4.5 Features of NIR Spectra of Polyatomic Molecules

4.5.1 Overtones and combination frequencies

Overtones and combination bands are the heart of NIR spectroscopy and the key quantity which determines the occurrence and the spectral properties (frequency, intensity) of the NIR bands is anharmonicity. When the restriction to simple harmonic motion is lifted we have again, as in the case of diatomic molecule the possibility of first, second, etc. overtones occurring at frequencies near $2\nu_1, 3\nu_1, \dots, 2\nu_2, 3\nu_2, \dots, 2\nu_3, 3\nu_3$, etc. where each ν_i is a fundamental mode [3]. The intensities fall off rapidly. However, in addition, the selection rules permit combination bands and difference bands also. The former arises simply from the addition of two or more fundamental frequencies or overtones. Such combinations as $\nu_1 + \nu_2, 2\nu_1 + \nu_2, \nu_1 + \nu_2 + \nu_3$, etc., become allowed, although their intensities are normally very small. Similarly the difference bands, for example, $\nu_1 - \nu_2, 2\nu_1 - \nu_2, \nu_1 + \nu_2 - \nu_3$, etc. have small intensities but are often to be found in a complex spectrum. Symmetry considerations may restrict the number of allowed transitions. On the other hand, all normal vibrations are infrared active in unsymmetrical molecules.

4.5.2 Fermi resonance

The intensities of overtones or combination bands may sometimes be considerably enhanced by a resonance phenomenon. Such a resonance may occur between an overtone or a combination band which happens to have the same symmetry and nearly the same frequency as that of a fundamental vibration. This accidental degeneracy called Fermi resonance leads to two relatively strong bands of about the same intensity rather than one strong band for the fundamental. Here the overtone has gained intensity at the expense of the fundamental. The two bands are observed at somewhat higher and lower frequencies than the expected unperturbed positions of

the fundamental and overtone (or combination). Here the two close molecular vibrational frequencies, a fundamental and an overtone or a combination frequency, resonate and exchange energy - the phenomenon being known as Fermi resonance [1, 2, 16].

4.5.3 Darling–Dennison resonance

A rather less common resonance occurring between close-lying vibrational energy levels of the same symmetry is Darling-Dennison resonance [17-19]. This is most likely to be encountered when the first overtones of two different vibrations, having different symmetries, are of similar energies. This type of resonance occurs in water. H_2O is a non-linear symmetrical molecule exhibiting three normal modes of vibration: ν_1 (symmetrical stretch at 3657 cm^{-1}), ν_2 (bending vibration at 1595 cm^{-1}) and ν_3 (antisymmetric stretch at 3756 cm^{-1}). The two stretching modes ν_1 and ν_3 have similar wavenumbers but belong to different symmetry species and therefore cannot interact directly. However the symmetries of their first overtone levels ($\nu = 2$ of ν_1 and $\nu = 2$ of ν_3) are the same. These levels are expected to be fairly close together, giving rise to a Darling-Dennison resonance. In a similar way to a Fermi resonance, the effect is to push up in energy the higher of the two levels and to push down the lower.

4.6 Local Mode Model

The conventional normal mode description of molecular vibrations, which is generally used in the frequency region characteristic of the fundamental vibrations and low quanta overtone and combination modes is inefficient at high vibrational energies. An alternative approach involving the concept of 'local' vibrational modes has been applied to bond stretching vibrations involving only hydrogen or deuterium stretching modes. Bonds with the highest anharmonicity are those involving hydrogen, the lightest of atoms. These bonds, which vibrate at high energy and with large amplitude when undergoing stretching motion, carry the most intensity. The main idea of the local mode model is to treat a molecule as if it was made up of a set of equivalent diatomic oscillators and the reason for local mode behaviour at high

energy may be understood as follows. As the stretching vibrations become more highly excited, the anharmonicity ($X = x_e \bar{\omega}_e$) term which increases as v^2 , tends to dominate the effect of the interbond coupling which is only v dependent, giving rise to uncoupled vibrations and thus local mode behaviour [11]. The cause of this decoupling is the strong bond anharmonicity which can in certain cases quench any interbond coupling term. Experimentally, it is found that a switch from normal to local mode character occurs for high energy transitions corresponding to $\Delta v \geq 3$. The important parameter which gives rise to "near-normal" or "near-local" behaviour is the ratio of coupling strength to bond anharmonicity.

For the description of higher excited vibrational levels, the local mode model (LM) introduced by Henry and Siebrand is used [14, 20-22]. In their attempt to model nonradiative electronic transition in polyatomic molecules they found a semi-quantitative agreement between the anharmonicity parameter in the Franck-Condon factors and the known anharmonicity of the CH molecule. This led the authors to find the relation between the CH anharmonicity constant in the CH molecule and that in a hydrocarbon molecule. The local mode is the outcome of these investigations.

Very large vibrational amplitudes correspond to dissociation. In diatomic molecules, there is a clear-cut relation between the anharmonicity constant X and the dissociation energy D . When Morse potential is the actual vibrational potential, the relation takes the following form

$$X = \frac{\omega^2}{4D} \quad (24)$$

If we continually pump energy into the vibrational motions of a molecule, dissociation will be produced, which is a distinctly nonharmonic phenomenon. Moreover, intuition suggests that the molecule will follow low-energy pathways to dissociation. These pathways are unlikely to be those along normal coordinates. Consider, for example, the CH stretching motions of benzene. Dissociation along the normal coordinates Q_i associated with the totally symmetric stretching mode requires

the simultaneous breaking of all six CH bonds, a prohibitively high-energy process. The rupture of one or two CH bonds is more likely.

In polyatomic molecules the relation between normal mode anharmonicity constants X_{KL} , bond dissociation energies D_i and normal mode dissociation energies D_k , is not obvious. For those normal modes in which the vibrational energy is evenly distributed among a number of equivalent chemical bonds, the dissociation energy D_k refers to the sum of all bond energies D_i , so that $D_k = \sum D_i$. This implies a large value of D_k and thus a small value of the diagonal normal mode anharmonicity constant X_{kk} . As mentioned earlier the physically important dissociation is the rupture of a single chemical bond. The vibration associated with this rupture is not a normal mode but it is termed as a local mode. Its dissociation energy is much smaller than the normal mode dissociation energy; $D_i \ll D_k$ so that the corresponding anharmonicity constant X_{ii} will be much larger than X_{kk} . In other words for high vibrational quantum levels, the vibrational energy becomes increasingly more diagonal in a local mode representation than in a normal mode representation, so that the molecule oscillates in a pattern close to a local mode rather than a normal mode.

A familiar example of a local mode oscillator is a bond vibration with a frequency so disparate from others in the molecule that it is effectively uncoupled from other degrees of freedom, such as X-H stretching modes where X = C, N, O, etc.[23]. The principal bands in the spectra correspond to excitation of X-H stretching motion with all of the energy localized in a single X-H stretching oscillator. In the local mode representation the energy of the oscillator can be described [24, 25] by

$$E = E_0 + \sum_i v_i \omega_i + \sum_{i \geq j} c_{ij} \omega_{ij} + \sum_{i \geq j} v_i v_j X_{ij} \quad (25)$$

where v_i and ω_i are the vibrational quantum number and the harmonic frequency associated with local mode i . The X_{ij} correspond to local mode anharmonicity constants and the ω_{ij} are the harmonic coupling terms. If we are dealing with nearly degenerate oscillators, like a molecular set of CH stretching oscillators, then ω_{ij} are

small and can be neglected. When a single local oscillator is excited from the vibrational ground state ($v = 0$) to the vibrational state v , then the transition energy of the local mode overtone is given by Ellis [26, 27], by employing the Morse oscillator wave functions, as

$$\Delta\varepsilon_{0 \rightarrow v} = A v + B v^2 \quad (26)$$

A plot of $\Delta\varepsilon/v$ versus v will yield A , the local mode frequency as the intercept and B , the local mode diagonal anharmonicity as the slope. Here $A - B$ gives the mechanical frequency X_1 of the oscillator and $B = X_2$ is the anharmonicity of the bond. Here X_1 and X_2 are the spectroscopic parameters $\bar{\omega}_e$ and $x_e \bar{\omega}_e$ respectively. The local mode parameters X_1 and X_2 vary for non-equivalent X-H bonds and are sensitive to the inter and intra molecular environment of the X-H oscillator.

The local mode model has been widely used for the interpretation of overtone spectra of a wide variety of molecules [28-39], which will be discussed briefly in section 4.8. After the observations on a number of molecular systems Henry and co-workers have proposed the following empirical rules related to overtone spectra.

1. Local mode overtones involving high frequency oscillators are most intense but fall off rapidly in intensity with increasing vibrational quantum number.
2. Local-local and local-normal combinations occur generally with much less intensity than pure local mode overtones.
3. Combination bands fall off more quickly in intensity than do the pure overtones with increase in quantum number.

4.7 Quantum Mechanical Description of LM Model

Swofford et al. [40] gave a quantum mechanical description of the one-dimensional appearance of CH overtone spectra with particular application to benzene. They assumed that the vibrational Hamiltonian operator \hat{H} for the $(3N-6)$ molecular space is divided into a subspace of dimension S having coordinates R_1, \dots, R_S within

which \hat{H} is partitionable to one-dimensional Hamiltonians, and the remaining space $S' = (3N-6-S)$ is unpartitionable. We then write

$$\hat{H} = \sum_{j=1}^S \hat{H}_j + \hat{H}_{S'} \quad (27)$$

$$\text{with } \hat{H}_j = \frac{1}{2} g_{jj} P_j^2 + V_j(R_j) \quad (28)$$

$\hat{H}_{S'}$ is the Hamiltonian for the unpartitionable space. P_j are conjugate to R_j . The g_{jj} are the diagonal elements of the g matrix for the S coordinate system. For separability not only the S dimensional block in g matrix be diagonal but the variation of $|g|$ with respect to R_1, \dots, R_S also be negligible.

Once the Hamiltonian is partitioned the k^{th} molecular eigen state $|\psi_k\rangle$ is characterized by a set of quantum numbers $v_j(k)$ each belonging to a subspace.

$$\hat{H} |\psi_k\rangle = E_k |\psi_k\rangle \quad (29)$$

$$\text{with } |\psi_k\rangle = \prod_j |\phi_{v_j}(k)\rangle \quad (j=1 \dots S, S') \quad (30)$$

$$\text{and } \hat{H}_j |\phi_{v_j}(k)\rangle = E_{v_j}(k) |\phi_{v_j}(k)\rangle \quad (31)$$

The energy of the k^{th} state is given by

$$E_k = \sum_j E_{v_j}(k) \quad (32)$$

Any operator \hat{O} which can be partitioned in the same subspace such that

$$\hat{O} = \sum_j \hat{O}_j(R_j) \quad (33)$$

then $\langle \psi_k | \hat{O} | \psi_l \rangle \neq 0$ is possible only when $v_j(k) = v_j(l)$ for all j but one. Thus if the electric dipole moment operator (belongs to the class of operators like \hat{O}) is

separable in the same subspace as the Hamiltonian then electric dipole transitions which couple the ground state (all $v_j=0$) and excited states containing excitations ($v_j \neq 0$) in more than one coordinate of the partitioned space are forbidden. That is electric dipole moment operator couples ground state with only one of the coordinate in the excited state. Thus light incident on an unexcited state leads to excited states in only one local mode at a time. Thus the LM predicts a unique single state excitation at all ν . The workers verified that, in the case of benzene, the spectroscopic energies of these single state excitations are given by equation (26). In a later study, these authors further demonstrated the validity of the local mode model by comparing the fifth overtone band of benzene and benzene- d_5 . No significant difference in band shape or peak energy are observed for the two molecules in contrast to the predictions of the strongly coupled normal mode model. On the other hand, LM model predicts a similarity in the two spectra as observed experimentally.

4.8 Applications of Overtone Spectroscopy and Local Mode Model

Overtone spectroscopy and local mode model provide a valuable probe of molecular structure and conformation [41]. The model of local modes is used for the spectroscopic assignment and interpretation, an essential first step towards understanding the nature of vibrationally excited molecular motions. The most prominent bands in the near infrared are overtones and combination tones of O-H, N-H, C-H and S-H stretching vibrations and stretching-bending combinations [42]. Numerous cases of Fermi and higher anharmonic resonances occur in this region. The knowledge of the frequencies of such overtones and combination tones is necessary to determine anharmonicity and anharmonic coupling constants which might make possible to gain knowledge of the potential functions ruling these vibrations.

The most important application of overtone spectroscopy is the characterization of CH bonds in organic compounds. The CH stretching overtone spectra are characterized by one peak for each of the non-equivalent oscillators in a molecule and can be interpreted within the local mode model of molecular vibrations [33]. The infrared spectral study of vibrational fundamentals generally does not give

information on the influence of environment on a particular CH oscillator. There are a number of additional advantages for overtone spectral studies. First is the practical reason that one can avoid dependence on deuterated samples, which are often not readily available and also difficult to prepare. The overtone bands are quite well resolved even for very similar oscillators. Second, the CH stretching parameters obtained from fitting a number of sequential overtones for each local mode oscillator promise higher precision than single measurements in the infrared. Finally the overtone spectra also gives the anharmonicity values of the local mode oscillators, which determine the shape of the corresponding potential curves, whereas the infrared fundamentals of deuterated samples give only the frequencies of isolated CH bonds.

The local mode parameters X_1 and X_2 are characteristics of the particular CH oscillator and thus give rise to distinct absorption peaks corresponding to the distinct non-equivalent CH oscillators in the molecule. The non-equivalence of CH oscillators can arise from different reasons. The alkyl and aryl CH bonds are non-equivalent due to the difference in the states of carbon hybridization. Non-equivalent primary, secondary and tertiary CH bonds are present in alkanes. Conformational origin, inter and intramolecular environmental origin, etc. also causes non-equivalence among CH bonds.

The local mode description has been successfully applied to explain high overtone spectra of CH stretching modes of benzene [40, 43, 44]. The overtone spectrum of benzene shows no indication of the large number of excited vibrational states which are predicted on the basis of the normal mode or harmonic model. On the other hand, the benzene spectrum can be accurately described by the use of the LM model, as shown by Swofford et al. [40]. The success of the simple model stems from its ability to include the more realistic anharmonic potential function for the highly excited CH oscillator by using an internal coordinate system centred on the individual C-H bonds.

Overtone spectroscopy, through the local mode model, can be used to determine CH bond lengths in substituted aromatic molecules. These highly accurate bond

lengths correlate remarkably well with geometry-optimized *ab initio* MO calculations. Hayward and Henry in 1976 have shown that there is a very good correlation between the isolated (by selective deuteration) fundamental frequency and the CH stretching frequencies obtained from a local mode analysis of the overtone spectra of the undeuterated molecules [25]. Subsequently, Mizugai and Katayama [45] in liquid phase studies, and Wong and Moore [46] and Gough and Henry [32,47] in gas phase studies, have noted a correlation between CH overtone frequencies and CH bond lengths that holds over a wide variety of molecules. These overtone frequencies are a particularly sensitive probe of CH bond length changes. At $\Delta\nu_{\text{CH}} = 6$ a bond length change of .001 Å corresponds to a frequency shift of 69 cm^{-1} . Such shifts are easily measurable in gas phase overtone spectra. These spectral studies are more convenient in the sense that the difficult synthetic procedures involved with the selective deuteration process of McKean and collaborators [48, 49] are not required. In the analysis of bond length changes in substituted aromatic molecules the following relationship suggested by Gough and Henry [47] is used.

$$r_{\text{CH}}^{\text{LM}} (\text{Å}) = 1.084 - \left[\frac{\Delta\bar{\nu}}{11\Delta\nu_{\text{CH}}} \right] 0.001 \quad (34)$$

Here CH bond lengths of substituted benzenes are determined from the CH bond length in benzene (1.084 Å), and $\Delta\bar{\nu}(\text{cm}^{-1})$ is the overtone frequency shift from benzene for a given overtone $\Delta\nu_{\text{CH}}$. Here, actually the overtone spectral shifts measure the bond length changes.

In molecules which contain non-equivalent CH bonds, one can observe at every overtone a number of absorption peaks, each of which is explained as the excitation of an individual CH oscillator belonging to one of the types of CH bonds in the molecule. In toluene and xylene well resolved absorption peaks are seen which are assigned as the local mode excitation of either an alkyl or an aryl CH oscillator [25, 50]. Overtone spectroscopy is also used in assigning primary, secondary or tertiary CH oscillators in the normal and branched alkanes [29]. Axial and equatorial

environment of CH bonds in the cycloalkanes can also affect the overtone positions [51].

The results on the studies of toluenes, fluorotoluenes and xylenes show two sets of peaks [32, 33, 52]. The set at higher frequency corresponds to aryl CH bonds. The set at lower frequency corresponds to the methyl CH bonds. Two peaks are observed in the methyl region with an area ratio (low to high frequency) of approximately 2:1. The lower intensity, higher frequency peak is associated with the planar methyl CH, and the lower frequency peak is associated with the two methyl CH bonds at 60° .

The influence of mass, electronegativity and steric effect of halogens have been revealed by studies on halomethanes and allyl chloride [53-55]. Pross and Henry and Rong et al. carried out torsional barrier studies of 2-, 3- and 4-methyl substituted pyridines from their overtone spectra [56, 57].

The development of laser based techniques like thermal lensing spectroscopy and intracavity dye laser photoacoustic spectroscopy have produced dramatic improvements in resolution and application of overtone spectroscopy [45, 58-60].

Vibrational overtone spectroscopy is an effective tool in studying inter and intramolecular hydrogen bonding also. Since we have used vibrational overtone spectroscopy as an effective tool in hydrogen bonding studies, a qualitative idea of hydrogen bonding as well as some relevant applications of overtone spectroscopy are discussed in the following section. The rich literature available on overtone absorption spectroscopy itself is an evidence for its use as a valuable probe of molecular structure and conformation.

4.9 Hydrogen Bonding and Overtone Spectroscopy

The Hydrogen bond plays a very important role in our daily lives. For example, it is primarily responsible for the structure of the proteins and in determining the shape of nucleic acids. It is a big factor in the action of adhesives, in the binding of many dyes and in determining the properties of water. The widespread occurrence and importance of hydrogen bonds have made them an active topic. The published

definitions of the hydrogen bonds are many. The general definition of hydrogen bond by Pimental and McClellan [61] is "A hydrogen bond exists between the functional group, A-H, and an atom or group of atoms, B, in the same or different molecules when (a) there is evidence of bond formation, (b) there is evidence that this new bond linking A-H and B specifically involves a hydrogen atom already bonded to A". Hydrogen bonding is a donor-acceptor interaction specifically involving hydrogen atoms. Most frequently, a hydrogen bond is of A-H...B type, where A and B are electronegative elements and B possesses one or more lone electron pairs. The molecule providing a polar hydrogen for a hydrogen bond is called a donor (A-H). The molecule that provides the electron rich site to which the hydrogen is attracted is called an acceptor (B). All types of hydrogen bonds can be intramolecular (chelation) when donor and acceptor groups are on the same molecule or intermolecular (association) when they are on different molecules. When A and B are the same they are known as homonuclear hydrogen bonds, when different, heteronuclear hydrogen bonds. Very strong hydrogen bonds resemble covalent bonds, while very weak hydrogen bonds are close to van der Waals forces [62].

For studying hydrogen bonding spectroscopic, diffraction, thermochemical and theoretical methods are used. The spectroscopic methods include Infrared, Raman, N.M.R, etc. The infrared methods give information about hydrogen bonding from the spectra arising from transitions between the vibrational energy levels of the bonds involved in hydrogen bonding. The motion of the hydrogen atoms is greater than that of the heavier atoms to which they are covalently bonded. The formation of a hydrogen bond restricts the degree of vibrational motion, since the hydrogen atom is restrained by two bonds rather than one. A measure of the vibration of the A-H bonds is therefore a sensitive criterion of the formation and strength of hydrogen bonds. This is the basis for extensive use of IR spectroscopy for studying and classifying hydrogen bonds. The largest frequency change due to hydrogen bonding is observed in the A-H covalent bond stretching frequencies, and these changes are the most informative. Infrared spectroscopy provides insight into the potential energy surfaces

of the hydrogen bonds. When an A–H bond becomes involved in hydrogen bonding, the potential energy curve becomes broader, a second minimum develops and the A–H bond stretching vibrational levels become closer, as illustrated in Fig. 4.3 [63].

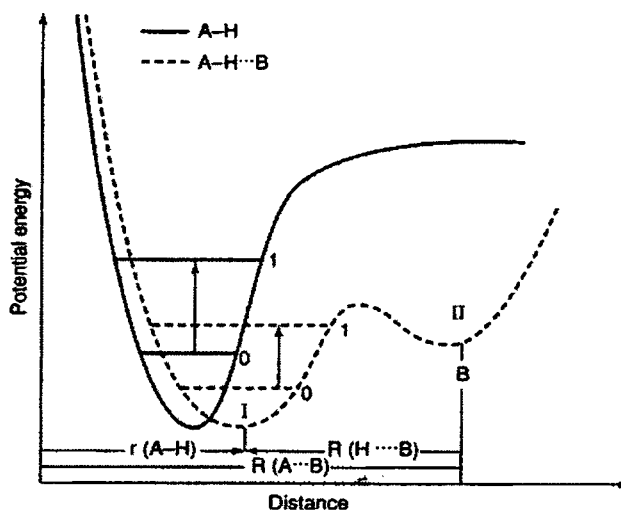


Fig.4.3 Qualitative potential energy curve for a free (—) and hydrogen-bond (---) A—H group (from Novak, 1974).

Hydrogen bonds having A, B = F, O and N are best studied [62,64,65]. The formation of the A–H...B hydrogen bond results in weakening of the A–H bond. This weakening is accompanied by bond elongation and a decrease of A–H stretch vibration frequency compared to the noninteracting species. This shift to lower frequencies is called a red-shift and represents the easily detectable manifestation of the formation of a hydrogen bond [66]. The presence of inter and intramolecular hydrogen bonding will be well reflected in the mechanical frequency and anharmonicity values. Since the existence of overtones is connected with anharmonicity, numerous studies were devoted to the effect of hydrogen bond formation on the anharmonicity of the potential function of vibrations affected by hydrogen bonding [67-69]. Shaji et al. [70] have analysed the overtone spectra of anilines and chloroanilines and established the presence of intramolecular bonding in o-chloroaniline. Eappen et al. [71] analysed the aryl CH and OH overtone spectrum of α -naphthol and found that there exists intramolecular hydrogen bonding

interaction between the hydroxyl group and aromatic nucleus. Rai et al. [72] studied the overtone spectra of aniline and its *ortho* and *meta* chloro derivatives at different concentrations. Vibrational frequencies and anharmonicity constants for the CH stretch vibration and for the symmetric and asymmetric NH stretch vibrations have been determined. The presence of intermolecular hydrogen bonding in all the three molecules and intramolecular hydrogen bonding involving N-H...Cl in *o*-chloroaniline have been detected. Chen and Hsu made investigations on a large number of five membered ring structures where intramolecular hydrogen bonding is present and found that the bonding strength is weaker compared to the six membered rings [73].

4.10 Present Work

In the following two chapters (chapter 5 & chapter 6) analyses of the near IR overtone spectra of a few amines and some hydrogen bonded systems are done. From the near infrared vibrational overtone absorption spectrum of liquid phase 2,6-dimethylaniline and 2,4-dimethylaniline, the aryl CH, methyl CH and NH local mode mechanical frequency values obtained are analysed and compared [74]. The near infrared vibrational overtone absorption spectra of cyclohexylamine and morpholine in carbon tetrachloride in different concentrations are examined. Free NH and bonded NH are located. The CH and NH local mode mechanical frequency values and anharmonicity values obtained from fitting the overtones are analysed and compared. Chapter 6 deals with the near IR overtone analysis of some hydrogen bonded systems. Overtone spectra of cyclohexanol in carbon tetrachloride in different concentrations are analysed using the local mode model. The aryl CH and free OH local mode parameters are almost insensitive to the variation in concentration. But the local mode parameters for the bonded OH stretching vibrations vary with concentration [75]. The near infrared vibrational overtone absorption spectra of cyclopentanol in liquid phase are examined. Due to hydrogen bonding in addition to free OH, a red shifted hydrogen bonded broad band appears in the spectrum. Near IR overtone spectrum of imidazole in carbon tetrachloride is analysed using the local mode model. Blue-shifted hydrogen bonded NH oscillators are observed. The mechanical anharmonicities of the bands are calculated using local mode model and analysed [76].

REFERENCES

- [1] G. Herzberg, Spectra of Diatomic Molecules, D. Van Nostrand Co., Inc., Canada, 1950.
- [2] G. Herzberg, Infrared and Raman Spectra of Polyatomic Molecules, D. Van Nostrand Co., Inc., Princeton, N.J., 1945.
- [3] C.N. Banwell, E.M. McCash, Fundamentals of Molecular Spectroscopy, Tata McGraw-Hill Publishing Company Ltd, New Delhi, 1995.
- [4] B.P. Straughan, S. Walker, Spectroscopy, (Vol.1 & Vol. 2), Chapman and Hall Ltd., London, 1976.
- [5] G.M. Barrow, Introduction to Molecular Spectroscopy, McGraw-Hill Kogakusha, Ltd., 1962.
- [6] W. Kemp, Organic Spectroscopy, ELBS/Macmillan Publishers Ltd., Hong Kong, 1975.
- [7] P.S. Kalsi, Spectroscopy of Organic Compounds, New Age International (P) Ltd., New Delhi, 1999.
- [8] G. Aruldhas, Molecular Structure and Spectroscopy, Prentice-Hall of India Pvt.Ltd., New Delhi, 2001.
- [9] B.S. Furniss, A.J. Hannaford, V. Rogers, P.W.G. Smith, A.R. Tatchell, Vogel's Text Book of Practical Organic Chemistry, ELBS/Longman Group Ltd., 1978.
- [10] A.M.C. Davies, Eur. Spectrosc. News 73 (1987) 10.
- [11] L. Bokobza, J. Near Infrared Spectrosc. 6 (1998) 3.
- [12] I. Ben-Gera, K.H. Norris, J. Food Sci. 18 (1968) 125.
- [13] I. Ben-Gera, K.H. Norris, J. Food Sci. 33 (1968) 64.
- [14] B.R. Henry, W. Siebrand, J. Chem. Phys. 49 (1968) 5369.
- [15] P.M. Morse, Phys.Rev.34 (1929) 57.
- [16] E.B. Wilson, J.C. Decius, P.C. Cross, Molecular Vibrations, Mc-Graw Hill Book Co., New York, 1955.
- [17] B.T. Darling, D.M. Dennison, Phys. Rev. 57 (1940) 128.
- [18] D.M. Dennison, Reviews of Modern Physics 12 (1940) 175.

- [19] J.M. Hollas, *High Resolution Spectroscopy*, John Wiley & Sons, 1998
- [20] W. Siebrand, D.F. Williams, *J. Chem. Phys.* 49(1968)1860.
- [21] B.R. Henry, *J. Phys. Chem.* 80 (1976) 2160.
- [22] B.R. Henry, *Acc. Chem. Res.* 10 (1977) 207.
- [23] M.S Child, *Acc. Chem. Res.* 18 (1985) 45.
- [24] B.R. Henry, I-Fu Hang, *Chem. Phys.* 29 (1978) 465.
- [25] R.J. Hayward, B.R Henry, *Chem. Phys.* 12 (1976) 387.
- [26] J.W. Ellis, *Phys. Rev.*, 33 (1929) 27.
- [27] J.W. Ellis, *Trans. Faraday. Soc.* 25 (1929) 888.
- [28] W.R.A. Greenlay, B.R. Henry, *Chem. Phys. Lett.* 53 (1978) 325.
- [29] W.R.A. Greenlay, B.R. Henry, *J. Chem. Phys.* 69 (1978) 82.
- [30] B.R. Henry, M.A. Mohammadi, J.A. Thomson, *J. Chem. Phys.* 75(1981)3165.
- [31] R.J. Hayward, B.R. Henry, *J. Mol. Struct.* 57 (1975) 221.
- [32] K.M. Gough, B.R. Henry, *J. Phys. Chem.* 88 (1984) 1298.
- [33] H.G. Kjaergaard, D.M. Turnbull, B.R. Henry, *J. Phys. Chem.* 101 (1997) 2589.
- [34] M.S. Child, L.Halonen, *Adv. Chem. Phys.* 57 (1984) 1.
- [35] I.M. Mills, A.G. Robiette, *Mol. Phys.* 743 (1985)56.
- [36] I.M. Mills, F.J. Mompean, *Chem. Phys Lett.* 425 (1986) 124.
- [37] M.S. Child, R.T. Lawton, *J. Chem. Soc. Faraday Discussions* 273 (1981) 1971.
- [38] O.S. Mortensen, B.R. Henry, M.A. Mohammadi, *J. Chem. Phys.* 75 (1981) 4800.
- [39] B.R. Henry, *Vibrational Spectra and Structure*, ed. J.R. Durig, Elsevier, Amsterdam, 10 (1981) 269.
- [40] R.L. Swofford, M.E. Long, A.C. Abrecht, *J. Chem. Phys.* 65 (1976) 179.
- [41] B.R. Henry, *Acc. Chem. Res.* 20 (1987) 429.
- [42] C. Sandorfy, *Bull. Polish. Acad. Sci. Chem.* 43 (1995) 7.
- [43] R.G. Bray, M.J. Berry, *J. Chem. Phys.* 71 (1979) 4909.



- [44] C.K.N. Patel, A.C. Tam, R.J. Kerl, *J. Chem. Phys.* 71 (1979) 1470.
- [45] Y. Mizugai, M. Kattayama, *Chem. Phys. Lett.* 73 (1980) 240.
- [46] J.S. Wong, C.B. Moore, *J. Chem. Phys.* 77 (1982) 603.
- [47] K.M. Gough, B.R. Henry, *J. Am. Chem. Soc.*, 106 (1984) 2781.
- [48] D.C. McKean, *Chem. Soc. Rev.* 7 (1978) 399.
- [49] D.C. McKean, R.A. Watt, *J. Molec. Spectrosc.* 61 (1976) 184.
- [50] M.S. Burberry, J.A. Morrel, A.C. Albrecht, R.L. Swofford, *J. Chem. Phys.* 70 (1979) 5522.
- [51] B.R. Henry, J.F. Hung, R.A. Macphail, H.L. Strauss, *J. Am. Chem. Soc.* 102 (1980) 515.
- [52] J. Susskind, *J. Chem. Phys.* 53 (1970) 2492.
- [53] H.L. Fang, R.L. Swofford, *J. Chem. Phys.* 72 (1980) 6382.
- [54] S. Kuriakose, K.K. Vijayan, S.M. Eappen, S. Shaji, K.P.R. Nair, T.M.A. Rasheed, *Asian J. Phys.* 11 (2002) 70.
- [55] B.R. Henry, I-Fu Hang, *Chem. Phys.* 29 (1978) 465.
- [56] R.J. Proos, B.R. Henry, *J. Phys. Chem.* 103 (1999) 8762.
- [57] Z. Rong, H.G. Kjaergaard, B.R. Henry, *J. Phys. Chem. A* 106 (2002) 4368.
- [58] H.G. Kjaergaard, B.R. Henry, A.W. Tarr, *J. Chem. Phys.* 94 (1991) 5844.
- [59] H.G. Kjaergaard, H. Yu, B. J. Schattka, B.R. Henry, *J. Chem. Phys.* 93 (1990) 6239.
- [60] T.M.A. Rasheed, V.P.N. Nampoori, *Pramana - J. Phys.* 42 (1994) 245.
- [61] G.C. Pimental, A.L. McClellan, *The Hydrogen Bond*, Freeman, San Francisco, 1960.
- [62] G.A. Jeffrey, *An Introduction to Hydrogen Bonding*, Oxford University Press, New York, 1997.
- [63] A. Novak, "Hydrogen Bonding in Solids. Correlation of Spectroscopic and Crystallographic Data." In: *Structure and Bonding*, Springer-verlag, New York, 1974.

- [64] G.R. Desiraju, T. Steiner, *The Weak Hydrogen Bond*, Oxford University Press, Oxford, 1999 .
- [65] S. Scheiner, *Hydrogen Bonding*, Oxford University Press, New York, 1997.
- [66] P. Hobza, Z. Havlas, *Chem. Rev.* 100 (2000) 4253.
- [67] C. Sandorfy, *Bull. Polish Acad. Sci. Chem.* 43 (1995) 7.
- [68] C. Sandorfy, in: P. Schuster, G. Zundel, C. Sandorfy (Eds.), *The Hydrogen Bond*, Vol. 2, North-Holland, Amsterdam, 1976.
- [69] C. Sandorfy, *Top. Curr. Chem.* 120 (1984) 41.
- [70] S. Shaji, T.M.A. Rasheed, *Spectrochim. Acta Part A* 57 (2001) 337.
- [71] S.M. Eappen, S. Shaji, K.P.R. Nair; *Asian. J. Spectrosc.* 2 (2001) 89.
- [72] V.K. Rai, S.B. Rai, D.K. Rai, *Spectrochim. Acta Part A* 59 (2003) 1299.
- [73] C. Chen, F.S. Hsu, *J. Mol. Structure (Theochem)*, 506 (2000) 147.
- [74] U. John, K.P.R. Nair, *Spectrochim. Acta Part A* 60 (2004) 2337.
- [75] U. John, K.P.R. Nair, *Spectrochim. Acta Part A* 61 (2005) 2555.
- [76] U. John, K.P.R. Nair, *Spectrochim. Acta Part A* 63 (2006) 169.

CHAPTER 5

NEAR IR OVERTONE ANALYSIS OF SOME AMINES

5.1 Analysis of the Overtone Spectra of 2, 4-Dimethylaniline and 2,6-Dimethylaniline

5.1.1 Introduction

As described in chapter 4, higher vibrational overtones often provide spectral simplification and greater resolution of peaks corresponding to nonequivalent X-H bonds where X is typically C, N or O. Hence vibrational overtone spectroscopy of molecules containing X-H oscillators is now a well established tool for molecular investigations [1-3]. Conformational and steric differences between bonds and structural inequivalence of CH bonds (methyl, aryl, acetylenic, etc.) are resolvable in the higher overtone spectra. The local mode model in which the X-H oscillators are considered to be loosely coupled anharmonic oscillators has been widely used for the interpretation of overtone spectra. If we are exciting a single local oscillator from the vibrational ground state to the state v , then the transition energy of the local mode overtone is given by $\Delta E_{0 \rightarrow v} = Av + Bv^2$. A plot of $\Delta E/v$ versus v will yield A , the local mode frequency as the intercept and B , the local mode diagonal anharmonicity as the slope [3,4]. Here $A - B$ gives the mechanical frequency X_1 of the oscillator and $B = X_2$ is the anharmonicity of the bond. The local mode parameters X_1 and X_2 vary for nonequivalent X-H bonds and are sensitive to the inter and intra molecular environment of the X-H oscillator [3-10].

Aniline and its derivatives are important starting materials in pharmaceutical and other chemical industries. 2,6-dimethylaniline (2,6-xylydine) is an important raw material for producing anaesthetic and 2,4-dimethylaniline (2,4-xylydine) is mainly used for producing pesticides (structures in Fig. 5.1). Both are used in the production of dyes and other chemicals also. The primary physiochemical property of importance in the drug chemistry of amino group is its basicity and this determines the chemical

behaviour of amines. The substituents on the ring have a marked effect on the basicity of aromatic amines. In the present paper we report the near infrared vibrational overtone absorption spectra of liquid phase 2,6-dimethylaniline and 2,4-dimethylaniline. A comparative study of the above spectra is done. The substituents on the aniline ring leads to variations of the charge distribution in the molecule and hence affect the frequencies of various X-H oscillators. This is discussed in the density functional studies of aniline and substituted anilines [11] and in *ab initio* calculations for the structural studies of various toluidines [12-14]. The methylation of aniline in *ortho* positions brings steric strain and how the strength of the base is weakened due to this has been explained by Brown [15]. The calculated aryl CH, methyl CH and NH mechanical frequency values of both the samples support the above conclusions.

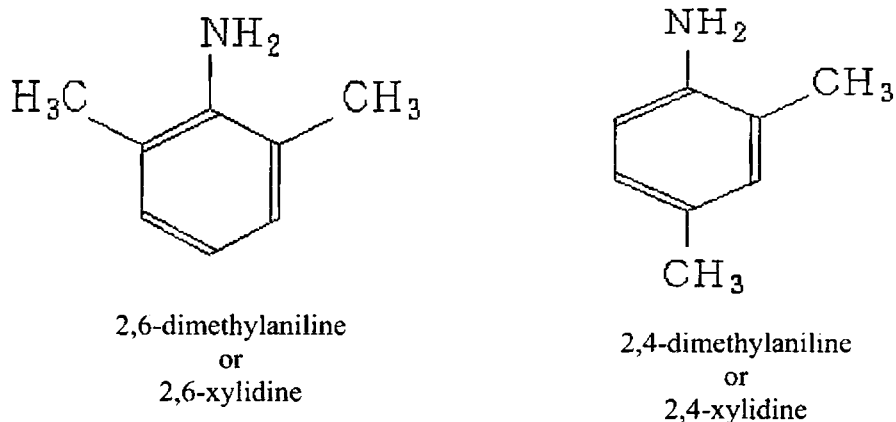


Fig. 5.1. Structures of 2,6-dimethylamine and 2,4-dimethylamine

5.1.2 Experimental

High purity (99%) 2,4-dimethylaniline and 2,6-dimethylaniline were obtained from Sisco Research Laboratories Pvt. Ltd, Mumbai, India. In order to avoid saturation of peaks the samples were near saturated in spectra-grade carbon tetrachloride. The liquid phase absorption spectra in the near infrared region (700-2000nm) were

recorded at room temperature ($26 \pm 1^\circ \text{C}$) with air as reference and pathlength 1cm, using a Hitachi model U-3410 UV-Vis-NIR Spectrophotometer which uses a tungsten lamp as the near IR source.

5.1.3 Results and Discussions

The near infrared vibrational overtone absorption spectra of 2,6- dimethylaniline and 2,4-dimethylaniline in the region 700-2000 nm show bands due to pure overtone transitions of NH, ring CH and methyl CH local mode oscillators and those due to combination transitions involving several vibrational degrees of freedom of the molecule. The sharp peak at 900nm is due to the detector change of the spectrophotometer. In the present analysis, only the pure overtones of NH, ring CH and methyl CH oscillators of the two molecules are considered. The bands in the $\Delta V = 2-4$ regions of the two molecules are shown in the Figs. 5.2-5.7. Here 'a' & 'b' represent NH overtones, 'c' represents ring CH overtones, 'd' & 'e' represent methyl CH overtones and the other peaks are combinations. The bands in the $\Delta V = 2$ region shows multiple peaks due to the presence of combinations whereas the higher overtone bands show single overtone peaks. The first overtone peak position in each case is assigned as the one giving the best fit in the Birge- Spomer plot with higher overtone peaks. Figs. 5.8-5.17 give the Birge-Spomer plots for various oscillators. The band assignments, overtone peak position and the local mode parameters of the NH, aryl CH and methyl CH oscillators of both the liquids are given in Tables 5.1 and 5.2.

Base is an electron pair donor. The most important property of Nitrogen is its basicity. The tendency of nitrogen to share the lone pair of electrons underlies the entire chemical behaviour of amines. Substituents on the ring have a marked effect on the basicity of aromatic amines. The electron releasing substituents like $-\text{CH}_3$ increases the basicity of aniline [16]. Strength of a base depends upon the availability of electrons on nitrogen in the amine. Any factor that can increase electron concentration on nitrogen will bring about increase in the basicity. Each amine has its

characteristic K_b , the basicity constant. The larger the K_b , the stronger the base. Basicity constants of aniline and substituted anilines are given below [17].

Substituent	K_b of <i>para</i> isomer	K_b of <i>meta</i> isomer	K_b of <i>ortho</i> isomer
-CH ₃	12×10^{-10}	5×10^{-10}	2.6×10^{-10}

K_b of aniline = 4.2×10^{-10}

Even though the electron releasing substituents like -CH₃ increases the basicity of aniline, the basicity is weakened when they are *ortho* to the amino group. The introduction of first one and then two *ortho* methyl groups into aniline progressively decreases the base strength of aniline [18]. Methylation of aniline in *ortho* position brings steric strain and due to this strength of the base is weakened. Steric nature of *ortho* effect is operating between the amino group and the two *o*-methyl groups in 2,6-dimethylaniline. The methyl groups in the *meta* and *para* position exert inductive effect, without a steric change. In 2,4-dimethylaniline the *o*-methyl group is base weakening but the *p*-methyl group is base strengthening. Since the K_b value of the *p*-isomer differ largely from aniline compared to *o*-isomer, basicity of 2,4-dimethylaniline is greater compared to 2,6-dimethylaniline.

It is well known that the substitution of an electron donating group to benzene decreases the ring CH mechanical frequency and hence a red shift [19] in overtone energy values. The Hammett σ constants which indicate the donating or withdrawing nature of the substituent [20] shows that -NH₂ group and -CH₃ group are electron donors to the benzyl ring through resonance or induction. Both the amino group and methyl groups in 2,6-dimethylaniline and 2,4-dimethylaniline are electron donating groups. Now let us examine the calculated NH, aryl CH and methyl CH oscillator frequencies of both the samples.

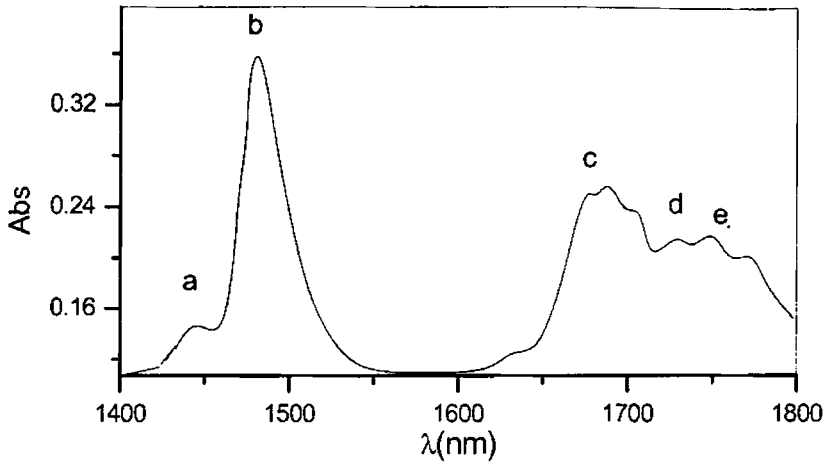


Fig. 5.2. Overtone spectrum of 2,6-xylylene
in the region $\Delta v = 2$

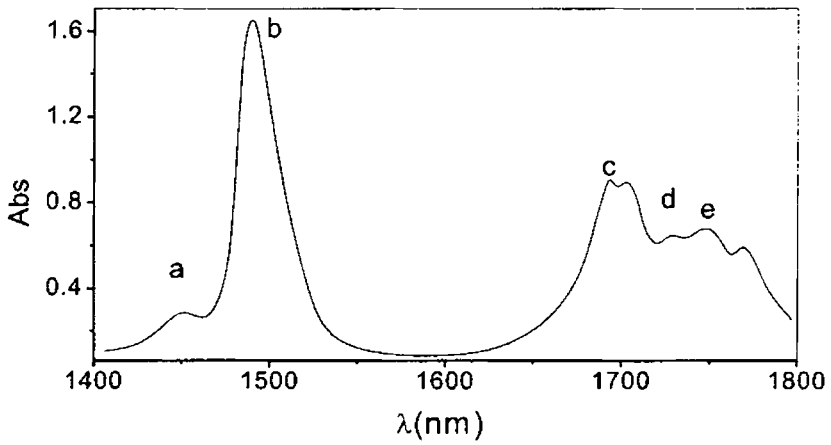


Fig. 5.3. Overtone spectrum of 2,4-xylylene
in the region $\Delta v = 2$

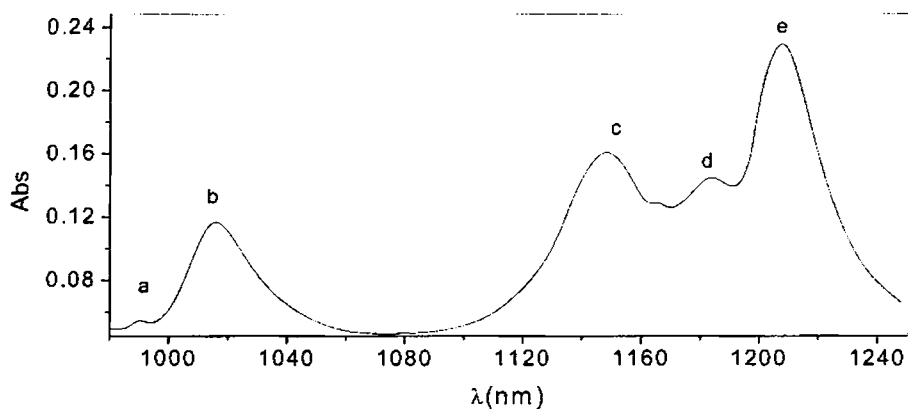


Fig. 5.4. Overtone spectrum of 2,6-xylylidine
in the region $\Delta\nu = 3$

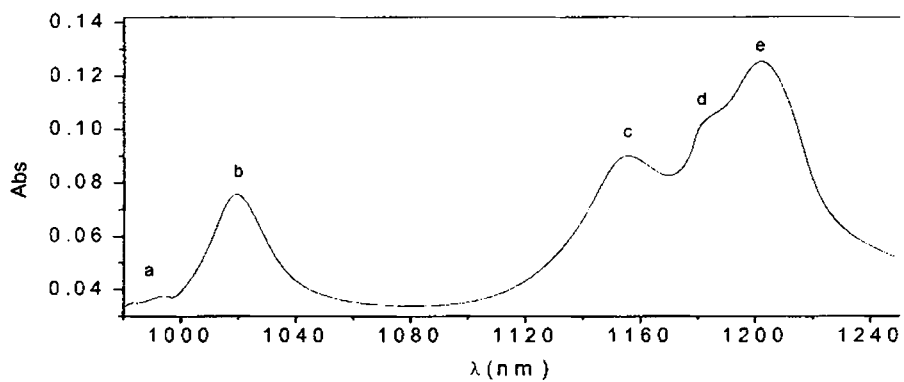


Fig. 5.5. Overtone spectrum of 2,4-xylylidine
in the region $\Delta\nu = 3$

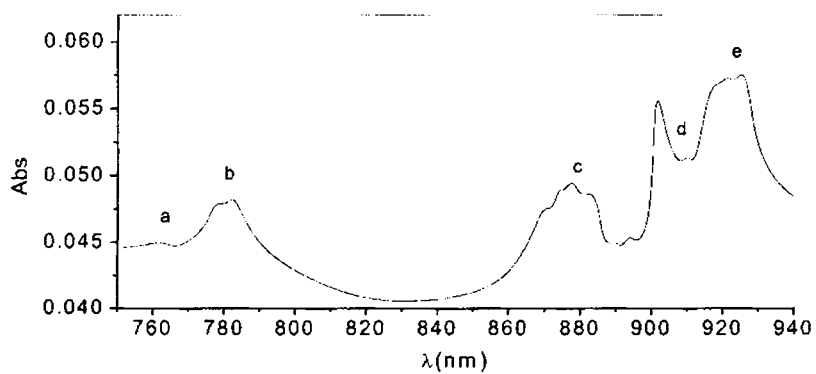


Fig. 5.6. Overtone spectrum of 2,6-xylylene
in the region $\Delta v = 4$

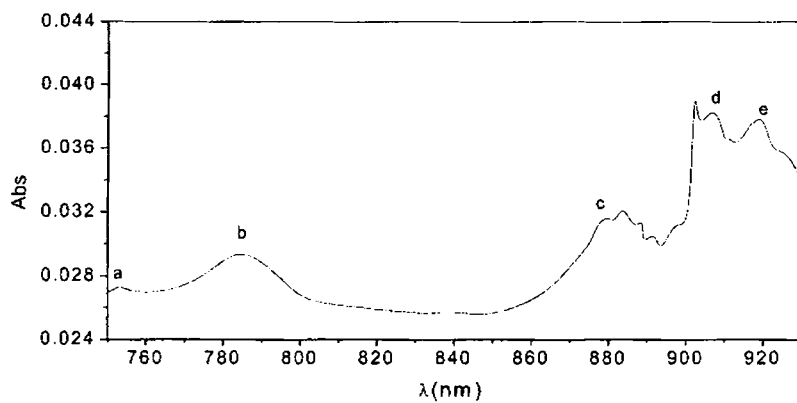


Fig. 5.7. Overtone spectrum of 2,4-xylylene
in the region $\Delta v = 4$

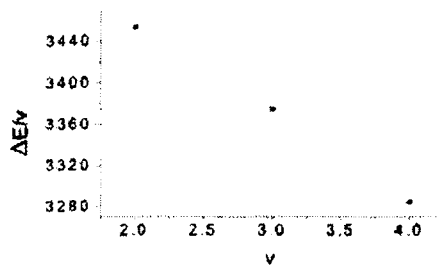


Fig. 5.8 Birge-Sponer plot for NH-asymmetric overtones of 2,6-xylylidine

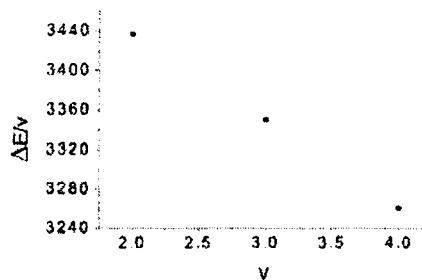


Fig. 5.9 Birge-Sponer plot for NH-asymmetric overtones of 2,4-xylylidine

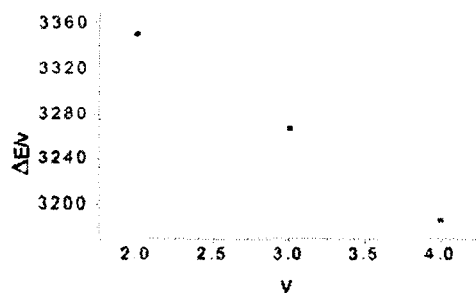


Fig. 5.10 Birge-Sponer plot for NH-symmetric overtones of 2,6-xylylidine

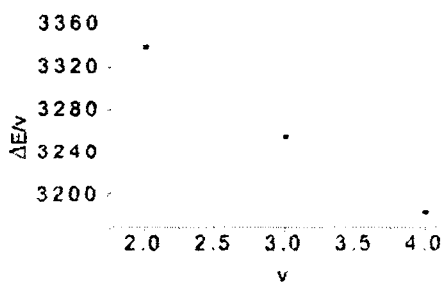


Fig. 5.11 Birge-Sponer plot for NH-symmetric overtones of 2,4-xylylidine

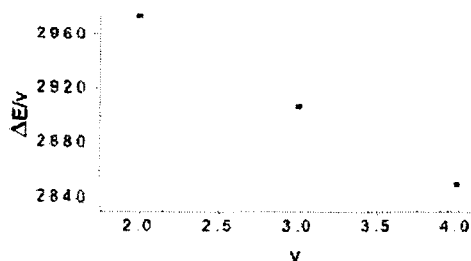


Fig. 5.12 Birge-Sponer plot for aryl CH overtones of 2,6-xylylidine

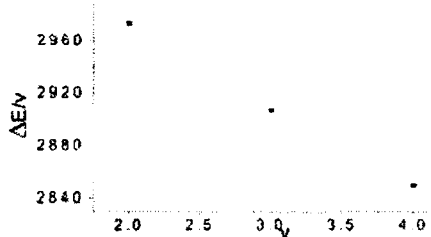


Fig. 5.13 Birge-Sponer plot for aryl CH overtones of 2,4-xylylidine

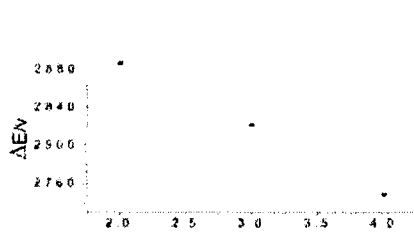


Fig. 5.14 Birge-Sponer plot for in-plane methyl CH overtones of 2,6-xylylidine

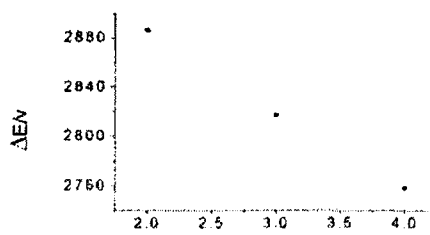


Fig. 5.15 Birge-Sponer plot for in-plane methyl CH overtones of 2,4-xylylidine

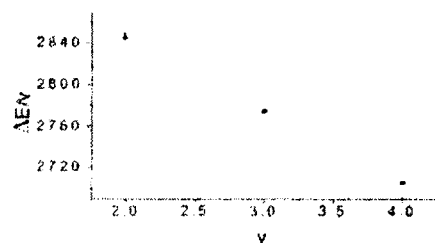


Fig. 5.16 Birge-Sponer plot for out-of-plane methyl CH overtones of 2,6-xylylidine

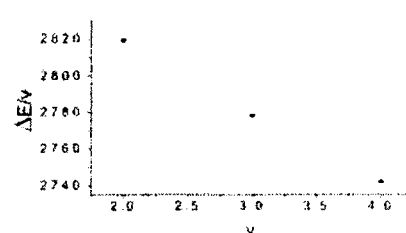


Fig. 5.17 Birge-Sponer plot for out-of-plane methyl CH overtones of 2,4-xylylidine

NH oscillators: It is interesting to note that overtones corresponding to both asymmetric and symmetric stretching vibrations are obtained as is expected for a primary amine. As can be seen in Tables 5.1 & 5.2 the NH frequency is high in 2,6-xylylidine. Here the steric repulsion occurs between the hydrogens of NH_2 and the bulky methyl groups so that shortening of NH bonds takes place, which in turn increases the force constant. Thus the wavenumber of the NH absorption in 2,6-xylylidine increases. In 2,4-xylylidine the steric strain is less compared to 2,6-xylylidine and hence its wave number of absorption is less. Hence an increase in the frequency of NH oscillator is an indication of the weakening of the basicity of the methyl substituted anilines.

Table 5.1

The band assignments, overtone peak position and the local mode parameters of the NH and aryl CH oscillators

Stretch type	v	Overtone peak position in nm (cm^{-1})		Local mode parameters & γ for	
		2,6-xylylidine	2,4-xylylidine	2,6-xylylidine	2,4-xylylidine
NH-Asymmetric stretch	2	1447.8 (6907.03)	1454.7 (6874.27)	$X_1 = 3707.79$	$X_1 = 3701.76$
	3	987.8 (10123.51)	994.7 (10053.28)	$X_2 = 84.18$	$X_2 = 87.99$
	4	761 (13140.60)	766.6 (13044.61)	$\gamma = -0.9994$	$\gamma = -999$
NH-Symmetric stretch assignment	2	1492.3 (6701.07)	1497.7 (6676.90)	$X_1 = 3596$	$X_1 = 3567.72$
	3	1020 (9803.92)	1023.9 (9766.58)	$X_2 = 81.90$	$X_2 = 77.07$
	4	784.5 (12746.97)	785.1 (12737.23)	$\gamma = -1$	$\gamma = -9990$
Aryl CH- stretch assignment	2	1681.3 (5947.78)	1695.9 (5897.97)	$X_1 = 3158.62$	$X_1 = 3111.24$
	3	1146.7 (8720.68)	1150.6 (8691.12)	$X_2 = 62.12$	$X_2 = 54.01$
	4	877.3 (11398.61)	880.2 (11361.05)	$\gamma = -.9990$	$\gamma = -.9996$

v = vibrational quantum number, X_1 = mechanical frequencies (cm^{-1}), X_2 = anharmonicities (cm^{-1}) and γ = the least square correlation coefficient.

Table 5.2

The band assignments, overtone peak position and the local mode parameters of the methyl CH oscillators

Stretch type	v	Overtone peak position in nm (cm^{-1})		Local mode parameters & γ for	
		2,6-xylydine	2,4-xylydine	2,6-xylydine	2,4-xylydine
In-plane methyl CH stretch	2	1732 (5773.67)	1732 (5773.67)	$X_1 = 3094.76$	$X_1 = 3078.40$
	3	1181.3 (8465.25)	1182.8 (8454.52)	$X_2 = 68.89$	$X_2 = 64.36$
	4	909.4 (10996.26)	906.4 (11032.66)	$\gamma = -.9995$	$\gamma = -.9993$
Out-of-plane methyl CH stretch	2	1753.5 (5702.80)	1749.6 (5715.59)	$X_1 = 3057.65$	$X_1 = 3058.46$
	3	1201.3 (8324.32)	1199.7 (8335.41)	$X_2 = 69.53$	$X_2 = 68.13$
	4	921.7 (10849.5)	918.6 (10886)	$\gamma = -.998$	$\gamma = -.996$

v = vibrational quantum number, X_1 = mechanical frequencies (cm^{-1}),
 X_2 = anharmonicities (cm^{-1}) and γ = the least square correlation coefficient.

Aryl CH oscillators: The introduction of alkyl groups causes positive inductive effect which results in the lengthening or the weakening of the aryl CH bonds and hence the force constant is lowered and wave number of absorption decreases. In 2,6-xylydine and 2,4-xylydine we have three ring CH bonds. In 2,6-xylydine two bonds are (o+p) type and one is (m+m) type w.r.to methyl substitution. In 2,4-xylydine the bonds are (o+o) type, (o+p) type and (m+m) type. We have the frequency of ring CH in 2,4 < frequency of ring CH in 2,6 which agrees with the expected order (o+p) > (o+o) in the work of Khalique and Henry on conformationally non-equivalent ring CH bonds in trimethylbenzenes [9]. The aryl CH frequencies of *ortho* substituted anilines reported from our laboratory by

Shaji et al. [21] and *ab initio* calculations of o-methylaniline [12] agree with our results [22].

Methyl CH oscillators: The presence of inequivalent methyl CH bonds similar to toluene, xylene and trimethylbenzenes are [10, 6, 9] observed. The less intense high frequency peak is associated with the in-plane methyl CH stretch, when the methyl groups have one CH bond in the ring plane. The highly intense low frequency peak is associated with the out-of-plane methyl stretch when the two methyl CH bonds are at 60° . The frequencies of the methyl stretches are almost the same in both the liquids.

5.1.4 Conclusions

The frequency of the NH oscillator in 2,6-xylidine is higher compared to 2,4-xylidine. Since 2,6-xylidine is a weak base compared to 2,4-xylidine, we can conclude that the increase in the NH oscillator frequency is an indication of the weakening of the basicity in methylated anilines. Again we have observed that methylation of aniline in *ortho* position brings a blue shift in the overtone energy values of the ring CH oscillator.

5.2 Analysis of the Overtone Spectrum of Cyclohexylamine

5.2.1 Introduction

Cyclohexylamine is a nonaromatic cyclic primary amine with six-member saturated ring (Fig. 5.18). Cyclohexylamine is a colourless liquid and is widely used in rubber industry for the preparation of vulcanization accelerator. Another important application of cyclohexylamine is its use in the manufacturing of artificial sweeteners (cyclamates).



Fig. 5.18 Cyclohexylamine

Being a primary amine two bands corresponding to NH stretch are expected, one for asymmetric stretch and the other due to symmetric stretch [23]. Amines are usually weakly bonded systems. The formation of the hydrogen bond results in weakening of the N-H bond which is accompanied by bond elongation and a decrease of NH stretch vibration frequency compared to the noninteracting species. This shift to lower frequencies, called the red-shift represents the easily detectable manifestation of the formation of a hydrogen bond [24]. NH stretch frequencies of amines are usually confused with OH stretch. However, since oxygen is more electronegative than nitrogen, OH stretch results in a greater change in bond moment than does NH stretch [23]. The associated NH stretch absorption is sharper than associated OH, because of much weaker tendency to form hydrogen bonds. Overtones of free NH bands are obtained but the associated NH bands are too weak to be observed at room temperature in the higher overtone region as is concluded by Sadorfy et al. [25, 26]. Cyclohexylamine is a far stronger base than is aniline [27]. The CH and NH local mode mechanical frequency values and anharmonicity values obtained from fitting the overtones are analysed and is compared with that of aniline [28]. The strong basicity of cyclohexylamine compared to aniline is reflected in NH stretch frequency values obtained.

5.2.2 Experimental

High purity (99.5 %) cyclohexylamine was obtained from Sisco Research Laboratories Pvt. Ltd, Mumbai, India. Solutions of the liquid in spectra-grade carbon tetrachloride in different concentrations are made. The liquid phase absorption spectra in the near infrared region (700-2000nm) were recorded at room temperature ($26\pm 1^{\circ}\text{C}$) with air as reference and pathlength 1cm, using a Varian (Cary 5000 model) UV- Vis- NIR Spectrophotometer which uses a tungsten lamp as the near IR source.

5.2.3 Results and Discussions

The near infrared vibrational overtone absorption spectra of the amine in carbon tetrachloride in the region 700-2000 nm show bands due to pure overtone transitions of CH, free NH and bonded NH local mode oscillators and those due to combination

transitions involving several vibrational degrees of freedom of the molecule. In the present analysis, only the pure overtones of oscillators are considered. The bands in the $\Delta\nu = 2, 3, 4$ and 5 regions (for 100% concentration) are shown in Figs. 5.19–5.22. Here ‘a’ represents CH overtones, ‘b’ represents bonded NH-stretching overtones, ‘c’ and ‘d’ represent free NH-stretching overtones corresponding to symmetric and antisymmetric stretch of the primary amine and the other peaks are combinations. The sharp change in $12,500\text{ cm}^{-1}$ in Fig.5.21 is due to the detector change at 800 nm. In the CH region in $\Delta\nu = 2$ we have two peaks corresponding to two nonequivalent CH bonds, the axial and equatorial, similar to the case of cyclohexane [29]. Bonded NH stretch region is observed only in $\Delta\nu = 2$. But such associated bands are not resolvable in the $\Delta\nu = 3, 4$ and 5 regions. This is because of the fact that what is observed for fairly strong OH...O bonds cannot be expected for weakly bonded NH...N bonds [25]. Fig. 5.23 gives the bonded NH stretch region in $\Delta\nu = 2$ under various concentrations. From the figure it is evident that as the concentration is increased the associated bands shift to lower wavenumber side, which is the normal red-shifting due to hydrogen bonding. Since associated bands are not resolvable in the $\Delta\nu = 3, 4$ and 5 regions, the spectra at those regions for lower concentrations are not shown. Figs. 5.24-5.26 give the Birge-Sponer plots for CH stretch, free symmetric NH stretch and asymmetric NH stretch (for 100% concentration). The band assignments, overtone peak positions and local mode parameters of the CH and free NH (both symmetric and antisymmetric) oscillators are given in Table 5.3.

These values agree with the already established results by Sandorffy et al. for NH oscillators [25] and Kjaergaard et al. for CH oscillators [29]. The NH-stretching local mode parameters of aniline from the work of Shaji et al. is also given for comparison in Table 5.3 itself. As discussed in 5.1.3 the most important property of nitrogen is its basicity. In the case of aromatic amines like aniline the phenomenon of ‘resonance’ also affect the base strength. Aniline being a resonance hybrid of many structures, the lone pair on nitrogen is partly shared with the benzene ring and is obviously less available for sharing with a proton, thus lowering the basicity of aniline. In the case of saturated amine like cyclohexylamine such effect is not there or cyclohexylamine is a far stronger base than aniline [27]. The calculated value of NH frequency (symmetric) of cyclohexylamine

is smaller than that of aniline. This establishes the fact that cyclohexylamine is a far stronger base than aniline, since the increase in NH oscillator frequency is an indication of weakening the basicity as explained in section 5.1.3 [22].

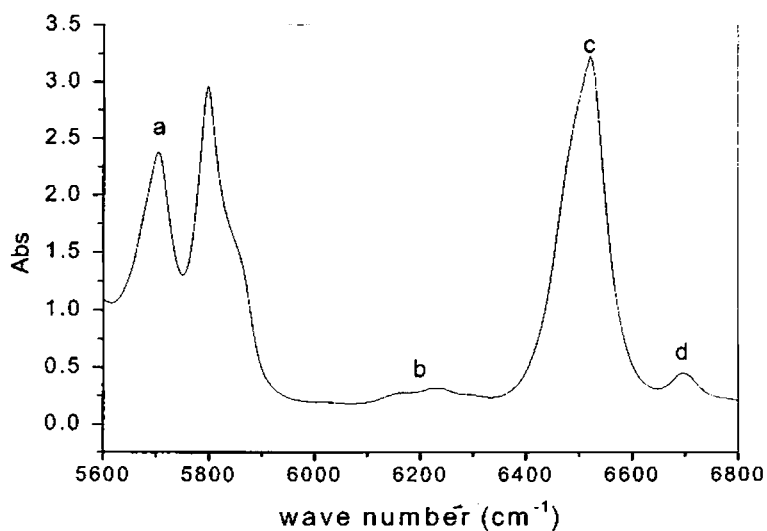


Fig. 5.19. Overtone spectrum of cyclohexylamine in the region $\Delta v = 2$

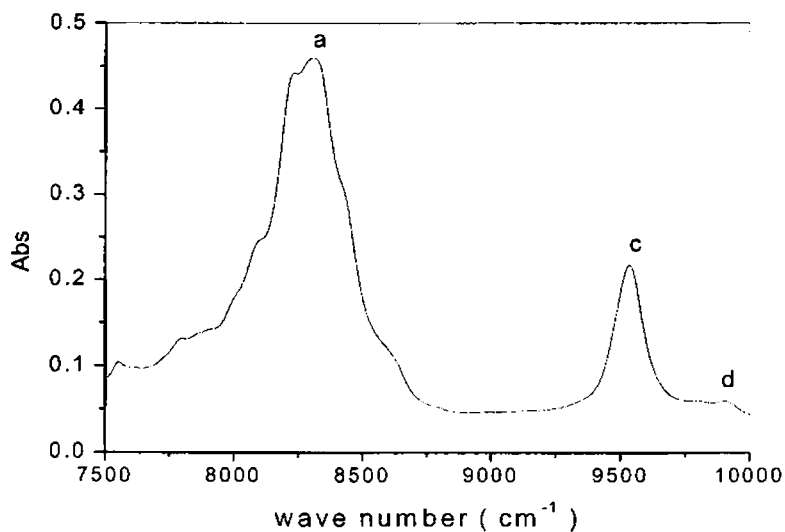


Fig. 5.20. Overtone spectrum of cyclohexylamine in the region $\Delta v = 3$

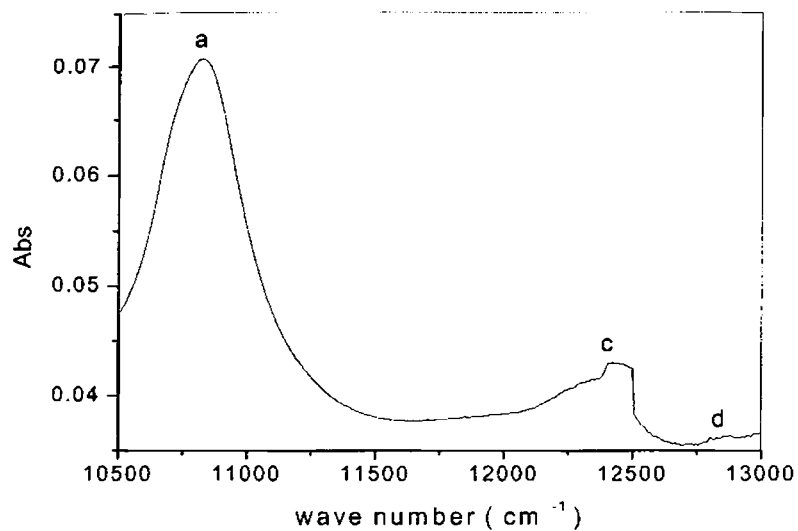


Fig. 5.21. Overtone spectrum of cyclohexylamine in the region $\Delta v = 4$

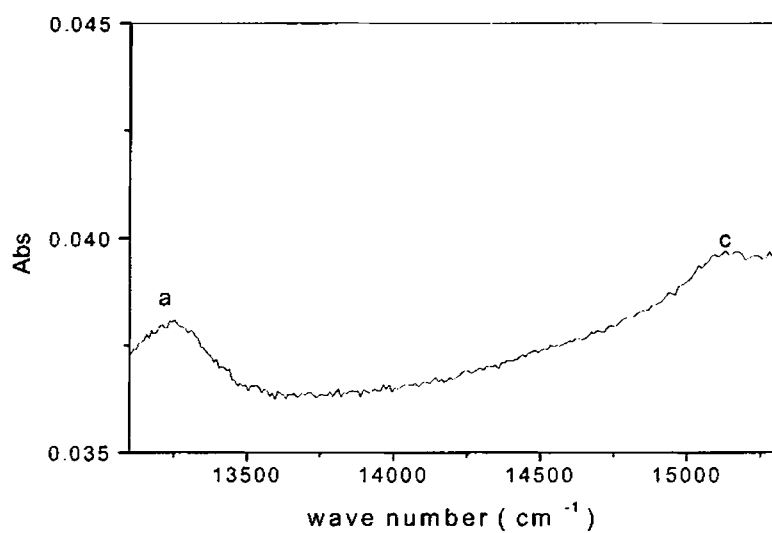


Fig. 5.22. Overtone spectrum of cyclohexylamine in the region $\Delta v = 5$

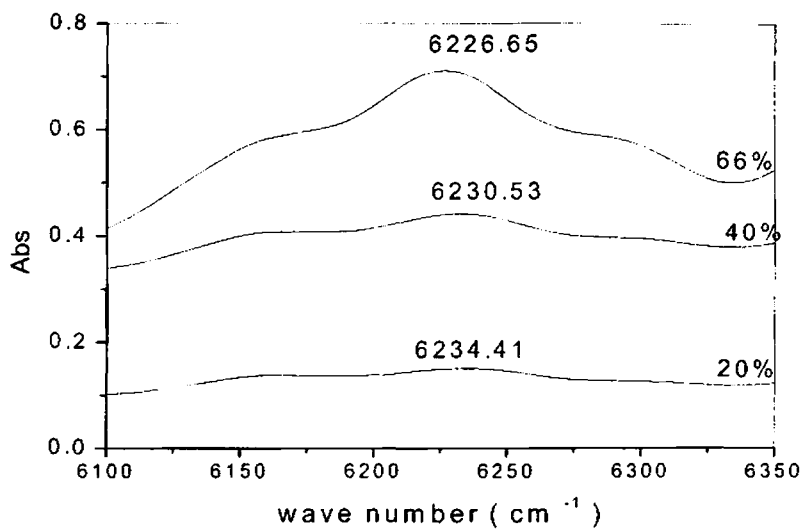


Fig. 5.23. Overtone spectrum of bonded NH oscillators of cyclohexylamine under various concentrations in the region $\Delta v = 2$

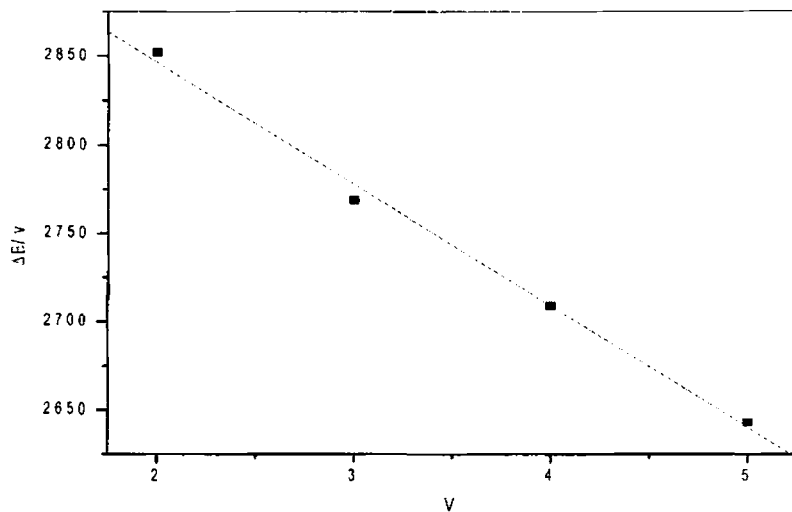


Fig. 5.24. Birge-Spinner plot for CH stretch overtones of cyclohexylamine

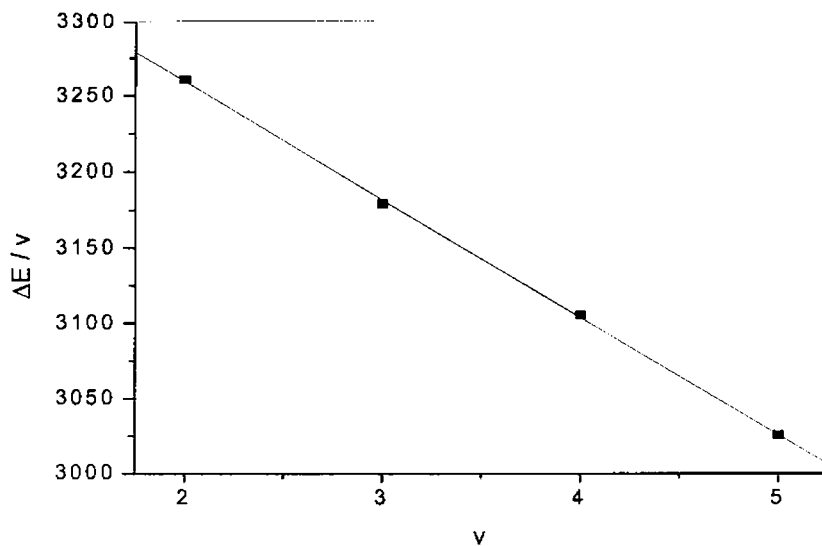


Fig. 5.25. Birge-Sponer plot for free NH-symmetric overtones of cyclohexylamine

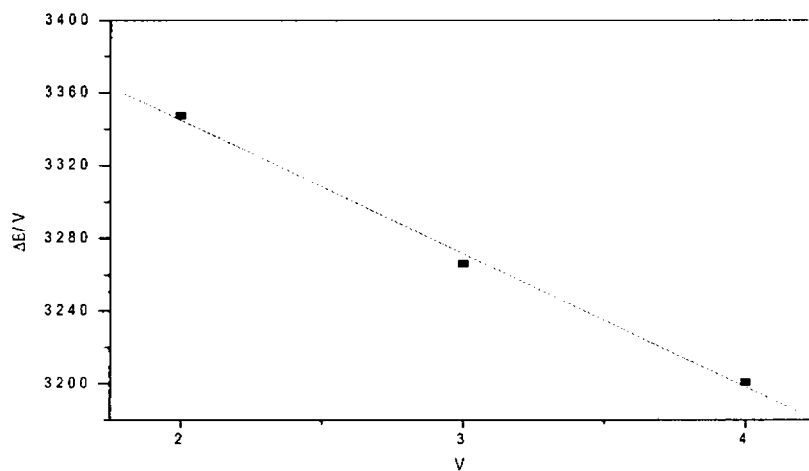


Fig. 5.26. Birge-Sponer plot for NH-asymmetric overtones of cyclohexylamine

Table 5.3

The band assignments, overtone peak position and the local mode parameters of the CH and NH oscillators of cyclohexylamine & overtone peak position and local mode parameters of the NH oscillators of aniline from reference [28]

Stretch type	Overtone peak positions in (cm^{-1}) for $\nu =$				Local mode parameters and correlation coefficient
	2	3	4	5	
CH	5702.88	8305.65	10822.51	13236.27	$X_1 = 3047.19$ $X_2 = 67.55$ $\gamma = -.997$
Free NH (symmetric)	6521.03	9537.43	12422.36	15128.59	$X_1 = 3492.81$ $X_2 = 77.79$ $\gamma = -.9998$
Free NH (asymmetric)	6695.68	9799.12	12804.1	-	$X_1 = 3565.38$ $X_2 = 73.41$ $\gamma = -.998$
Free NH (symmetric) of aniline [28]	6636.14	9722.9	12655.02	-	$X_1 = 3549.56$ $X_2 = 77.16$ $\gamma = -.1$

ν = vibrational quantum number, X_1 = mechanical frequencies (cm^{-1}),
 X_2 = anharmonicities (cm^{-1}) and γ = the least square correlation coefficient .

5.2.4 Conclusions

It is interesting to note that in the case of cyclohexylamine, overtones corresponding to both asymmetric and symmetric NH-stretching vibrations are obtained as is expected for a primary amine. Due to the weak hydrogen bonding in amines higher overtones for bonded NH oscillators are too weak to be resolved. Still weak and broad red-shifted bands at lower overtones are identified due to the formation of hydrogen bonds. The low value of NH-stretching frequency of cyclohexylamine compared to aniline is an indication of its strong basicity.

5.3 Analysis of the Overtone Spectrum of Morpholine

5.3.1 Introduction

Morpholine is a nonaromatic heterocyclic amine with six-member saturated ring (Fig. 5.27). Morpholine ring contains two heteroatoms. It is one of the important organic bases which has become an article of commerce in recent years. Soaps made from morpholine and fatty acids are excellent emulsifying agents useful in the production of floor polishes, paper coatings and other products. Morpholine finds its major application in food preservation and is added to waxes used to coat apples.

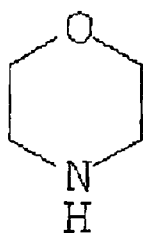


Fig. 5. 27. Morpholine

For the secondary amine morpholine only one NH stretch is expected [23]. Like cyclohexylamine, here also weak hydrogen bonds are formed, resulting in weakening of the N-H bond which is accompanied by bond elongation and a decrease of NH stretch vibration frequency compared to the noninteracting species. The main

difference here is that it is the NH...O hydrogen bonded structure [30] instead of the NH...N hydrogen bonded structure in cyclohexylamine. Piperidine is a far stronger base than morpholine [27]. Studies on the vibrational spectra of piperidine and morpholine was done by Vedal et al. [32]. Overtone positions of morpholine are compared with that of piperidine from the work of Sauvageau and Sandorfy [31]. The weak basicity of morpholine is reflected in the NH stretch frequency values.

5.3.2 Experimental

High purity (99.5%) morpholine was obtained from Sisco Research Laboratories Pvt. Ltd, Mumbai, India. Solutions of the liquid in spectra-grade carbon tetrachloride in different concentrations are made. The liquid phase absorption spectra in the near infrared region (700-2000nm) were recorded at room temperature ($26 \pm 1^{\circ}$ C) with air as reference and pathlength 1cm, using a Varian (Cary 5000 model) UV-Vis-NIR Spectrophotometer which uses a tungsten lamp as the near IR source.

5.3.3 Results and Discussions

The near infrared vibrational overtone absorption spectra of morpholine in carbon tetrachloride in liquid phase in the region 700-2000 nm shows bands due to pure overtone transitions of CH, free NH and bonded NH local mode oscillators and those due to combination transitions involving several vibrational degrees of freedom of the molecule. The bands in the $\Delta v = 2, 3, 4$ and 5 regions (for 100% concentration) for morpholine are shown in Figs. 5.28 – 5.31. The sharp change in $12,500 \text{ cm}^{-1}$ in Fig. 5.30 is due to the detector change at 800nm. In the present analysis focus is on overtones only. Here 'a' represents CH overtones, 'b' represents bonded NH-stretching overtones and 'c' represents free NH-stretching overtones of the secondary amine and the other peaks are combinations. Bonded NH stretch region is observed only in $\Delta v = 2$ and 3 . But such associated bands are not resolvable in the $\Delta v = 4$ and 5 regions. This too is because of the fact that the hydrogen bonding is weak in amines compared to alcohols [25]. The bonded NH stretch region in $\Delta v = 2$ under various

concentrations is given in Fig. 5.32. Here the situation is same as in the case of cyclohexylamine. As the concentration is increased the associated bands shift to lower wavenumber side, which is the normal red-shifting due to hydrogen bonding. But the shift from the free NH position to bonded NH position is greater in morpholine compared to cyclohexylamine (sec.5.2.3), since we have the NH...O hydrogen bonded structure here compared to the NH...N type in cyclohexylamine. Indrisa et al. determined the molecular structure of morpholine by FT microwave spectroscopy and the NH...O hydrogen bonded structure was found to be consistent with the derived molecular parameters [30]. Since associated bands are not resolvable in the $\Delta v = 4$ and 5 regions, it is not possible to obtain the local mode parameters of bonded NH bands and that is why the spectra at higher Δv regions for lower concentrations are not shown. Figs.5.33 and 5.34 give the Birge-Sponer plots for CH stretch and free NH stretch of the secondary amine respectively. The band assignments, overtone peak positions and local mode parameters of the CH and free NH oscillators are given in Table 5.4.

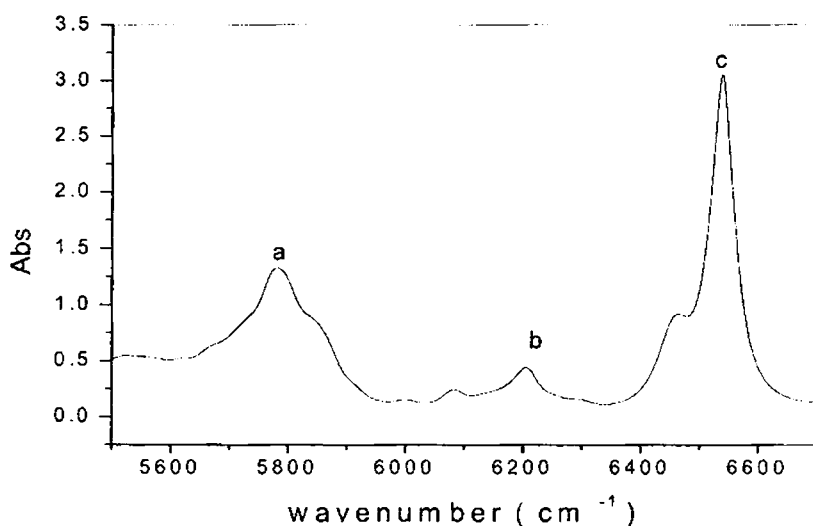


Fig. 5.28. Overtone spectrum of morpholine in the region $\Delta v = 2$

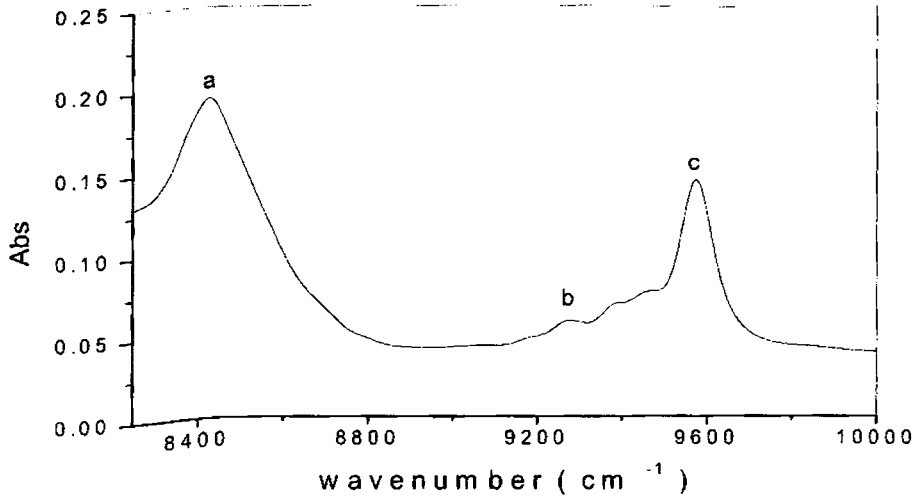


Fig. 5.29. Overtone spectrum of morpholine
in the region $\Delta v = 3$

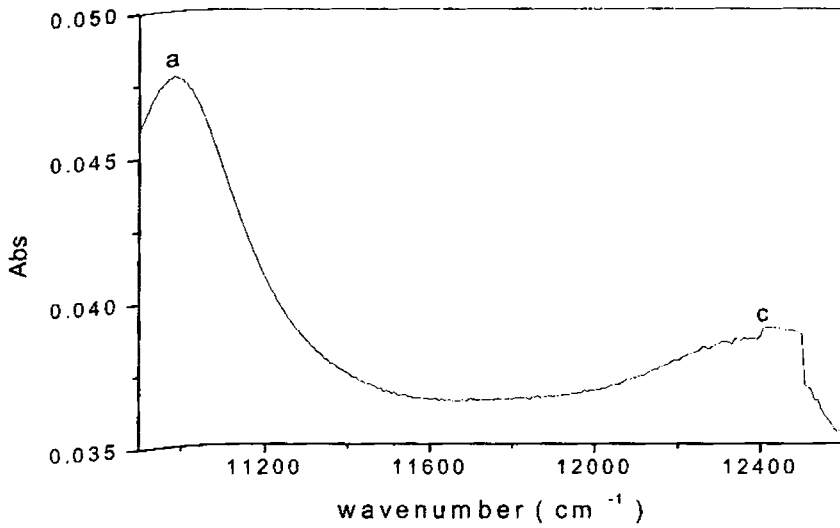


Fig. 5.30. Overtone spectrum of morpholine
in the region $\Delta v = 4$

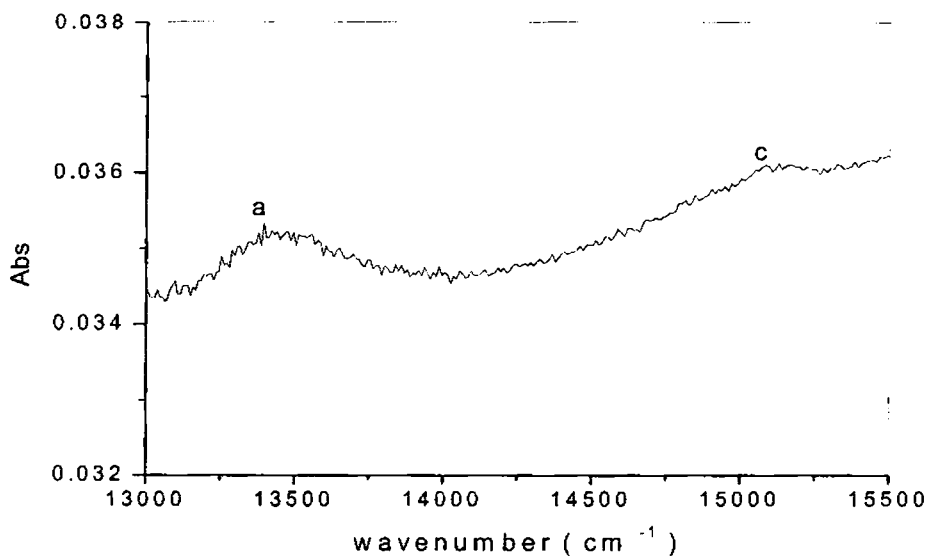


Fig. 5.31. Overtone spectrum of morpholine in the region $\Delta\nu = 5$

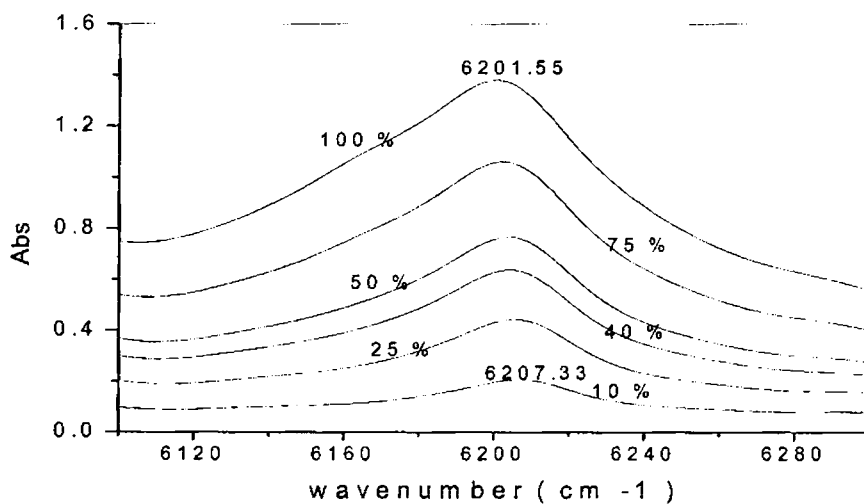


Fig. 5.32. Overtone spectrum of bonded NH oscillators of morpholine under various concentrations in the region $\Delta\nu = 2$

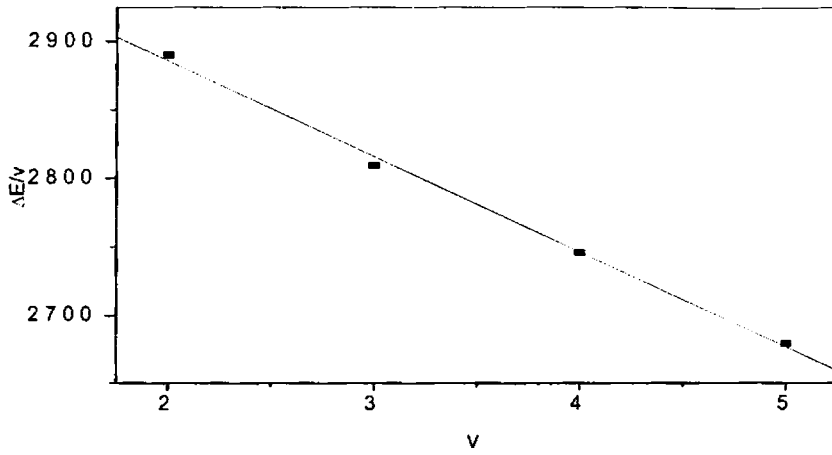


Fig. 5.33. Birge-Sponer plot for CH stretch overtones of morpholine

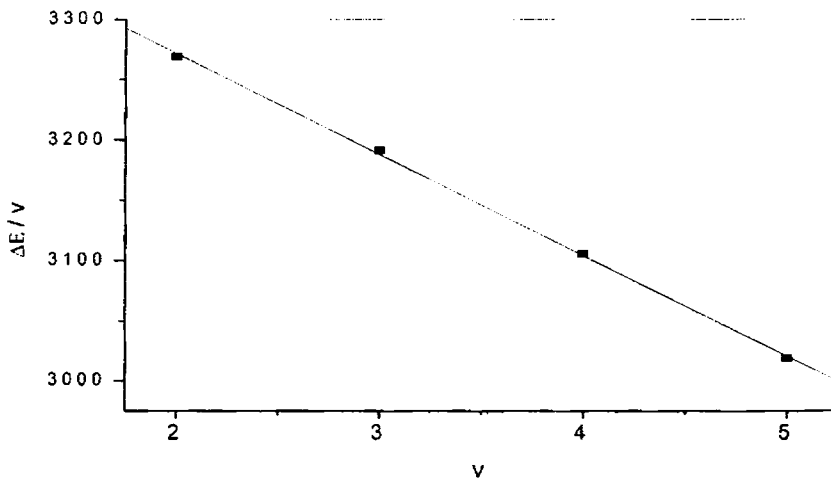


Fig. 5.34. Birge-Sponer plot for free NH overtones of morpholine

Table 5.4

The band assignments, overtone peak position and the local mode parameters of the CH and NH oscillators morpholine

Stretch type	Overtone peak positions in (cm ⁻¹) for v =				Local mode parameters and correlation coefficient
	2	3	4	5	
CH	5780.35	8428.15	10982.98	13395.85	X ₁ = 3070.30 X ₂ = 65.11 γ = -.9999
Free NH	6538.08	9573.96	12422.36	15094.34	X ₁ = 3450.16 X ₂ = 86.23 γ = -.1

v = vibrational quantum number, X₁ = mechanical frequencies (cm⁻¹), X₂ = anharmonicities (cm⁻¹) and γ = the least square correlation coefficient.

Comparing the structures of morpholine and piperidine, we can see that the oxygen atom in morpholine is electron withdrawing, making the nitrogen more positive [27], weakening its basicity. Studies on the vibrational spectra of piperidine and morpholine was done by Vedal et al. [32]. NH overtone positions of piperidine are given in the work of Sauvageau and Sandorfy [31]. The NH overtone peaks for morpholine (Figs. 5.28-5.31) are greater compared to piperidine. Thus the weak basicity of morpholine is reflected in the NH- stretch frequency values itself [22].

5.3.4 Conclusions

Morpholine being a secondary amine overtones corresponding to only one type of NH stretch is there. Due to the weak hydrogen bonding in amines higher overtones for bonded NH oscillators are too weak to be resolved. Still weak and broad red-shifted bands at lower overtones are identified due to the formation of NH...O hydrogen bonds. The high values of NH-stretching overtone positions of morpholine compared to piperidine is an indication of its weak basicity.

REFERENCES

- [1] B.R. Henry, *Acc. Chem. Res.* 20 (1987) 429.
- [2] B.R. Henry, in: J.R. Durig (Ed.), *Vibrational Spectra and Structure*, Vol.10, Elsevier, Amsterdam, 1981.
- [3] W.R.A. Greenlay, B.R. Henry, *Chem. Phys. Lett.*, 53 (2) (1978) 325.
- [4] W.R.A. Greenlay, B.R. Henry, *J. Chem. Phys.* 69 (1) (1978) 82.
- [5] B.R. Henry, M.A. Mohammadi, J.A. Thomson, *J.Chem. Phys.*, 75 (1981) 3165.
- [6] K.M. Gough, B.R. Henry, *J. Phys. Chem.*, 88 (1984)1298.
- [7] H.G. Kjaergaard, D.M. Turnbull, B.R. Henry, *J.Phys.Chem.*, 101 (1997) 2589.
- [8] B.R. Henry, R.J.D. Miller, *Chem. Phys. Lett.* 60 (1) (1978) 81.
- [9] M.K. Ahamed, B. R. Henry, *J. Phys. Chem.*, 90 (1986) 1737.
- [10] P.N. Ghosh, P.K. Panja, C.M. Pal, *Chem. Phys. Lett.*, 148 (4) (1988) 337.
- [11] M.E. Vaschetto, B.A. Retamal, A.P. Monkman, *J. Mol. Struct. (Theochem)*, 468 (1999) 209.
- [12] W.B. Tzeng, K. Narayanan, J.L. Lin, C.C. Tung, *Spectrochim. Acta Part A* 55 (1999) 153 .
- [13] L. Santos, E. Martinez, B. Ballesteros, J. Sanchez, *Spectrochim. Acta Part A* 56 (2000) 1905.
- [14] W.B. Tzeng, K. Narayanan, *J. Mol. Struct.* 446 (1998) 93.
- [15] H.C. Brown, A. Cahn, *J. Am. Chem. Soc.*, 72 (1950) 2939.
- [16] R.T. Morrison, R.N. Boyd, *Organic Chemistry*, Prentice-Hall of India, New Delhi, 2000, p. 853.
- [17] R.T. Morrison, R.N. Boyd, *Organic Chemistry*, Prentice-Hall of India, New Delhi, 2000, p.850.
- [18] L.N. Ferguson, *The Modern Structural Theory of Organic Chemistry*, Prentice-Hall of India, New Delhi, 1973, p. 353.
- [19] R. Nakagaki, I. Hanazaki, *Spectrochim. Acta* 404 (1984) 57.

- [20] L.N. Ferguson, *The Modern Structural Theory of Organic Chemistry*, Prentice-Hall of India, New Delhi, 1973, p. 421.
- [21] S. Shaji, S.M. Eapen, K.P.R. Nair, T.M.A. Rasheed, *Spectrochim. Acta Part A* 60 (2004) 351.
- [22] U. John, K. P. R. Nair, *Spectrochim. Acta Part A* 60 (2004) 2337.
- [23] P.S. kalsi, *Spectroscopy of Organic Compounds*, New Age International Limited, Publishers, New Delhi, Fourth edition, 1999, p.90 .
- [24] P. Hobza, Z. Havlas, *Chem.Rev.* 100 (2000) 4253.
- [25] C. Berthomieu , C. Sandorfy, *J.Mol.Spectrosc.*15 (1965) 15.
- [26] M.C.B. Houplain, C. Sandorfy, *J. Chem. Phys.* 56 (1972) 3412.
- [27] R.J. Fessenden, J.S. Fessenden, *Organic Chemistry*, 5th ed., Brooks/Cole Publishing Company, California, 1993, p. 789.
- [28] S. Shaji, T.M.A. Rasheed, *Spectrochim. Acta Part A* 57 (2001) 337.
- [29] H.G. Kjaergaard, B.R. Henry, *J. Chem. Phys.* 96 (1992) 4841.
- [30] O. Indrisa, W. Stahla, U. Kretschmerb, *J. Mol. Spectrosc.*190 (1998) 372.
- [31] P. Sauvageau, C. Sandorfy, *Can. J. Chem.* 38 (1960) 1901.
- [32] D. Vedal, O.H. Ellestad, P. Klaboe, G. Hagen, *Spectrochim. Acta Part A* 32 (1976) 877.

CHAPTER 6

NEAR IR OVERTONE ANALYSIS OF SOME MODERATELY STRONG HYDROGEN BONDED SYSTEMS

6.1 Analysis of the Overtone Spectra of Cyclohexanol

6.1.1 Introduction

Self associated alcohols are a good example for relatively weak hydrogen bonds. Cyclohexanol or cyclohexyl alcohol ($C_6H_{12}O$, Fig. 6.1) is a viscous liquid used mainly as a laboratory and industrial solvent. It is an intermediate in making chemicals used in nylon manufacture. The near infrared vibrational overtone absorption spectrum of liquid phase cyclohexanol in carbon tetrachloride in different concentrations are reported here. In the liquid state and concentrated solutions, OH compounds associate through hydrogen bonds. As the solutions are progressively diluted, the solute molecules are separated more and more, and the hydrogen bonds are gradually broken. The mean state of aggregation passes successively from polymeric through tetrameric, trimeric, dimeric states until the solute is essentially monomeric [1]. Jones and Sandorfy [2] studied the fundamentals from the infrared spectrum of cyclohexanol at various concentrations in carbon tetrachloride solution. In the region of OH stretching vibrations, they observed the free (non-hydrogen bonded) and bonded OH bands. Huisken et al. [3] made theoretical investigations on water clusters and were able to assign two main transitions in the IR region corresponding to the nonbonded and bonded OH-stretching vibrations for the dimer, trimer, tetramer and pentamer. At very low concentration, only the free OH band is seen. At higher concentration the intensity of the so-called polymer band increases. This band is broad and this is a characteristic of many hydrogen bonded systems.

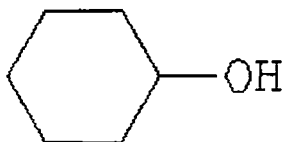


Fig. 6.1 Structure of cyclohexanol

Since the existence of overtones is connected with anharmonicity, numerous studies were devoted to the effect of hydrogen bond formation on the anharmonicity of the potential function of vibrations affected by hydrogen bonding [4-6]. For all concentrations of cyclohexanol the OH frequencies and anharmonicities (for both free and bonded) calculated using local mode model support the conclusions made by Durocher and Sandorfy by measuring the fundamental and first two overtones [7, 8]. Low and Kjaergaard [9] have calculated local mode parameters of water dimer and trimer from scaled *ab initio* calculations and noted that the significant difference between the monomer and the dimer and trimer is the appearance of the red shifted hydrogen bonded OH-stretching band in the dimer and trimer spectra. They have noted that the red shift is larger for the trimer than the dimer. Also they obtained slightly larger anharmonicity for the bonded OH-stretching bonds in the trimer compared to the dimer. These theoretical investigations also support our conclusions.

6.1.2 Experimental

High purity (99%) cyclohexanol were obtained from Sisco Research Laboratories Pvt. Ltd., Mumbai, India. Solutions of cyclohexanol in carbon tetrachloride in different concentrations (100%, 66% and 33%) are made. The liquid phase absorption spectra in the near infrared region (700–2000 nm) were recorded for the three concentrations, at room temperature ($26 \pm 1^{\circ}$ C) with air as reference and pathlength 1cm, using a Jasco Corp. model V-570 UV-Vis-NIR spectrophotometer which uses a tungsten lamp as the near IR source.

6.1.3 Results and Discussions

The near infrared vibrational overtone absorption spectra of cyclohexanol in carbon tetrachloride in each concentration in the region 700-2000 nm show bands due to pure overtone transitions of CH, bonded OH and free OH local mode oscillators and those due to combination transitions involving several vibrational degrees of freedom of the molecule. In the present analysis, only the pure overtones of oscillators are considered. The bands in the $\Delta\nu = 2, 3$ and 4 regions for all the three concentrations are shown in Figs. 6.2-6.4. Here 'a' represents CH overtones, 'b' represents bonded OH-stretching overtones, 'c' represents free OH-stretching overtones and the other peaks are combinations. In Fig. 6.4 'a₅' is the CH stretching overtone corresponding to $\Delta\nu = 5$. The bands in the $\Delta\nu = 2$ region show multiple peaks due to the presence of combinations whereas the higher overtone bands show single overtone peaks. In the CH region in $\Delta\nu = 2$ and 3 we have two peaks corresponding to two nonequivalent CH bonds, the axial and the equatorial, similar to the case of cyclohexane [10]. Similarly in the free OH region also we have two peaks corresponding to the axial and equatorial conformations, since the cyclohexanol being a monosubstituted cyclohexane [11]. The hydrogen bonded band is broad and this is a characteristic of all hydrogen bonded systems [4]. Actually it is this breadth whose study can lead us to the understanding of the nature of the hydrogen bonding. Bonded OH bands are shown in Figs. 6.5-6.7 corresponding to $\Delta\nu = 2, 3$ and 4 respectively. In the particular case of self associated alcohols one of the causes of the breadth is the existence of a variety of associated species in the solution, like dimers, trimers, tetramers, etc. Even when only one associated species is present, the bands are broad [4]. This is due to the anharmonic coupling between the free OH and the low frequency bridge (bonded) vibration. The result of this anharmonic coupling would be the appearance of combination bands, both summation and difference tones, which gives breadth to the region.

Anyway the first overtone peak position in each case is assigned as the one giving the best fit in the Birge-Sponer plot with higher overtone peaks. Figs. 6.8-6.10 give the Birge-Sponer plots for CH stretching, bonded OH-stretching and free OH-

stretching vibrations respectively, at different concentrations. The band assignments, overtone peak positions and local mode parameters of the CH, bonded OH and free OH oscillators for different concentrations are given in Tables 6.1- 6.3.

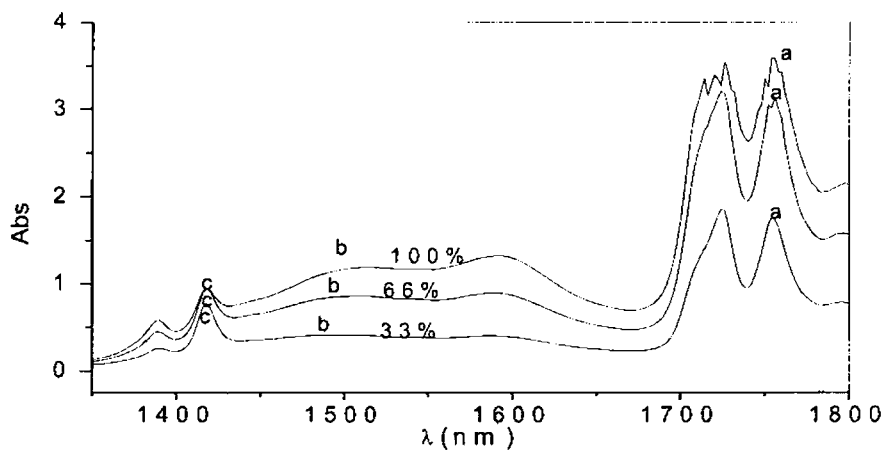


Fig. 6.2. Overtone spectrum of cyclohexanol in carbon tetrachloride in different concentrations in the region $\Delta v = 2$

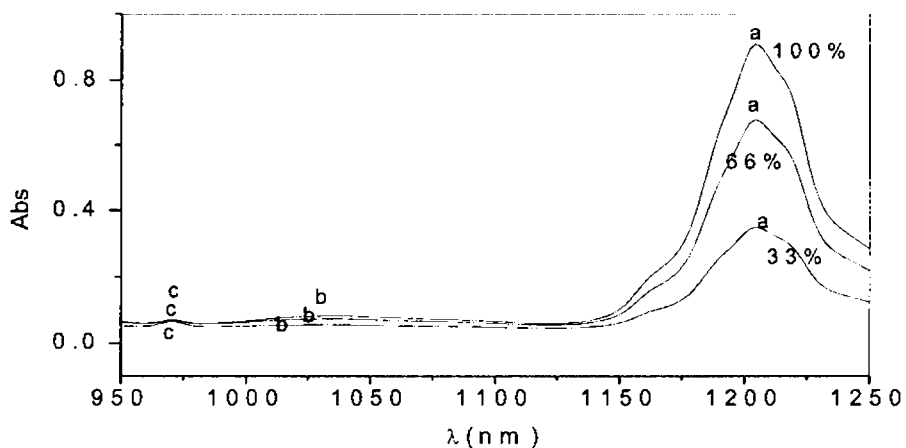


Fig. 6.3. Overtone spectrum of cyclohexanol in carbon tetrachloride in different concentrations in the region $\Delta v = 3$

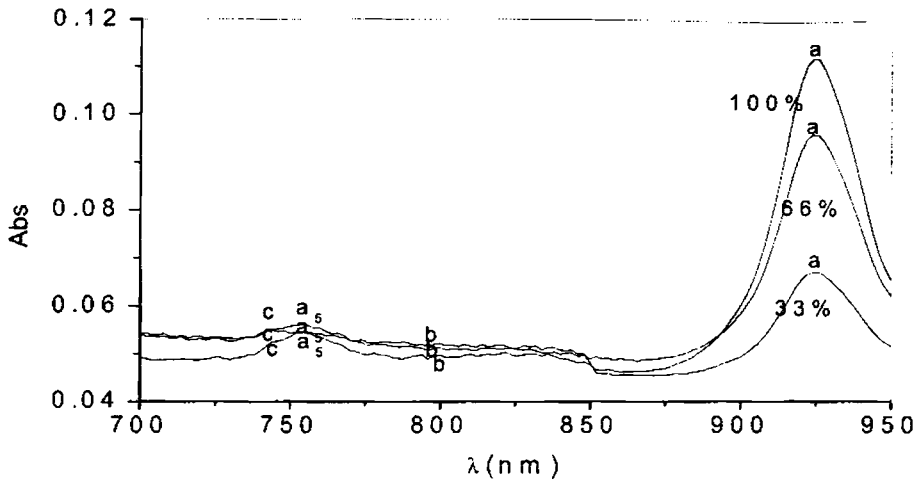


Fig. 6.4. Overtone spectrum of cyclohexanol in carbon tetrachloride in different concentrations in the region $\Delta\nu = 4$. a_5 is the CH stretching overtone corresponding to $\Delta\nu = 5$

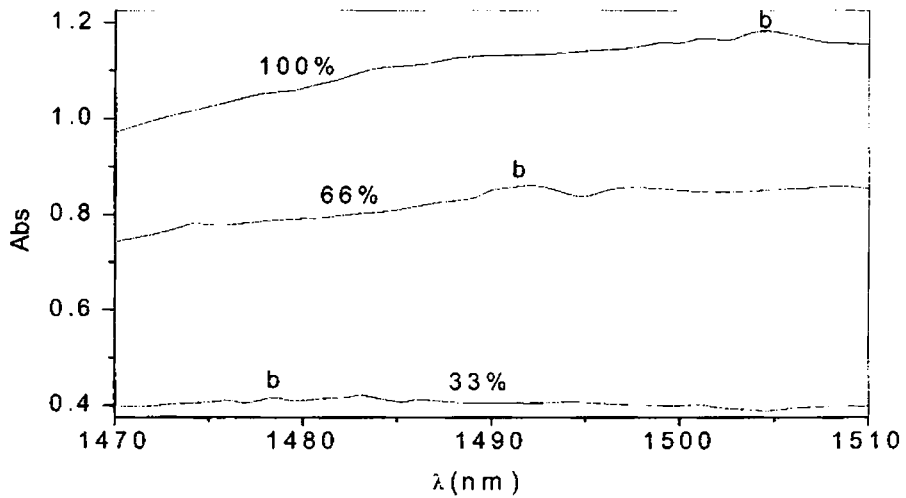


Fig. 6.5. Bonded OH bands in the region $\Delta\nu = 2$

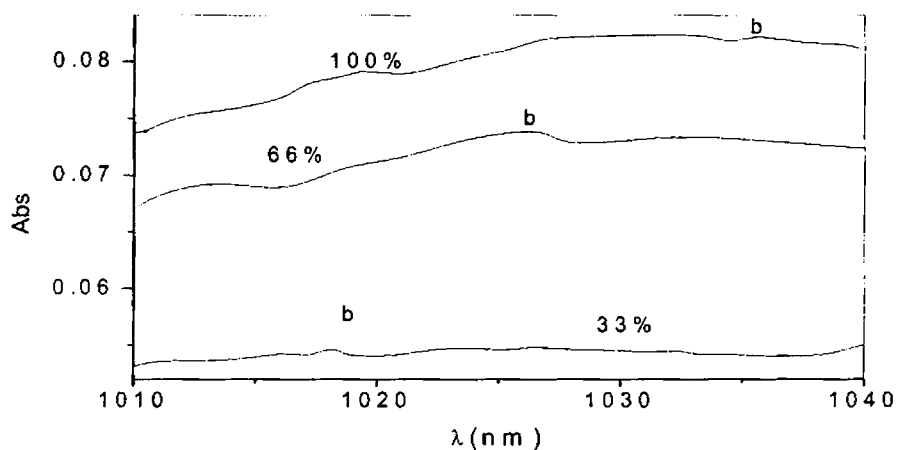


Fig. 6.6. Bonded OH bands in the region $\Delta\nu = 3$

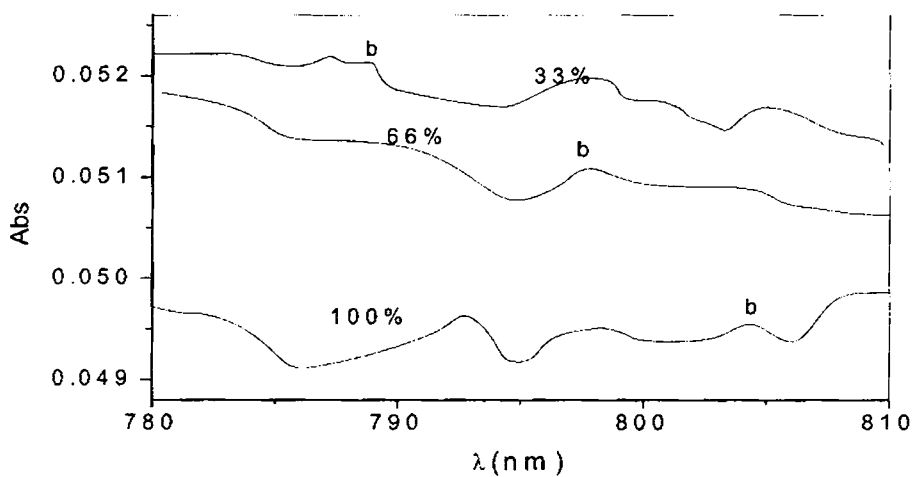


Fig. 6.7. Bonded OH bands in the region $\Delta\nu = 4$

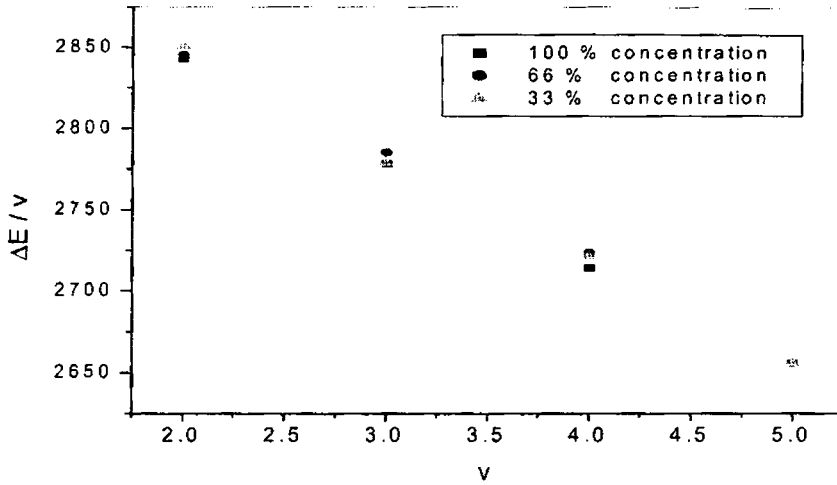


Fig. 6.8. Birge-Sponer plots for CH stretching overtones of cyclohexanol at different concentrations

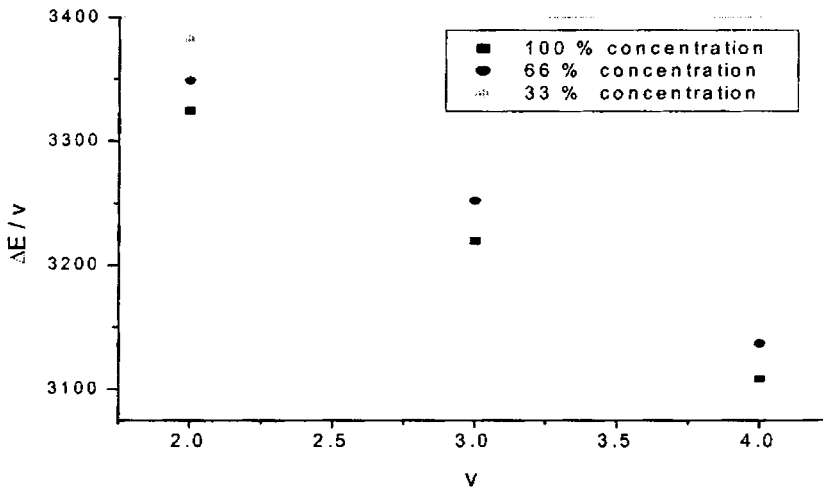


Fig. 6.9. Birge-Sponer plots for bonded OH-stretching overtones of cyclohexanol at different concentrations

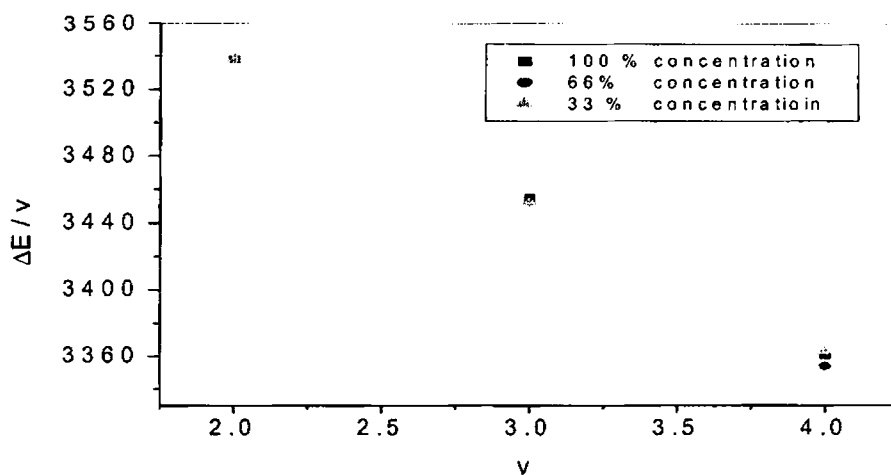


Fig. 6.10 Birge-Sponer plots for free OH-stretching overtones of cyclohexanol at different concentrations

Table 6.1
CH-stretch assignment

v	Overtone peak positions in nm (cm^{-1}) for cyclohexanol concentration			Local mode parameters and γ for cyclohexanol concentration		
	100%	66%	33%	100%	66%	33%
2	1758.8 (5685.70)	1757.3 (5690.55)	1754 (5701.25)	$X_1=3028.96$	$X_1=3031.39$	$X_1=3040.37$
3	1199.7 (8335.42)	1199.7 (8335.42)	1199.7 (8335.42)	$X_2=62.45$	$X_2=62.36$	$X_2=64.18$
4	921 (10857.76)	917.9 (10894.43)	918.6 (10886.13)	$\gamma=-.9997$	$\gamma=-.9992$	$\gamma=-.9991$
5	753 (13280.21)	753.1 (13278.45)	753.1 (13278.45)			

v = vibrational quantum number, X_1 = mechanical frequencies (cm^{-1}), X_2 = anharmonicities (cm^{-1}) and γ = the least square correlation coefficient.

Table 6.2

Bonded OH-stretch assignment

v	Overtone peak positions in nm (cm ⁻¹) for cyclohexanol concentration			Local mode parameters and γ for cyclohexanol concentration		
	100%	66%	33%	100%	66%	33%
2	1503.9 (6649.38)	1493.1 (6697.48)	1478.5 (6763.61)	X ₁ =3650.24	X ₁ =3669.8	X ₁ =3688.3
3	1035.4 (9658.10)	1025 (9756.10)	1017.7 (9826.08)	X ₂ = 108.2	X ₂ =106	X ₂ = 102.59
4	804.3 (12433.17)	797 (12547.05)	787 (12706.48)	$\gamma = -.9999$	$\gamma = -.9990$	$\gamma = -.9998$

v = vibrational quantum number, X₁ = mechanical frequencies(cm⁻¹), X₂ = anharmonicities (cm⁻¹) and γ = the least square correlation coefficient .

Table 6.3

Free OH-stretch assignment

v	Overtone peak positions in nm (cm ⁻¹) for cyclohexanol concentration			Local mode parameters and γ for cyclohexanol concentration		
	100%	66%	33%	100%	66%	33%
2	1413.2 (7076.14)	1413.2 (7076.14)	1413.2 (7076.14)	X ₁ =3806.9	X ₁ =3816.47	X ₁ =3802.19
3	964.7 (10365.92)	965.5 (10357.33)	965.5 (10357.33)	X ₂ = 88.93	X ₂ =92.08	X ₂ = 87.80
4	744 (13440.86)	745.4 (13415.62)	743.5 (13449.90)	$\gamma = -.9992$	$\gamma = -.9992$	$\gamma = -.9999$

v = vibrational quantum number, X₁ = mechanical frequencies(cm⁻¹), X₂ = anharmonicities (cm⁻¹) and γ = the least square correlation coefficient .

The calculated CH, bonded OH and free OH oscillators under various concentrations are examined below.

CH oscillators: The CH stretching frequencies and anharmonicities are almost unaffected by variation in concentration. The CH stretching frequencies and anharmonicities are in agreement with the local mode parameters calculated by Kjaergaard and Henry for cyclohexane [10].

Bonded OH oscillators: Due to hydrogen bonding, in addition to the free OH, a red shifted hydrogen bonded broad band appears in the spectrum. This red shift increases with concentration. The mechanical frequencies and anharmonicities experience a systematic variation as concentration is changed [12]. For hydrogen bonded polymers where oxygen atom is both proton donor and acceptor it increases to about 95 cm^{-1} – 120 cm^{-1} [4]. The frequency decreases and anharmonicity increases with concentration, which is in agreement with the experimental conclusions made by Durocher and Sandorfy [7] and with the theoretical investigations by Low and Kjaergaard [9].

Free OH oscillators: The free OH local mode parameters are almost unaffected by variation in concentration. For the free stretching OH bands the anharmonicity is small and frequency is high compared to bonded OH [7, 9].

6.1.4 Conclusions

Overtone spectra of cyclohexanol in carbon tetrachloride in three different concentrations are analysed using the local mode model. The mechanical frequencies and anharmonicities for various oscillators are calculated. The aryl CH and free OH local mode parameters are almost insensitive to the variation in concentration. But the local mode parameters for the bonded OH stretching vibrations vary with concentration. We have observed that as the concentration is increased, mechanical frequency of the bonded OH vibrations tends to decrease and anharmonicity tends to increase due to strong intermolecular hydrogen bonding.

6.2 Analysis of the Overtone Spectra of Cyclopentanol

6.2.1 Introduction

Just like cyclohexanol, cyclopentanol too is a self-associated alcohol. Cyclopentanol ($C_5H_{10}O$, Fig. 6.11) is a thick, colourless liquid with a pleasant odour. It is used as a solvent, and as an intermediate in making perfumes, pharmaceuticals, dyes and other organic chemicals. Cyclopentanol is having a puckered shape. Just like cyclopentane, the actual structure of cyclopentanol is of 'envelope' shape [13, 14]. A number of studies of substituted cyclopentanes have been reported [15-18]. Ekejiuba and Hallam [19] observed an ill-resolved doublet for the free hydroxyl stretching band at 3612 cm^{-1} in the IR spectrum of cyclopentanol in CCl_4 . They interpreted this as evidence of an equilibrium between axial and equatorial conformers. Later Abraham et al. reported a theoretical and LIS (Lanthanide Induced Shifts) investigations of cyclopentanol [20]. They showed that the conformation of cyclopentanol in solution is not symmetrical but is a non-symmetric conformation. All the previous investigations of the conformations of monosubstituted cyclopentanes have assumed a symmetric envelope conformation with the substituent at the flap of the envelope. Both the theoretical and LIS results presented by these authors show clearly that the major conformation of cyclopentanol in solution is an unsymmetric envelope conformation with the axial hydroxyl substituent at the fold of the envelope (Fig. 6.12) The symmetric conformation with an axial hydroxyl at the flap of the envelope (Fig. 6.13) is present but is of higher energy than the unsymmetric conformer. The symmetric equatorial conformer is a minor component in solution. Accordingly one would expect the OH stretching frequency in Fig. 6.12 and Fig. 6.13 to differ and therefore two free OH bands would be observed in dilute solutions. These theoretical investigations support our observations of the overtone spectra of cyclopentanol

The near infrared vibrational overtone absorption spectrum of liquid phase cyclopentanol in carbon tetrachloride is examined in the region $\Delta v = 2, 3$ and 4. In the region of OH stretching vibrations, besides the free OH (non-hydrogen bonded),

bonded OH bands are also observed, as in the case of cyclohexanol. The CH, bonded OH and free OH local mode mechanical frequency values and anharmonicity values obtained from fitting the overtones are analysed and compared.



Fig. 6.11. structure of cyclopentanol

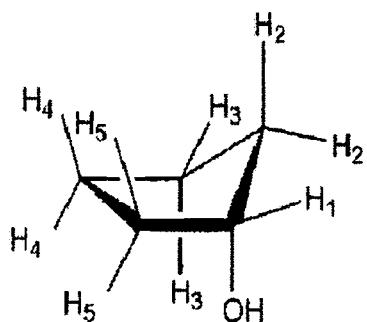


Fig. 6.12. unsymmetric envelope conformation

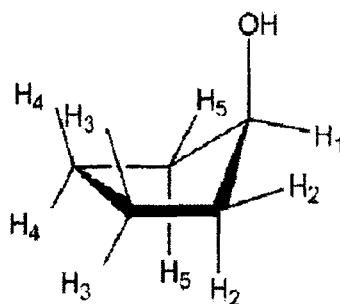


Fig. 6.13. symmetric envelope conformation

6.2.2 Experimental

High purity (99%) cyclopentanol were obtained from Sigma-Aldrich Chemicals Private Limited, Bangalore, India. Solutions of cyclopentanol in carbon tetrachloride under various concentrations are made. The liquid phase absorption spectra in the near infrared region (700-2000 nm) were recorded at room temperature ($26 \pm 1^\circ\text{C}$) with air as reference and path length 1 cm, using a Varian (Cary 5000 model) UV- Vis-NIR Spectrophotometer which uses a tungsten lamp as the near IR source.

6.2.3 Results and Discussions

Kanno et al. in their Raman studies of alcohol solutions (21-25) measured Raman OH-stretching spectra of alcoholic solutions with inert solvents, such as CCl_4 , CHCl_3 , etc. OH stretching spectrum below 3600 cm^{-1} in which the bonded OH bands for dimer and trimer should exist, it was impossible to detect expected Raman bands due to the stretching vibrations of the dimers and trimers, because the Raman spectrum below 3600 cm^{-1} was broad and rather featureless. Concentrated solutions of cyclopentanol in CCl_4 gave unresolvable bands in the bonded OH stretch region. So the observation is made only on a less diluted solution of cyclopentanol. The near infrared vibrational overtone absorption spectra of diluted solution of cyclopentanol in carbon tetrachloride in the region 700-2000 nm show bands due to pure overtone transitions of CH, bonded OH and free OH local mode oscillators and those due to combination transitions involving several vibrational degrees of freedom of the molecule. In the present analysis, only the pure overtones of oscillators are considered.

The bands in the $\Delta\nu = 2, 3$ and 4 regions are shown in Figs. 6.14 – 6.16. Here 'a' represents CH overtones, 'b' represents bonded OH stretching overtones, 'c' represents free OH-stretching overtones and other peaks are combinations. In the CH region in $\Delta\nu = 2$ we have two peaks corresponding to two nonequivalent CH bonds, the axial and the equatorial, similar to the case of cyclopentane [26]. Similarly in the free OH region in $\Delta\nu = 2$ also we have two peaks. This observation is supported by both the theoretical and LIS investigations of cyclopentanol by Abraham et al. [20]. They suggested two optimised geometries for cyclopentanol. These authors showed clearly that the major conformation of cyclopentanol in solution is an unsymmetric envelope conformation with the axial hydroxyl substituent at the fold of the envelope as in Fig. 6.12. The symmetric conformation with an axial hydroxyl at the flap of the envelope as in Fig. 6.13 is also present but is of higher energy than the unsymmetric conformer. Hence the low intensity band in the free OH region is identified as due to the symmetric conformer and the other one due to the unsymmetric conformer. The red-shifted

hydrogen bonded band is broad and this is a characteristic of all hydrogen bond systems. This breadth is due to the existence of a variety of associated species in the solution, like dimers, trimers, tetramers, etc. and also due to the anharmonic coupling between the free OH and the low frequency bridge (bonded) vibration [4].

The first overtone peak position in each case is assigned as the one giving the best fit in the Birge-Sponer plot with the higher overtone peaks. Figs. 6.17-6.19 give the Birge-Sponer plots for CH-stretching overtones, bonded OH-stretching overtones and free OH-stretching overtones respectively. The band assignments, overtone peak positions and local mode parameters of the CH, bonded OH and free OH oscillators are given in Table 6.4.

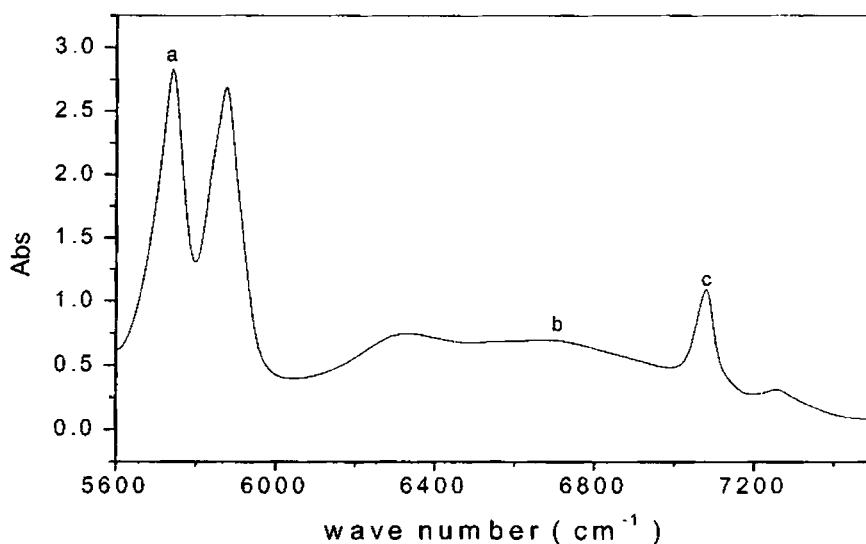


Fig. 6.14. Overtone spectrum of cyclopentanol
in the region $\Delta v = 2$

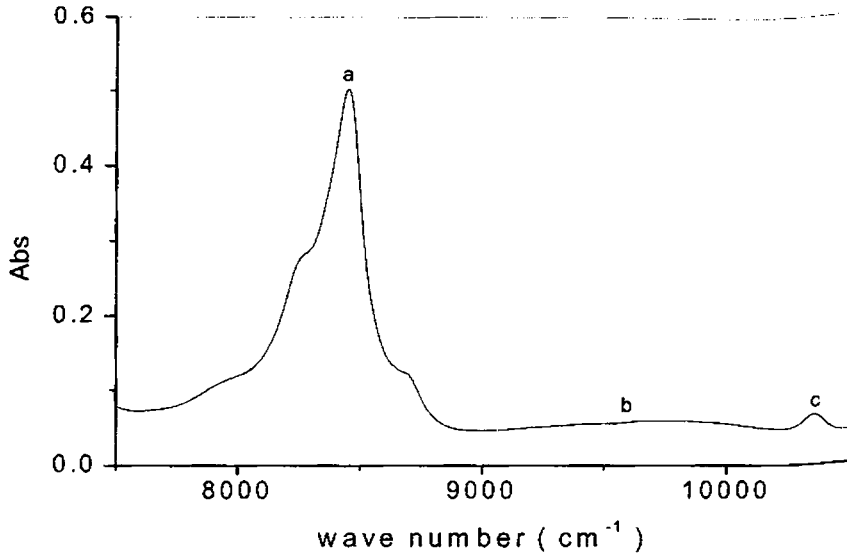


Fig. 6.15. Overtone spectrum of cyclopentanol
in the region $\Delta v = 3$

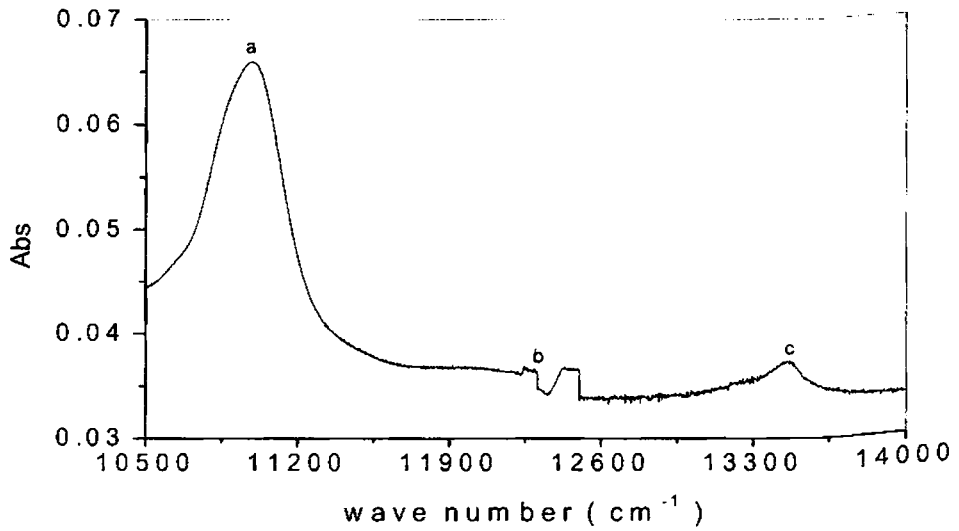


Fig. 6.16. Overtone spectrum of cyclopentanol
in the region $\Delta v = 4$

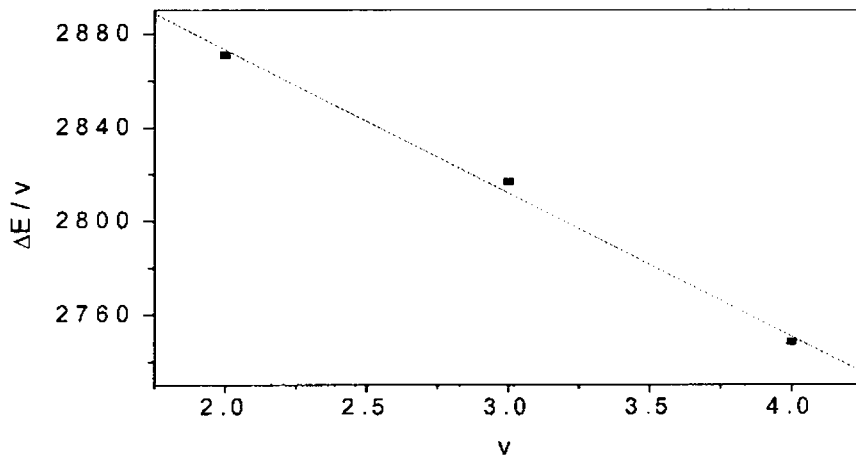


Fig. 6.17. Birge-Sponer plot for CH stretching overtones

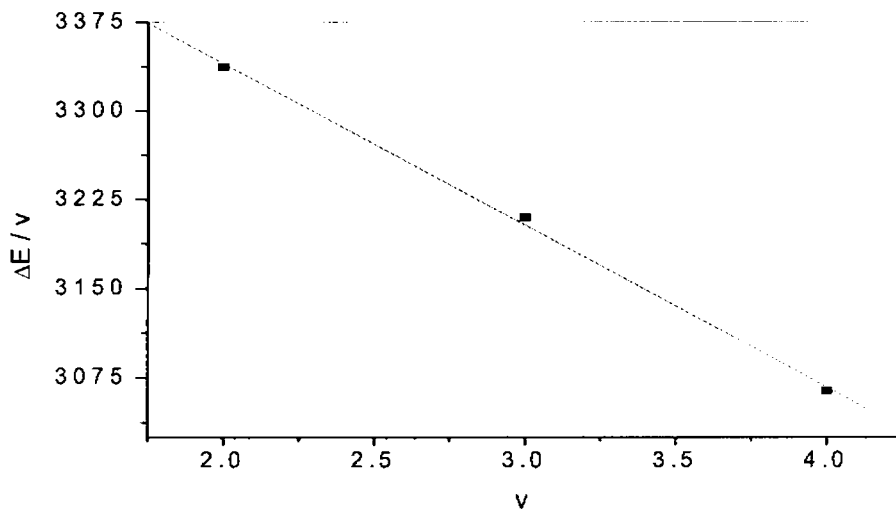


Fig. 6.18. Birge-Sponer plot for bonded OH-stretching overtones

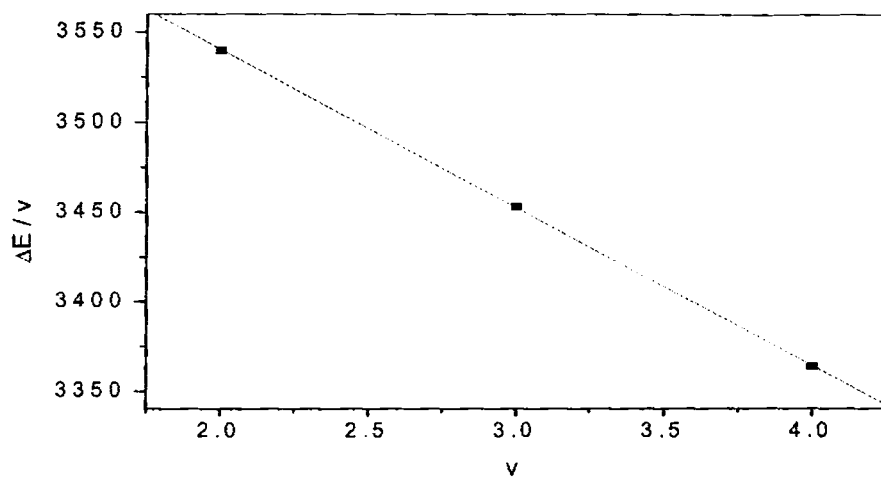


Fig. 6.19. Birge-Sponer plot for
free OH stretching overtones

Table 6.4

The band assignments, overtone peak positions and the local mode parameters of the CH, bonded OH and free OH oscillators of cyclopentanol

Stretch type	V	Overtone peak positions in nm (cm^{-1})	Local mode parameters and γ
CH	2	1741.70 (5741.52)	$X_1 = 3057.09$
	3	1183.40 (8450.23)	$X_2 = 61.30$
	4	909.70 (10992.63)	$\gamma = -.998$
Bonded OH	2	1498.400 (6673.79)	$X_1 = 3749.90$
	3	1038.40 (9630.09)	$X_2 = 136.59$
	4	816.00 (12254.9)	$\gamma = -.9992$
Free OH	2	1412.50 (7079.65)	$X_1 = 3804.256$
	3	965.30 (10359.47)	$X_2 = 87.996$
	4	743.20 (13455.33)	$\gamma = -.99996$

V = vibrational quantum number, X_1 = mechanical frequencies (cm^{-1}),
 X_2 = anharmonicities (cm^{-1}) and γ = the least square correlation coefficient.

The CH, bonded OH and free OH oscillators under various concentrations are examined briefly below.

CH oscillators: The CH stretching frequencies and anharmonicities are in agreement with the local mode parameters calculated by Henry et al. for cyclopentane [26].

Bonded OH oscillators: Due to hydrogen bonding, in addition to the free OH, a red-shifted hydrogen bonded broad band appears in the spectrum. The frequency decrease and anharmonicity increase due to hydrogen bonding is in agreement with the experimental conclusions made by Durocher and Sandorfy [7] and with the theoretical investigations by Low and Kjaergaard [9].

Free OH oscillators: The frequency and anharmonicity of the free stretching OH bands agree with the already established results for free OH bands [7, 9, 12].

6.2.4 Conclusions

Overtone spectra of cyclopentanol in carbon tetrachloride is analysed using the local mode model. In the CH region in $\Delta v = 2$ we have two peaks corresponding to two nonequivalent CH bonds, the axial and the equatorial, similar to the case of cyclopentane. The CH stretching frequencies and anharmonicities are in agreement with the local mode parameters calculated by Henry et al. for cyclopentane. In the OH region both free and red-shifted hydrogen bonded OH oscillators are observed. The mechanical anharmonicity of the red-shifted OH bands is calculated using local mode model and is found to be greater than that of free OH. In the free OH region in $\Delta v = 2$ two peaks are there, which suggest the two optimised geometries for cyclopentanol, an unsymmetric envelope conformation with the axial hydroxyl substituent at the fold of the envelope and the symmetric conformation with an axial hydroxyl at the flap of the envelope. The frequency and anharmonicity of the free stretching OH bands agree with the already established results for free OH bonds.

6.3 Analysis of the Overtone Spectra of Imidazole

6.3.1 Introduction

Aromatic heterocycles are widely distributed in nature and often play an important role in various biochemical processes. The volume of literature on five-membered heteroaromatic rings has experienced an enormous expansion over the past few decades [27]. Five membered aromatic heterocycles containing two heteroatoms represent a large and structurally diverse group. For example, Imidazole, which contains two similar hetero atoms is derived from pyrrole by replacement of the methine (-CH group) by an sp^2 -hybridized nitrogen atom. The lone pair of the electrons of the nitrogen atom provides a site for protonation and alters the acidity and basicity of these heterocycles. The unique ring structure of imidazole (Fig. 6.20)

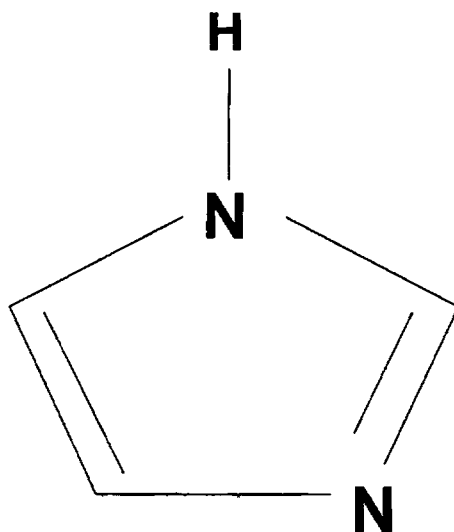


Fig. 6.20. Ring structure of Imidazole ($C_3N_2H_4$)

permits the proton to be picked up by one N atom and the other H/H^+ to be released from the other N atom. Imidazole occurs in histidine, an essential amino acid. The use of imidazoles and their derivatives in chemical processes is becoming increasingly

important. Their potential for hydrogen bond formation is also widely used in pharmaceuticals [28]. The incorporation of an imidazole ring in medicinal chemistry has grown considerably as judged from the large number of therapeutically useful imidazole based compounds including antifungals, anticonvulsants and inhibitors [29]. Proton transfer properties of Im-ImH⁺ complex are recently suggested in polymer electrolyte fuel cells [30]. The fuel cell technology is expected to become one of the key technologies for energy production.

As discussed in chapter 4, the hydrogen bond is a bond between electron deficient hydrogen and a region of high electron density. Most frequently, a hydrogen bond is of X-H...Y type, where X and Y are electronegative elements and Y possesses one or more lone electron pairs. Here there is a significant charge transfer or electron density transfer from the proton acceptor (Y) to the proton donor (X-H). Hydrogen bonds having X, Y = F, O and N are best studied [31-33]. The formation of the X-H...Y hydrogen bond results in weakening of the X-H bond. This weakening is accompanied by bond elongation and a decrease of XH stretch vibration frequency compared to the noninteracting species. As already discussed in many cases, this shift to lower frequencies is called a red-shift and represents the easily detectable manifestation of the formation of a hydrogen bond [34]. But a different situation called blue-shifting of hydrogen bonds was reported [35] first in 1989 where the IR spectrum of triformylmethane in chloroform was measured and the presence of a distinct, sharp band close to the CH stretch of chloroform but slightly shifted to higher wave numbers were detected. Another observation of the blue shift was reported in 1997 by Boldeskul et al. [36].

Two schools of thought have mainly emerged in trying to explain the physical basis for blue-shifted frequencies in hydrogen bonded systems [37]. In both cases it is acknowledged that the frequency (blue) shift results from the shortening of the bond that occurs on hydrogen bonding. One group, represented by Hobza and co-workers, views such bonds as fundamentally different from traditional red-shifted bonds. They initially termed them "anti-hydrogen bonds" and subsequently revised this to

improper “blue-shifting hydrogen bonds” [34, 38-44]. According to them, the origin of the bond shortening is attributed primarily to a two step mechanism that involves electron density transfer from the proton acceptor to the antibonding orbitals in the remote part of the proton donor, which causes elongation of bonds in that part of the complex. This primary effect is accompanied by a secondary effect of structural reorganization of the proton donor, leading to a contraction of the X–H bond and a blue shift of the XH stretch frequency [34,44]. The other group, represented by Scheiner and Dannenberg and their co-workers, views such bonds as basically no different in nature from red shifted hydrogen bonds [45-47]. According to them the change in X–H bond length is the net resultant of one set of forces tending toward elongation and another that pulls toward a shorter bond. The same forces are in operation in both types of hydrogen bond: electrostatic, polarization, charge transfer and dispersion push the hydrogen away from the donor atom, while exchange pulls it away from the acceptor. When the former set are together slightly stronger than the exchange, red shift follows due to the bond stretch. If the latter overcomes the former set, a blue shift follows due to contraction of the bond [45].

In the present paper, we report the near infrared vibrational overtone absorption spectrum of imidazole dissolved in carbon tetrachloride. In the $\Delta\nu = 2$ region we have observed two NH stretch positions. One is blue shifted and is broad and intense compared to the other low wave number band. Our experimental evidence for this blue shifted hydrogen bond is supported by the recent (2004) theoretical investigations of Shihai Yan et al. [48] on Im-ImH⁺ complex. On the basis of the reliable B3LYP/6-311+G* method they have found different coupling modes for the complexes of imidazole and imidazole cation through the geometry optimisations. There is one common phenomenon for these complexes, where one NH bond is blue shifted for each of them. This observation should be due to the interaction of two fragments; therefore, the electron redistribute in two fragments, leading to the strengthening of the NH bond of ImH⁺.

6.3.2 Experimental

High purity (>99%) imidazole was obtained from E. Merck (India) Ltd, Mumbai. Imidazole being a solid, its near saturated solution in spectrargrade carbon tetrachloride is prepared. By adding more carbon tetrachloride, a less concentrated solution also is prepared. The liquid phase absorption spectra in the near infrared region (700–2000 nm) were recorded for the two concentrations, at room temperature ($26 \pm 1^\circ \text{C}$) with air as reference and pathlength 1 cm, using a Varian (Cary 5000 model) UV-Vis–NIR spectrophotometer which uses a tungsten lamp as the near IR source.

6.3.3 Results and Discussions

The near infrared vibrational overtone absorption spectra of imidazole in carbon tetrachloride in the region 700–2000 nm show bands due to pure overtone transitions of CH, free NH and bonded NH local mode oscillators and those due to combination transitions involving several vibrational degrees of freedom of the molecule. In the present analysis, only the pure overtones of oscillators are considered. The bands in the $\Delta v = 2, 3$ and 4 regions for all the three concentrations are shown in Figs. 6.21–6.23. Here 'a' represents CH overtones, 'b' represents free NH-stretching overtones, 'c' represents blue-shifted hydrogen bonded NH-stretching overtones and the other peaks are combinations. The sharp rise in $12,500 \text{ cm}^{-1}$ in Fig. 6.23 is due to the detector change at 800nm. The peak position in each case is assigned as the one giving the best fit in the Birge-Sponer plot. Figs. 6.24–6.26 give the Birge-Sponer plots for CH, free NH and blue shifted NH oscillators. The band assignments, overtone peak positions and local mode parameters of the CH, free NH and blue shifted NH oscillators are given in Table 6.5.

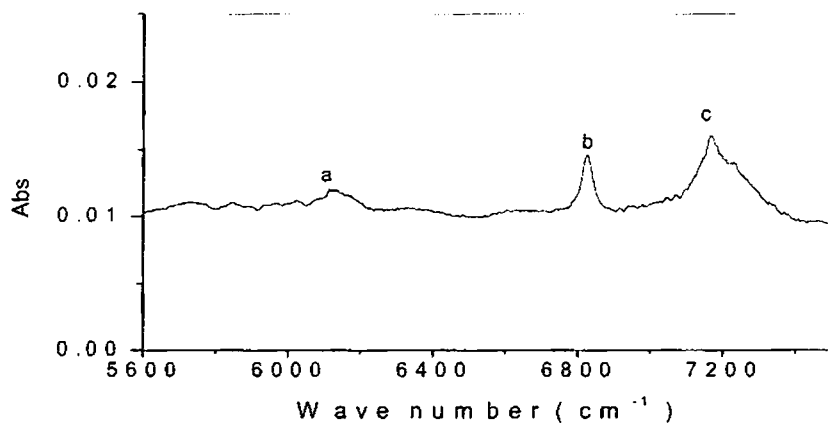


Fig. 6.21. Overtone spectrum of imidazole in carbon tetrachloride in the region $\Delta v = 2$

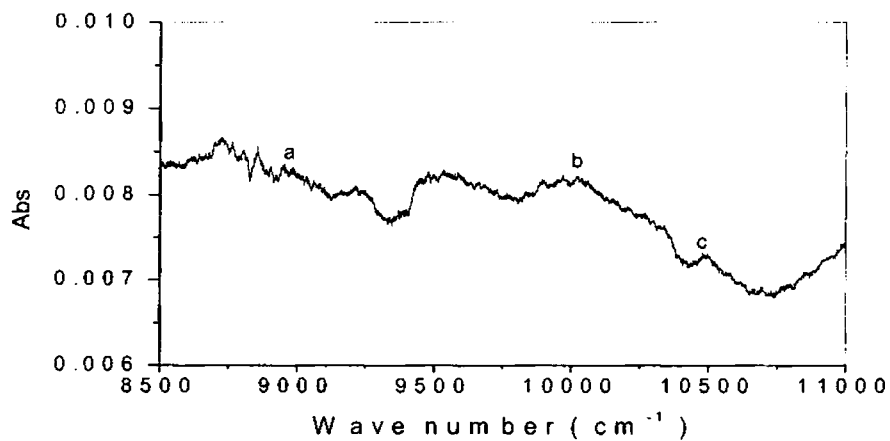


Fig. 6.22. Overtone spectrum of imidazole in carbon tetrachloride in the region $\Delta v = 3$

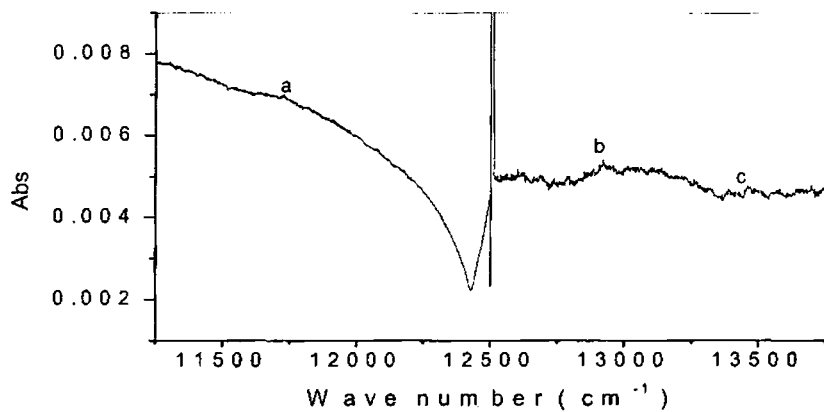


Fig. 6.23. Overtone spectrum of imidazole in carbon tetrachloride in the region $\Delta v = 4$

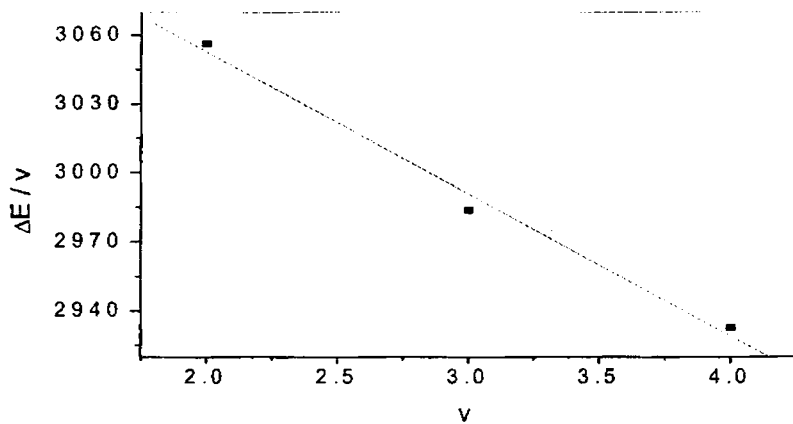


Fig. 6.24. Birge-Sponer plot for CH stretching overtones

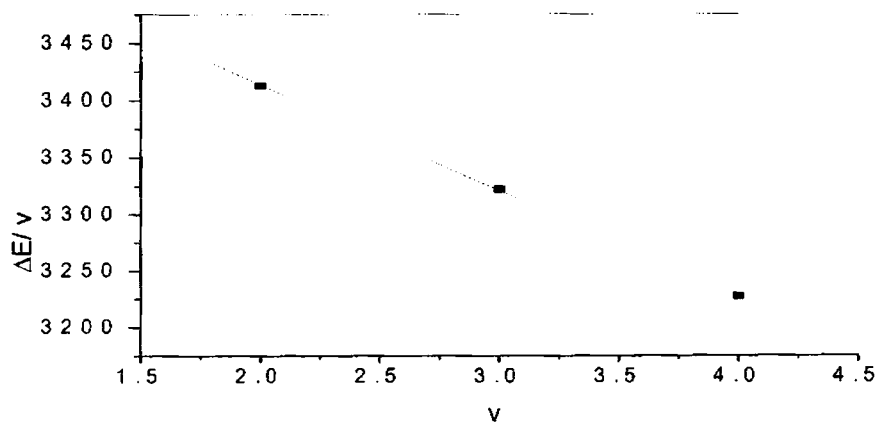


Fig. 6.25. Birge-Sponer plot for free NH-stretching overtones

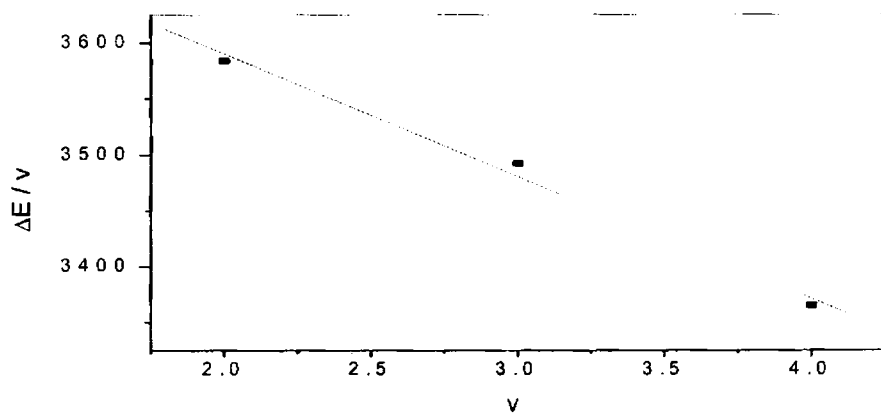


Fig. 6.26. Birge-Sponer plot for blue shifted NH-stretching overtones

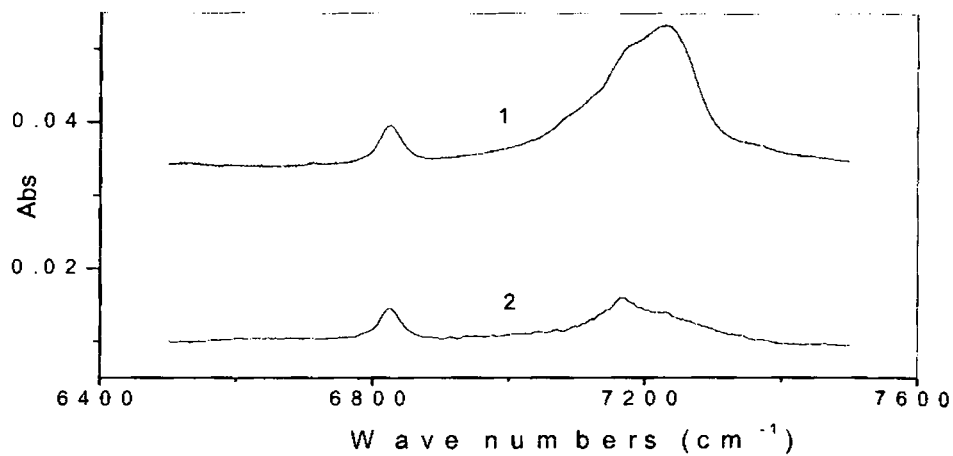


Fig. 6.27. NH positions in the region $\Delta\nu \approx 2$ for two concentrations.
 Curve 1-high concentration
 Curve 2-low concentration

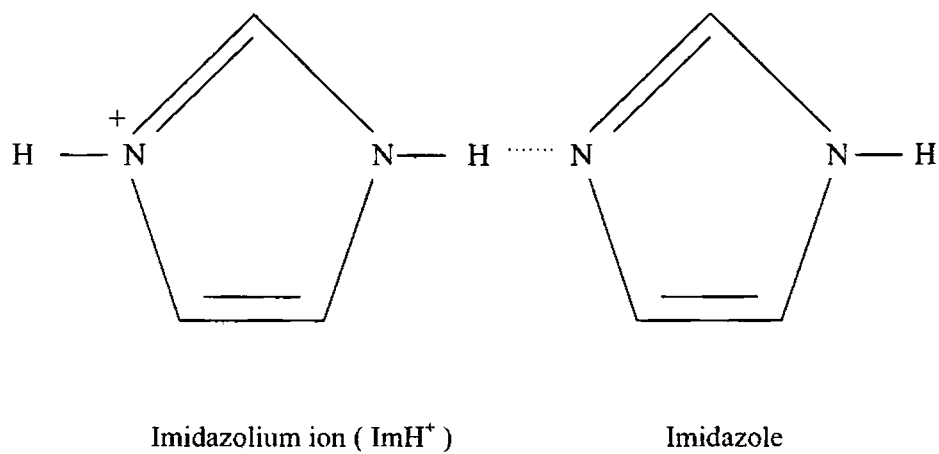


Fig. 6.28. Coupling between imidazole and imidazolium ion through hydrogen bonding

Table 6.5

The band assignments, overtone peak positions and the local mode parameters of the CH, free NH and blue shifted NH oscillators of Imidazole

Stretch type	ν	Overtone peak positions in (cm^{-1})	Local mode parameters and γ
CH	2	6112.47	$X_1 = 3238.18$
	3	8950.95	$X_2 = 61.84$
	4	11730.21	$\gamma = -.995$
Free NH	2	6825.94	$X_1 = 3692.52$
	3	9966.12	$X_2 = 92.96$
	4	12908.22	$\gamma = -.9999$
Blue-shifted NH	2	7168.46	$X_1 = 3918.65$
	3	10476.84	$X_2 = 109.52$
	4	13460.76	$\gamma = -.996$

ν = vibrational quantum number, X_1 = mechanical frequencies (cm^{-1}), X_2 = anharmonicity (cm^{-1}) and γ = the least square correlation coefficient .

Due to the small size and rigidity of the five membered ring and also due to its biological importance, there were significant amount of studies [49-52] of the structure and vibrational spectrum of imidazole, both theoretically and experimentally. But the agreement between the two was worse. The unique structure of imidazole allows a hydrogen bonded chain. In the spectra of molecular aggregates sometimes the X–H band contours for the hydrogen bonded associates exhibit their own fine structure [50]. The fine structure of the spectra has been found to be extremely sensitive to the influence of molecular interactions, changing with the condensation state of the material and with the temperature. In the $\Delta v = 2$ region we have two positions corresponding to NH stretch. The blue shifting is found to increase with concentration as in Fig. 6.27. Those at low wave number side is almost unchanged due to variation of concentration, which correspond to the almost free NH stretch vibrations. This itself is an evidence for the existence of strong intermolecular hydrogen bonding exhibited by imidazole. In their theoretical studies on the basis of B3LYP/6-311+G* method, Tatara et al. [53] and Shihai Yan et al.[48] have found one common phenomenon for all coupling modes for the complexes of imidazole and imidazole cation – that is one NH bond is blue shifted spectroscopically for each of them. This observation should be due to the interaction of two fragments; therefore, the electrons redistribute in two fragments, leading to the contraction and strengthening of the NH bond of ImH^+ . We haven't detected any red shifted bands, may be the bands are too broad and the hydrogen bonded samples are giving very complex spectra in the overtone region. The Im-ImH^+ complex is a strongly hydrogen bonded system (Fig.6.28) with a low energy barrier for the proton-transfer reaction and the rotation of the imidazolium ion along the axis of the complex [53]. The calculations predict that a classical motion of the proton between the two molecules in the complex is allowed. The aryl CH, free NH and blue shifted NH oscillators are examined in brief below.

Aryl CH oscillators: The aryl CH stretching frequency calculated using local mode model from the overtone spectrum agrees with the theoretical studies of Im-ImH^+ complex by Tatara et al. [53] and Shihai Yan et.al [48]. The mechanical frequency

and anharmonicity of the CH stretching vibration agree with the vibrational overtone study of five-membered aromatic heterocycles by Michael G. Sowa and Bryan R. Henry [54].

Free and blue shifted NH oscillators: The free NH oscillator frequency and anharmonicity values are in agreement with the earlier studies by Berthomieu and Sandorfy [55] on secondary amines. It is interesting to note that the mechanical anharmonicity of the blue shifted hydrogen bonds also is greater compared to the nonbonded (free) NH bonds. Thus the unusual blue-shifted hydrogen bonding as well as the standard red shifted one brings a higher anharmonicity value [56].

6.3.4 Conclusions

Near IR overtone spectrum of imidazole in carbon tetrachloride is analysed using the local mode model for the first time. Blue-shifted hydrogen bonded NH oscillators are observed. This is an indication of the formation of Im-ImH⁺ complex. The mechanical anharmonicity of the blue-shifted bands is calculated using local mode model and is found to be greater than that of free NH, similar to the case of standard red-shifted hydrogen bonding.

REFERENCES

- [1] L.N. Ferguson, *The Modern Structural Theory of Organic Chemistry*, Prentice-Hall of India, New Delhi, 1973, p. 530.
- [2] R.N. Jones, C. Sandorfy, *The application of Infrared and Raman Spectrometry on the Elucidation of Molecular Structure*, in: Weissberger's *Technique of Organic Chemistry*, Vol.9, ed. W.West, Interscience, New York, 1956.
- [3] F. Huisken, M. Kaloudi, A. Kulcke, *J. Chem. Phys.* 104 (1996) 17.
- [4] C. Sandorfy, *Bull. Polish Acad. Sci. Chem.* 43 (1995) 7.
- [5] C. Sandorfy, in: P. Schuster, G. Zundel, C. Sandorfy (Eds.), *The Hydrogen Bond*, vol. 2, North-Holland, Amsterdam, 1976, p. 613.
- [6] C. Sandorfy, *Top. Curr. Chem.* 120 (1984) 41.
- [7] G. Durocher, C. Sandorfy, *J. Mol. Spectrosc.* 15 (1965) 22.
- [8] C. Sandorfy, *J. Mol. Struct.* 614 (2002) 365.
- [9] G.R. Low, H.G. Kjaergard, *J. Chem. Phys.* 110 (1999) 9104.
- [10] H.G. Kjaergard, B.R. Henry, *J. Chem. Phys.* 96 (1992) 4841.
- [11] E. Juaristi, *Conformational Behaviour of Six-Membered Rings*, VCH Publishers, Inc. New York, 1995.
- [12] U. John, K.P.R. Nair, *Spectrochim. Acta Part A* 61 (2005) 2555.
- [13] E.L. Eliel, *Stereochemistry of Carbon compounds*, Tata McGraw-Hill Publishing Company Ltd., New Delhi, 1975.
- [14] P.S. Kalsi, *Stereo chemistry-Cofirmation and Mechanism New Age International (P) Ltd, New Delhi, Third Edition, 1995.*
- [15] C. Altona, H. J. Geise, C. Romers, *Tetrahedron*, 24 (1968) 13.
- [16] R. Loyd, S.N. Marthur, M.D. Harmony, *J. Mol. Spectrosc.* 72 (1978) 359.
- [17] R.L. Hilderbrandt, Q. Shen, *J. Phys. Chem.* 86 (1982) 587.
- [18] B. Fuchs, *Top. Stereochem.* 10 (1978) 1.
- [19] I.O.C. Ekejiuba, H. E Hallam, *J. Chem. Soc. B*, (1970) 209.

- [20] R.J. Abraham, R. Koniotou, F. Sancassan, *J. Chem. Soc., Perkin Trans. 2* (2002) 2025.
- [21] H. Kanno, M. Honshoh, Y. Yoshimura, *Journal of Solution Chemistry*, 29 (2000) 1007.
- [22] S. Yamauchi, H. Kanno, *Chem. Phys. Lett.* 154 (1989) 248.
- [23] S. Yamauchi, H. Kanno, *J. Phys. Chem.* 94 (1990) 6594.
- [24] H. Kanno, S. Yamauchi, *J. Solution Chem.* 20 (1991) 589.
- [25] H. Kanno, S. Yamauchi, *J. Raman Spectrosc.* 24 (1993) 403.
- [26] B. R. Henry, I-Fu Hung, R.A. MacPhail, H.L. Strauss, *J. Am. Chem. Soc.* 102 (1980) 515.
- [27] R.J. Fessenden, J.S. Fessenden, *Organic Chemistry*, 5th ed, Brooks/Cole Publishing Company, California, 1993.
- [28] U. Domanska, A. Pobudkowaska, M. Rogalski, *J. Chem. Eng. Data* 49 (2004) 1082.
- [29] D.k. Dalvie, A.S. kalgutkar, S. Cyrus Khojasteh-Bakht, R.S. Obach, J.P. O'Donnell, *Chem. Res. Toxicol.* 15 (2002) 269.
- [30] K.W. Boddeker, K.V. Peinemann, S.P. Nunes, *J. Membr. Sci.* 185 (2001) 1.
- [31] G.A. Jeffrey, *An Introduction to Hydrogen Bonding*, Oxford University Press, New York, 1997.
- [32] G.R. Desiraju, T. Steiner, *The Weak Hydrogen Bond*, Oxford University Press, Oxford, 1999.
- [33] S. Scheiner, *Hydrogen Bonding*, Oxford University Press, New York, 1997.
- [34] P. Hobza, Z. Havlas, *Chem. Rev.* 100 (2000) 4253.
- [35] M. Budesinsky, P. Fiedler, Z. Arnold, *Synthesis* (1989) 858.
- [36] I.E. Boldeskul, I.F. Tsymbal, E.V. Ryltsev, Z. Latajka, A.J. Barnes, *J. Mol. Struct.* 436 (1997) 167.
- [37] Q. Weili, K. Samuel, *J. Phys. Chem. A* 106 (2004) 6628.
- [38] P. Hobza, V. Spirko, H.L. Selzle, E.W. Schiag, *J. Phys. Chem. A* 102 (1998) 2501.

- [39] P. Hobza, V. Spirko, Z. Havlas, K. Buchhold, B. Reimann, H.D. Barth, B. Brutschy, *Chem. Phys. Lett.* 299 (1999) 180.
- [40] P. Hobza, Z. Havlas, *Chem. Phys. Lett.* 303 (1999) 447.
- [41] E. Cubero, M. Orozco, P. Hobza, F. J. Luque, *J. Phys. Chem. A* 103 (1999) 6394.
- [42] P. Hobza, J. Sponer, E. Cubero, M. Orozco, F.J. Luque, *J. Phys. Chem. A* 104 (2000) 6286.
- [43] P. Hobza, *Phys. Chem. Chem. Phys.* 3 (2000) 2555.
- [44] B.J. Van der Veken, W.A. Herrebout, R. Szostak, D.N. Shchepkin, Z. Havlas, P.J. Hobza, *J. Am. Chem. Soc.* 123 (2001) 12290.
- [45] Y. Gu, T. Kar, S. Scheiner, *J. Am. Chem. Soc.* 121 (1999) 9411.
- [46] S. Scheiner, T. Kar, *J. Phys. Chem. A* 106 (2002) 1784.
- [47] J.J. Dannenberg, L. Haskamp, A. Masunov, *J. Phys. Chem. A* 103 (1999) 7083.
- [48] Shihai Yan, Yuxiang Bu, Zhaohua Cao, Ping Li, *J. Phys. Chem. A* 108 (2004) 7038.
- [49] M. Cordes, J.L. Walters, *Spectrochim. Acta Part A* 24 (1968) 237.
- [50] H.R. Flakus, A. Bryk, *J. Mol. Struct.* 372 (1995) 215.
- [51] H.R. Flakus, A. Bryk, *J. Mol. Struct.* 385 (1996) 35.
- [52] A.A. El-Azhary, *Spectrochim. Acta Part A* 59 (2003) 2009.
- [53] W. Tatara, M.J. Wojcik, J. Lindgren, M. Probst, *J. Phys. Chem. A* 107 (2003) 7827.
- [54] M.G. Sowa, B.R. Henry, Y. Mizugai, *J. Phys. Chem.* 95 (1991) 7659.
- [55] C. Berthomieu, C. Sandorfy, *J. Mol. Spectrosc.* 15 (1965) 15.
- [56] U. John, K.P.R. Nair, *Spectrochim. Acta Part A* 63 (2006) 169.

CHAPTER 7

SUMMARY AND CONCLUSIONS

The first part of the thesis deals with photothermal investigations on certain plasma polymerized thin films. Photothermal effects originate from the non-radiative excited state relaxation resulting in the heat generation. PT techniques are best suited for thermal characterization of materials. Thermal diffusivity is an important thermal transport parameter in thin film characterization. Plasma polymerization is an inexpensive tool for fabricating organic thin films. These films have potential applications in microelectronics. They are finding use in fabricating storage batteries, sensors, supercapacitors, etc. Using r.f polymerization technique, three different polymer thin film samples, namely, poly 2,6 dimethylaniline, poly diethylamine and poly dimethylamine are prepared. FTIR analysis of the monomer and polymer are done to suggest the possible linkage in the formation of polymer. The FTIR spectra are recorded in the range $400\text{-}4000\text{ cm}^{-1}$. Since the r.f plasma polymerized samples are highly branched and highly cross-linked, the exact structure cannot be predicted with the IR analysis alone. Still, some conclusions are made. The most important observation is that pertaining to NH stretching frequencies in 2,6-dimethylaniline. Being a primary amine, in 2,6-dimethylaniline there are two bands in the monomer spectrum in the NH stretch region corresponding to asymmetric (3462 cm^{-1}) and symmetric stretch (3383 cm^{-1}). But in the polymer spectrum only a single frequency (3343 cm^{-1}) is there. The presence of this single frequency is characteristic of a secondary amine, which has only one NH bond. Hence it can be inferred that NH_2 group in the monomer is changed to NH group in the polymer. Thus the possible linkage is through the hydrogen abstraction of the NH_2 group in the monomer.

The thermal diffusivity of the low absorbing, optically transparent and thermally thin polymer thin film samples coated on bulk substrates is suitably evaluated by probe beam deflection (PBD) experimental set up. Here the thin film sample is irradiated with a focused laser beam (pump). The thermal waves generated diffuse in all directions.

Here carbon tetrachloride is used as a coupling fluid since its thermal diffusivity is very low compared to that of the sample. A refractive index gradient is generated in the coupling fluid in contact with the heated surface of the solid sample. A probe beam traveling through this gradient gets deflected. The probe beam is directed to the sample surface in the skimming configuration, in which the probe beam just grazes the sample surface. The probe is scanned across the sample surface perpendicular to the pump beam. The phase or amplitude of the deflection signal holds a linear relationship with pump-probe offset. The thermal diffusivity of the sample is calculated from the slope of the plot. For each sample, measurements are taken at two different modulation frequencies and the signal is analysed using the phase method and amplitude method. Both methods at the two modulation frequencies yielded similar results for thermal diffusivity. The values obtained for all the samples lie in the same order as those of polymer thin films. Thus the very low values of the thermal diffusivity of organic thin film samples are successfully determined by employing PBD experimental set up. It has the advantage that no knowledge of the thickness of the sample is required for the evaluation of thermal diffusivity.

Near IR overtone investigations of a few organic molecules using local mode model are also done for characterizing the CH, NH and OH bonds. Normal mode model is successful for fundamental vibrations of molecules but fails for anharmonic higher overtones. Higher vibrations are localized or they are effectively uncoupled from other degrees of freedom since their frequencies are disparate from others in the molecule. This local mode model can be applied very successfully for X-H (X = C, O, N, S, etc.) containing molecules as a probe for molecular structure and conformation. The liquid phase absorption spectra of the molecules in the near infrared region (700–2000 nm) are recorded at room temperature ($26 \pm 1^\circ \text{C}$) with air as reference and pathlength 1 cm, using commercial UV-Vis-NIR spectrophotometers [Varian-Cary 5000 model, Jasco Corp. V-570 model and Hitachi U-3410 model] which use a tungsten lamp as the near IR source. The overtone spectra of 2,6-dimethylaniline, 2,4-dimethylaniline, cyclohexylamine, morpholine, cyclohexanol, cyclopentanol and imidazole are analysed using local mode model.

The pure overtones of NH, ring CH and methyl CH oscillators of 2,6-dimethylaniline and 2,4-dimethylaniline are considered. It is interesting to note that overtones corresponding to both asymmetric and symmetric stretching vibrations are obtained for both the molecules as is expected for a primary amine. The frequency of the NH oscillator in 2,6-dimethylaniline is higher compared to 2,4-dimethylaniline. Since 2,6-dimethylaniline is a weak base compared to 2,4-dimethylaniline, it is concluded that the increase in the NH oscillator frequency is an indication of the weakening of the basicity in methylated anilines. Again it is observed that methylation of aniline in *ortho* position brings a blue shift in the overtone energy values of the ring CH oscillator. In the case of cyclohexylamine, overtones corresponding to both asymmetric and symmetric NH-stretching vibrations are obtained as is expected for a primary amine. Due to the weak hydrogen bonding in amines higher overtones for bonded NH oscillators are too weak to be resolved. Still weak and broad red-shifted bands at lower overtones are identified due to the formation of hydrogen bonds. The low value of NH-stretching frequency of cyclohexylamine compared to aniline is an indication of its strong basicity. Morpholine being a secondary amine overtones corresponding to only one type of NH stretch is there. Due to the weak hydrogen bonding in amines higher overtones for bonded NH oscillators are too weak to be resolved. Still weak and broad red-shifted bands at lower overtones are identified due to the formation of NH...O hydrogen bonds. The high values of NH-stretching overtone positions of morpholine compared to piperidine is an indication of its weak basicity.

Overtone spectra of cyclohexanol in carbon tetrachloride in different concentrations are analysed using the local mode model. The mechanical frequencies and anharmonicities for various oscillators are calculated. The aryl CH and free OH local mode parameters are almost insensitive to the variation in concentration. But the local mode parameters for the bonded OH stretching vibrations vary with concentration. We have observed that as the concentration is increased, mechanical frequency of the bonded OH vibrations tends to decrease and anharmonicity tends to increase due to strong intermolecular hydrogen bonding. Overtone spectra of cyclopentanol in carbon tetrachloride is analysed using the local mode model. In the CH region in $\Delta\nu = 2$ we

have two peaks corresponding to two nonequivalent CH bonds, the axial and the equatorial, similar to the case of cyclopentane. The CH stretching frequencies and anharmonicities are in agreement with the local mode parameters for cyclopentane. In the OH region both free and red-shifted hydrogen bonded OH oscillators are observed. The mechanical anharmonicity of the red-shifted OH bands is calculated using local mode model and is found to be greater than that of free OH. In the free OH region in $\Delta v = 2$ two peaks are there, which suggest the two optimised geometries for cyclopentanol, an unsymmetric envelope conformation with the axial hydroxyl substituent at the fold of the envelope and the symmetric conformation with an axial hydroxyl at the flap of the envelope. The frequency and anharmonicity of the free stretching OH bands agree with the already established results for free OH bonds. Near IR overtone spectrum of imidazole in carbon tetrachloride is analysed using the local mode model. Blue-shifted hydrogen bonded NH oscillators are observed. This is an indication of the formation of Im-ImH^+ complex. The mechanical anharmonicity of the blue-shifted bands is calculated using local mode model and is found to be greater than that of free NH, similar to the case of standard red-shifted hydrogen bonding.

Thus in the above discussed cases of molecules, overtone spectroscopy and local mode model provide a valuable probe of molecular structure and conformation. Here the overtone spectroscopy is used for the characterization of X-H (X = C, N and O) bonds in the organic compounds. The X-H stretching parameters obtained from fitting a number of sequential overtones for each local mode oscillator promise higher precision than single measurements in the infrared. The overtone spectra and local mode model also give the anharmonicity values of the local mode oscillators, which determine the shape of the corresponding potential curves, whereas the infrared fundamentals of samples give only the frequencies of isolated X-H bonds. Vibrational overtone spectroscopy with local mode model is used as an effective tool in hydrogen bonding studies as well.

G 9025

LIST OF PAPERS PUBLISHED IN INTERNATIONAL JOURNALS

1. Ionic character and dipole moments of alkali halides from their electronegativity data.

K. P. R. Nair, **Usha John**, Asian Journal of Physics 9 (2000) 93.

2. Photothermal Investigations on weakly absorbing plasma polymerized diethylaniline thin film.

Jyotsna Ravi, B.Syamalakumari, **Usha John**, K.P.R. Nair, T.M.A. Rasheed, Journal of Material Science Letters 22 (2003) 1073.

3. Liquid phase overtone spectral investigations of 2,6-dimethylaniline and 2,4-dimethylaniline—evidence for steric nature of the *ortho* effect and the consequent base weakening.

Usha John, K.P.R. Nair, Spectrochimica Acta Part A: Mol.& Biomol. Spectroscopy 60 (2004) 2337.

4. Near IR overtone spectral investigations of Cyclohexanol using local mode model—evidence for variation of anharmonicity with concentration due to hydrogen bonding .

Usha John, K.P.R. Nair, Spectrochimica Acta Part A: Mol.&Biomol. Spectroscopy 61 (2005) 2555.

5. Near IR overtone spectral investigations of liquid phase Imidazole and the blue- shifting hydrogen bonds.

Usha John, K.P.R. Nair, Spectrochimica Acta Part A: Mol.& Biomol. Spectroscopy 63 (2006) 169.

